NORTHWESTERN UNIVERSITY

Highly Conductive and Transparent Cadmium Oxide Thin Films Grown by

MOCVD - Epitaxial Growth and Doping Effects

A DISSERTATION

SUBMITTED TO THE GRADUATE SCHOOL IN PARTIAL FULFILLMENT

OF THE REQUIREMENTS

for the degree

DOCTOR OF PHILOSOPHY

Field of Chemistry

By

Shu Jin

EVANSTON, ILLINOIS

December 2006

ABSTRACT

Highly Conductive and Transparent Cadmium Oxide Thin Films Grown by

MOCVD - Epitaxial Growth and Doping Effects

Shu Jin

Four series of doped CdO thin films have been grown on both amorphous glass and single-crystal MgO(100) substrates by metal-organic chemical vapor deposition (MOCVD), and their phase structure, microstructure, electrical, and optical properties investigated. Epitaxial films grown on single-crystal MgO(100) exhibit biaxial, highly textured microstructures. These as-deposited doped CdO thin films exhibit excellent optical transparency, with an average transmittance of > 80 % in the visible range. Doping widens the optical band gap up to 3.4 eV via a Burstein-Moss shift. Epitaxial doped CdO films on single-crystal MgO(100) exhibit significantly higher mobilities (up to 236 cm^2/V·s) and carrier concentrations than that of films on glass, arguing that the epitaxial CdO films possess fewer scattering centers and higher doping efficiencies due to the highly textured microstructure. Room temperature thin film conductivities of 20,000 S/cm on MgO(100), is obtained at an optimum In-doping level of 2.6%, which is the highest up to date grown by CVD technique.

Both experimental and theoretical results reveal that dopant ionic radius and electronic structure have a significant influence on the CdO-based TCO crystal and band structure: (1)

lattice parameters contract as a function of dopant ionic radii in the order Y (1.09 Å) < In (0.94 Å) < Sc (0.89 Å), Ga (0.76 Å), with the smallest radius ion among the four dopants, only shrinking the lattice slightly and exhibiting low doping efficiency; (2) carrier mobilities and doping efficiencies decrease in the order In > Y > Sc>Ga; (3) the dopant d state has substantial influence on the position and width of the s-based conduction band, which ultimately determines the intrinsic charge transport characteristics.

Highly conductive and transparent CdO thin films have been grown on glass and on single-crystal MgO(100) by MOCVD at 400 ^{o}C, and were used as transparent anodes for fabricating small-molecule organic-light emitting diodes (OLEDs). Device response and applications potential have been investigated and compared with those of control devices based on commercial ITO anodes.

Advisor: Professor Tobin J. Marks

ACKNOWLEDGEMENTS

Hersam. Dr. Julia Medvedeva did an amazing job on theoretical calculations, which provided great direction about my experimental work; Dr. Shuyou Li did great work on TEM measurements, the sample preparation takes great patience and needs deft skills which Shuyou has both. Dr. Qinglan Huang fabricated OLED devices and did characterization on them. Dr. John Ireland and Norma Cortes measured variable temperature charge transport properties of my films. I would also want to express my gratitude to Dr. Jerry Carsello for his assistance with X-ray diffraction measurements and Dr. Nick Wu for his assistance with XPS measurements at Keck-II/NUANCE facility.

Lastly I want to thank my parents, who taught me the importance of independence thinking and trying my best whatever I do; without their constant encouragement and support, this work will not be possible. To mom and dad I dedicate this dissertation.

LIST OF ABBREVIATIONS

μ	carrier mobility
σ	conductivity
AFM	atomic force microscopy
Alq	tris-8-hydroxyquinoline aluminum
BCP	2,9-dimethyl-4,7-diphenyl-1,10-phenanthroline
CGO	gallium doped cadmium oxide
CIO	indium doped cadmium oxide
CSO	scandium doped cadmium oxide
CYO	scandium doped cadmium oxide
CVD	chemical vapor deposition
DIQA	di-isoamylquinacridone
dpm	dipivaloylmethanate or 2,2,6,6-tetremethyl-3,5-heptanedionate
eV	electron volts
FLAPW	full-potential linear augmented plane wave
FPD	flat panel display
FWHM	full width at half maximum
GBS	grain boundary scattering
Hdpm	dipivaloylmethane or 2,2,6,6-tetremethyl-3,5-heptanedione
hfa	1,1,1,5,5,5-hexafluoro-2,4-pentanedionate
Hhfa	1,1,1,5,5,5-hexafluoro-2,4-pentanedione

ICP-AES	inductively coupled plasma atomic emission spectroscopy
IIS	ionized impurity scattering
ITO	indium tin oxide or Sn-doped In_2O_3
LCD	liquid crystal display
LVS	lattice vibration scattering
MOCVD	metal-organic chemical vapor deposition
n	carrier concentration
NIS	neutral impurity scattering
NMR	nuclear magnetic resonance
NPB	N,N'-di(1-napthyl)-N,N'-diphenylbenzidine
OLED	organic light-emitting diodes
PLD	pulsed laser deposition
PLED	polymer light emitting diodes
PSS-PEDOT	polystyrenesulfonate-poly (3,4-ethylenedioxythiophene)
RMS	root mean-squared
SAED	selected area electron diffraction
sccm	standard cubic centimeter per minute
SEM	scanning electron microscopy
SIMS	secondary ion mass spectrometry
sX-LDA	screened-exchange local density approximation
TCO	transparent conducting oxide
TEM	transmission electron microscopy
TGA	thermogravimetric analysis

TMEDA	*N*, *N*, *N'*, *N'*-tetramethylethylenediamine
UPS	ultraviolet photoelectron spectroscopy
UV-Vis-NIR	ultraviolet-visble-infrared spectroscopy
XPS	X-ray photoelectron spectroscopy
XRD	X-ray diffraction
ZITO	zinc- and tin-doped indium oxide

TABLE OF CONTENTS

LIST OF TABLES

LIST OF FIGURES

CHAPTER ONE

Dopant Ion Size and Electronic Structure Effects on Transparent Conducting Oxides. Sc-Doped CdO Thin Films Grown by MOCVD

1.1. INTRODUCTION

Transparent conducting oxides (TCOs), a fascinating class of materials that are both optically transparent and electrically conductive, are finding increasing application in opto-electronic devices such as flat panel displays (FPDs), OLEDs, photovoltaics, solar cells, heat reflectors, de-icers, and energy-efficient windows. Advances in all of these technologies would greatly benefit from new TCO materials with, among other characteristics, greater charge transport capacities and broader transparency windows.[1-3] Recently, CdO-based TCOs received much attention due to their exceptional carrier mobilities, nearly metallic conductivities, and relatively simple crystal structures.[2,4-7] Sn doping of CdO thin films grown epitaxially on MgO(111) by pulsed laser deposition (PLD) achieved thin film mobilities and conductivities as high as 607 cm^2/V·s and 42,000 S/cm, respectively, rendering them the most conductive TCO thin films with the highest carrier mobilities grown to date.[7] In addition, Cd_2SnO_4, $CdIn_2O_4$, and CdO-ZnO thin films have been grown with good-excellent conductivities (up to 8,300 S/cm) and excellent optical transparencies (band gaps as large as 3.7 eV) for photovoltaic applications[3,8]. Although the optical band gap of pure bulk CdO is only 2.3 eV,[9] leading to relatively poor optical transparency in the short wavelength range, aliovalent metal doping offers the possibility of tuning the electronic structure and the optical band gap through a carrier concentration-dependent Burstein-Moss (B-M) energy level shift.[10] CdO, with a simple cubic rock salt structure, broadly dispersed s-like conduction bands, and a small carrier effective mass,

is seen to represent an ideal model material in which to study the effects of doping on TCO band structure, crystal chemistry, and charge transport.

In our previous work, undoped and doped CdO thin films were successfully grown by MOCVD using optimized metal-organic Cd precursors.[5,6] In-doped CdO thin films grown on glass by MOCVD exhibit conductivities as high as 16,800 S/cm.[6] It was found that In doping dramatically alters the CdO band structure by extensive mixing of In 5s and Cd 5s states, also yielding a hybridization gap in the conduction band. Our continued interest in CdO-based TCOs focuses on understanding crystal structure-charge transport relationships by doping CdO with a wide variety of dopants which: (1) offer controlled lattice parameter excursions via varying ionic radius; (2) offer varying degrees of orbital overlap between Cd^{2+} conduction band states and dopant ions; (3) contribute varying formal numbers of conduction band electrons to increase the effective carrier density by substituting for Cd^{2+}. For all these reasons, Sc^{3+} with a six-coordinate ionic radius of 0.89 Å,[11] which is substantially smaller than that of Cd^{2+}, 1.09 Å, would be of great interest in the study of dopant size effects. In addition, compared with In^{3+} and Sn^{4+}, Sc^{3+} does not have an energetically comparable s state that can hybridize with the Cd 5s states in the conduction band.[12] Hence, Sc-doped CdO would also be of great interest to probe orbital hybridization effects by comparison with the corresponding In- and Sn-doped CdO thin films.

In this contribution, we report the growth of Sc-doped CdO (CSO) thin films on amorphous glass and single crystal MgO(100) by MOCVD. The CSO thin film phase structure, microstructure, and electrical and optical properties are investigated in detail. In addition, we

report first-principles full-potential linear augmented plane wave (FLAPW)[5b,6,13] electronic band structure calculations within the screened exchange local density approximation (sX-LDA) to treat both the ground and the excited states, which allow us to compare the structural, electronic, and optical properties of In- and Sc-doped CdO systems. It is found both experimentally and theoretically, that (as might, a priori, be expected) Sc doping shrinks the CdO lattice parameter substantially due to its smaller ionic radius. As-deposited CSO thin films are highly conductive and transparent, with an average transmittance > 80% in the visible range. Thin film conductivities as high as 18,100 S/cm on MgO(100) are obtained at the optimum Sc doping level of 1.8 atom %. This conductivity is roughly 5 × greater than that of commercial ITO.

1.2. EXPERIMENTAL

1.2.1. MOCVD Precursors and Thin Film Growth

The volatile metal-organic Cd precursor Cd(hfa)$_2$(N,N-DE-N',N'-DMEDA) (**1**) (hfa = hexafluoroacetylacetonate, N,N'-DE-N,N'-DMEDA = N,N'-diethyl-N,N'-dimethyl-ethyldnediamine) was prepared from high-purity Cd(NO$_3$)$_2$·4H$_2$O (99.999%, Aldrich),[15] and was triply vacuum-sublimed. Sc(dpm)$_3$ (**2**) (dpm = dipivaloymethanate) was prepared from Sc$_2$O$_3$ (99.99%, Alfa Aesar) by a literature procedure.[16]

1   **2**

CSO thin film growth was carried out in a previously described horizontal, cold-wall MOCVD reactor.[14] For CdO and Sc-doped CdO thin film growth, the precursor reservoir temperatures/Ar carrier gas flow rates were optimized at: $Cd(hfa)_2$(N,N'-DE-N,N'-DMEDA) (**1**), 85 ^{o}C /15 sccm; $Sc(dpm)_3$ (**2**), 110 ^{o}C/5-50 sccm. The O_2 oxidizing gas was introduced upstream at 400 sccm after bubbling through distilled water. A system operating pressure of 4.0±0.1 Torr and a substrate temperature of 400 ^{o}C was maintained during the thin film deposition. Corning 1737F glass and polished single-crystal MgO(100) (a = 4.216 Å) substrates were purchased from Precision Glass and Optics and MTI Corporation, respectively. Both the glass and the MgO(100) substrate surfaces were cleaned with acetone prior to the film deposition, and were placed side-by-side on a SiC-coated susceptor in the growth reactor for simultaneous growth experiments.

1.2.2. Film Physical Characterization Measurements

Composition analyses were carried out using inductively coupled plasma atomic emission spectrometry (ICP-AES). Fluorine and carbon contamination (mole %) were quantitatively analyzed using an Omicron ESCA Probe X-ray photoelectron spectrometer (XPS). Optical

transparency measurements were carried out in the range of 300 – 3300 nm with a Cary 500 Uv-Vis-NIR spectrophotometer. Film thicknesses were measured using a Tencor P-10 profilometer after etching a step in the film using 5% HCl solution. X-ray diffraction θ-2θ scans of CdO films on glass were obtained with a Rigaku DMAX-A powder diffractometer using Ni-filtered Cu K_α radiation. Rocking curves and ϕ scans of the epitaxial thin films on MgO(100) substrates were obtained on a home-built Rigaku four-circle diffractometer with detector-selected Cu K_α radiation. Film surface morphology was imaged using a Digital Instruments Nanoscope III atomic force microscope (AFM) operating in the contact mode. Film microstructure was imaged on a Hitachi S4500 FE scanning electron microscope (SEM). Ambient-temperature four-probe charge transport data were acquired on a Bio-Rad HL5500 Hall-effect measurement system. Variable-temperature Hall effect and 4-probe conductivity data were collected between 4K and 330K and used instrumentation described previously.[17]

1.2.3. Theoretical Methods

First-principles electronic band structure calculations were performed using the highly precise all-electron FLAPW method[13] that has no shape approximation for the potential and charge density. The exchange-correlation energies were treated via the local density approximation (LDA). Cut-offs of the plane-wave basis (14.4 Ry) and potential representation (81.0 Ry), and expansion in terms of spherical harmonics with $l \leq 8$ inside the muffin-tin spheres were used. To overcome the shortcomings of LDA for the determination of the excited state band

structure and optical properties of CSO, we used the self-consistent screened-exchange LDA

(sX-LDA) method[18] with cut-off parameters of 10.24 Ry in the wave vectors and $l \leq 3$ inside the

muffin-tin spheres. Summations over the Brillouin zone were carried using 10 special k points in

the irreducible wedge.

1.3. RESULTS AND DISCUSSION

We first describe a simple, effective, low-pressure MOCVD growth process for Sc-doped

CdO (CSO) thin films. Then, CSO film composition, morphology, microstructure, and epitaxy

are characterized as a function of doping level using a broad array of complementary physical

techniques. In addition, the optical and electrical properties of as-deposited CSO thin films are

investigated in detail, and microstructure-charge transport-optical properties relationships

discussed. Finally, band structure calculations using the highly precise sX-LDA formalism are

used to help understand CSO structural, electronic, and optical properties.

1.3.1. Film Growth

A series of CSO thin films was grown on 1737 F glass and single-crystal MgO(100) at 400

°C by low-pressure MOCVD using the metal-organic Cd precursor

$Cd(hfa)_2$(N,N-DE-N',N'-DMEDA) (**1**) and the Sc precursor $Sc(dpm)_3$ (**2**). Thin films with a

thickness of ~180 nm on glass and ~350 nm on MgO(100) are obtained after 2 h of growth, at a

growth rate of ~1.5 nm/min on glass and ~3 nm/min on MgO(100), respectively. The CSO thin

film growth rate on single-crystal MgO(100) is more rapid than that on amorphous glass

substrates, presumably due to epitaxy effects. Film growth is found to be very sensitive to the

substrate temperature and O_2 partial pressure. At a given Cd precursor delivery rate (precursor

temperature/Ar carrier gas flow rate of 85 ^{o}C/15 sccm), the film growth rate decreases with

increasing substrate temperature over the range 300-400 ^{o}C. This is because CdO itself is

relatively volatile,[19] leading to competition between the CdO film deposition and evaporation on

the substrate at higher temperatures. Films could only be deposited at temperatures below 425 ^{o}C

under the present reactor conditions. More importantly, low precursor delivery rates proved to be

highly effective in obtaining highly epitaxial thin films (see below). In addition, as-deposited

films grown at low delivery rates (≤1.5 nm/min) exhibit larger grain sizes and higher measured

mobilities (see below) than films grown at higher delivery rates (>1.5 nm/min). These as-grown

films are uniformly pale-yellow in color but exhibit good optical transparency. The Sc doping

level can be incrementally varied from 0.7 to 15 atom % by varying the Ar carrier gas flow rate

and reservoir temperature of the Sc precursor.

1.3.2. Film Composition, Morphology, Microstructure, and Epitaxy

Fluorine and carbon contamination in the CSO films was quantitatively investigated by XPS

due to the use of a F-containing Cd-organic MOCVD precursor. To analyze the film composition,

the surface layer (~3-5 nm) exposed to air was first removed by Ar-ion sputtering (2 kV, 10 μA;

sputtering rate ~3 Å/min). There are no detectable changes in the composition or the chemical state

of the Cd, Sc, and O constituents after 10, 20, and 40 min sputtering. Less than 0.5 % F (atom %)

and 2.5 % C (atom %) are detected in the as-deposited CSO thin films, and hence F introduction is

minimal and should not contribute significantly as a doping mechanism for the high conductivity.

Previous SIMS analyses on CdO films grown under similar MOCVD conditions using an

analogous hfa precursor indicated F levels of 0.26 atom %.[15]

X-ray diffraction θ-2θ scans of CSO thin films grown on glass were carried out between 2θ

= 25° to 80°. Figure 1 shows the XRD data as a function of Sc doping level. All of the films are

phase-pure and polycrystalline, with the fcc CdO structure.[20] No Sc_2O_3[21] or other contaminating

phases are detected by XRD, even at the 15 atom % Sc doping level, indicating that Sc^{3+}

substitutes uniformly for Cd^{2+} in the lattice rather than forming a second phase. It is clear that the

presently determined solubility of Sc in CdO thin films is ≥ 15 %. In contrast to the present

polycrystalline microstructures of the MOCVD-derived CSO thin films grown on amorphous

glass substrates, all the epitaxial CSO thin films grown on single-crystal MgO(100) exhibit a

highly (200)-textured microstructure, even though the lattice mismatch between MgO(100)

substrate and CdO crystal structure is 10.2%. The textured structure of the as-deposited thin films

was further assessed by rocking curve and ϕ-scans (Figure 2). The rocking curves of the films

show good out-of-plane alignment (Figure 2A). The full-width-at-half-maximum (FWHM) is

increased from 0.5° for undoped CdO films to 1.5° for CSO at 6.4% Sc doping, suggesting that the

crystallite alignment decreases slightly with increased Sc doping. The in-plane orientation was

also investigated by ϕ-scans of the CdO(111) reflection at $\chi = 54.7^o$ (Figure 2B). The clear

four-fold rotational symmetry of the CdO(111) reflections along with the small FWHMs (0.5^o for

pure CdO, 0.7^o for CSO at 1.8% Sc doping) reveals excellent in-plane orientation of the films. The

orientation relation between CSO thin films and the MgO(100) substrates is therefore

CdO(100)∥MgO(100).

Using polycrystalline silicon as an internal calibration reference, the precise lattice

parameters of the MOCVD-derived CSO thin films on glass were calculated. It is found that the

lattice parameters decrease linearly with increasing Sc doping level (Figure 3), indicating that the

lattice dimensions contract monotonically with the introduction of Sc^{3+}, having a smaller

six-coordinate ionic radius, 0.89 Å, vs. 1.09 Å for Cd^{2+}. In addition, the lattice parameters of the

CSO films on MgO(100) were calculated using the MgO(200) reflection as an internal reference.

When Sc^{3+} doping is ≤ 2.8 %, there is no significant change in lattice parameters, doubtless

reflecting epitaxy effects. However, the lattice parameters decrease precipitously with further Sc^{3+}

doping, reaching 4.653 Å at 6.4% doping (Figure 3). It will be seen below that these results are in

good agreement with the FLAPW calculations. Ambrosini, et al, observed a similar lattice

shrinkage trend upon introducing Sc into bulk In_2O_3 samples.[22] However, the shrinkage is not as

large as estimated from a simple Vegards' law weighted average of the Sc^{3+} and Cd^{2+} ionic radii

(Figure 3).[23] One possible explanation is that some of the Sc^{3+} dopant ions exist as interstitial ions

instead of directly substituting for Cd^{2+} in the lattice. Another possibility is that the Sc^{3+}-induced

doping shrinkage is compensated by an expansion mechanism which originates from the

antibonding character of the conduction band formed from Cd 5s and O 2p states. This interesting

phenomenon was proposed for In- and Y-doped CdO bulk materials by Morozova, et al,[24] and Dou,

et al,[25] who reported that the In- and Y-doped CdO lattice parameters increase with increasing

doping levels, even though the dopant ions, In^{3+} and Y^{3+} (radii of 0.94 Å and 1.04 Å, respectively),

are again smaller than Cd^{2+}. This issue will be discussed further in the theory section. Besides

these possibilities, an expansion mechanism involving Cd^{2+} reduction to Cd^{1+} that could

compensate for the Sc^{3+}-induced doping shrinkage was proposed by Cimino, et al.[26] This issue will

also be discussed below.

The surface morphologies of the as-deposited CSO thin films were examined by SEM and

AFM. SEM surface images show that the as-deposited thin films on glass are densely packed with

a grained structure (Figure 4). At low doping levels, the films on glass have grains with rounded

shapes. As the doping levels increase to greater than 2.8 atom %, the grains of the films on glass

become triangular in shape, consistent with high in-plane order and with (111) planes parallel to

the surface, in agreement with the above XRD analysis. The thin films on glass exhibit a

root-mean-square (RMS) roughness ranging from 4.5 to 8.2 nm over a 25 μm^2 area (Figure 5A), as

determined by contact mode AFM. The average grain size of the films on the glass is 100-150 nm

(Figure 5A). Low doping level (< 2 atom %) films on MgO(100) are featureless by SEM, and their

surface morphology is found to be very smooth and uniform by AFM (Figure 5B). The

root-mean-square (RMS) roughness of the films on MgO(100) ranges from 1.6 to 1.9 nm at low

doping levels (< 2 atom %), indicating that the CSO thin films grown on MgO(100), with a nearly single-grained structure, are significantly smoother than CSO films grown on glass substrates.

1.3.3. Film Optical and Electrical Properties

The as-grown CSO films are pale-yellow but highly transparent. The color of the CSO films becomes lighter with increased Sc^{3+} doping as the band edge shifts to higher energies. CSO thin films with thicknesses of 180 nm on glass and 350 nm on MgO(100) exhibit an average transmittance at 550 nm of ≥ 80% (Figures 6A and 6B). As the Sc doping level increases, the band edges blue–shift dramatically, doubtless due to the Burstein-Moss (B-M) band-filling effect.[10] Band gap estimates were derived from the optical transmittance spectra by extrapolating the linear portion of the plot of $(\alpha h \nu)^2$ vs. $h\nu$ to $\alpha = 0$ (Figures 6C and 6D). The band gap increases from 2.7 eV to 3.4 eV with an increase in Sc^{3+} doping. Simultaneously, the plasma edge shifts to the blue due to the increased free carrier scattering with the increased levels of Sc doping.

All CSO thin films exhibit *n*-type conductivity as determined by negative Hall coefficients. The charge transport properties of the as-grown thin films as a function of Sc doping are shown in Figure 7. For undoped CdO thin films, carrier mobilities as high as 141 and 217 cm^2/V·s are achieved on glass and MgO(100), respectively, which are more than 5 × greater than those of commercial ITO films. With increased Sc doping, the carrier concentration increases from 2.3×10^{20} for undoped CdO thin films on glass to 6.7×10^{20} at ~5.0 atom % Sc doping. On

MgO(100) substrates, the carrier concentration increases from 1.9×10^{20} for pure CdO thin films to 18.7×0^{20} at ~5.0 atom % Sc doping. This indicates that most of the Sc^{3+} substitutes uniformly for Cd^{2+} in the lattice as an effective n-type dopant rather than forming a second phase. Beyond 5.0 atom % Sc doping, the carrier concentration does not increase with increasing Sc doping, suggesting that some Sc^{3+} may exist as interstitial ions or as free scandium oxide, which, however, is still below the XRD detection limit. The mobility, however, drops rapidly with increased Sc^{3+} doping. Compared to In-doped CdO on glass,[5,6] the present CSO thin films on glass exhibit lower carrier mobilities and concentrations, likely due to the lack of significant orbital hybridization between the Cd 5s conduction band and the Sc 4s states (see more below).

Thin films with conductivities of 6,000 S/cm and 18,100 S/cm on glass and MgO(100), are achieved at ~1.2% Sc doping on glass and 1.8% of Sc doping on MgO(100), respectively. Compared to films on glass, CSO films on MgO(100) at the same Sc doping level and similar grain sizes exhibit much greater carrier mobilities and carrier concentrations (Figure 7), arguing that the highly textured structure possesses fewer scattering centers and higher doping efficiency. When Sc^{3+} doping levels are greater than ~2.8 atom %, the carrier concentration plateaus and the mobilities decline precipitously. Although the lattice parameters are further compressed, the increased doping does not contribute additional free carriers. This explanation is consistent with the plasma edge trend: at the highest doping levels, further blue-shifting of the plasma edges is negligible.

Figure 7B shows the temperature dependence of CSO film charge transport properties

obtained from four-probe conductivity and Hall effect measurements for a 1.8% Sc-doped film on MgO (100), which achieves the highest conductivity of 18,100 S/cm at room temperature. In the low temperature region (<100 K), the mobility and conductivity are essentially independent of temperature, suggesting that neutral impurity scattering (NIS) and/or ionized impurity scattering (IIS) are dominant (the former mechanism is supported by the mobility vs. carrier concentration results of Figure 7).[15,26,27] In the high temperature range (>100 K), the mobility and conductivity decrease significantly with increasing temperature, reminiscent of metal-like character, and suggesting that lattice vibration scattering (LVS) has now become an important scattering contributor.[28,29,30a] In the present study, the highly textured epitaxial CSO thin films grown on MgO(100), having higher carrier concentrations and grain sizes similar to those grown in parallel on glass, possess significantly higher carrier mobilities, which is most likely attributable to a reduction in NIS caused by improved epitaxy-induced crystallinity.[15] The importance of grain boundary scattering (GBS) is an incompletely resolved mechanistic issue in most CdO-based TCOs. It has been argued that GBS is insignificant because the carrier mean-free-paths of highly degenerate TCOs are typically much smaller than the grain sizes of typical films.[26,28,30] Our recent microstructure-charge transport-optical reflectivity results on undoped MOCVD-derived CdO thin films also argue that GBS is not a dominant process, even in high-quality epitaxial CdO films with modest carrier concentrations and small grain sizes, 2×10^{20} cm^{-3} and ~100 nm, respectively.[15] However, it is conceivable that reduced large angle grain boundary scattering and better intergrain contact in the epitaxial thin films, due to the

highly ordered grain alignment, may contribute to some degree to the greater observed carrier mobilities.

1.3.4. Band Structure Calculations

The FLAPW total energy full structure optimization for CSO was performed at 12.5 atom % Sc doping. The lattice parameter, a, and the internal structure relaxation due to the Sc doping were first calculated. The smaller lattice parameter of CSO found at 12.5 atom % doping, $a = 4.63$ Å, than that of pure CdO (4.66 Å, obtained from a separate calculation) is found to be in agreement with the experimental findings discussed above. From similar band structure calculations for Ga-, Sc-, In- and Y-doped CdO to be discussed elsewhere,[12] we find that a smaller dopant ionic radius results in weaker Cd 5s – O 2p hybridization due to relaxation of the oxide anions around the dopant cations. Therefore, in the case of In^{3+} and Y^{3+}, whose ionic radii are relatively close to that of Cd^{2+}, the antibonding expansion mechanism is dominant, while Sc^{3+} has a sufficiently small ionic radius to weaken the s-p hybridization and, hence, to compress the lattice. In addition, the reduced ionic radius of Sc as well as the oxygen relaxation are clearly seen in the calculated FLAPW charge density distribution plot (Figure 8). Note here that we find negligible changes in the effective ionic radius of Cd for dopant concentrations as large as 12.5 % (Figure 8), so that the reduction from Cd^{2+} to Cd^{1+} as proposed by Cimino, et al,[26] seems unlikely.

The band structure of CSO at 12.5% Sc doping calculated within the sX-LDA method is shown in Figure 9. The prominent, highly dispersed single band, derived mainly from the 5s states

of Cd, crosses the Fermi level in the [100] (Δ), [110] (Σ) and [111] (Λ) directions. Similar electronic features were obtained[6] for In-doped CdO. However, in marked contrast to the case of In doping, the Sc 4s states in CSO are found to lie high up in the conduction band (at ~9.5 eV) and so do not hybridize with the Cd 5s states. On the other hand, the free-electron-like band is now separated away from Sc 3d states by a second band gap (Figure 9) which effectively decreases the dispersion of the s-type band. Indeed, we find that in CSO the width of the dispersed band (2.6 eV) is ~1 eV narrower than that in the In-doped CdO.[5b,6,12] Together with the lack of hybridization between Cd 5s and Sc 4s states, this convincingly explains the observed lower carrier mobilities in Sc-doped CdO as compared to the In-doped CdO materials. Finally, we find that the Sc doping results in a Burstein-Moss shift which significantly widens the optical transparency window, in agreement with the experimental results discussed above. As expected, the LDA is found to underestimate the band gap energies which determine optical transparency in the visible range, yielding 2.27, 2.89, and 2.92 eV in [100], [110], and [111] directions, respectively. Strikingly, the calculated sX-LDA band gap energies are found to be 3.02, 3.65 and 3.76 eV in [100], [110], and [111] directions, respectively – in good agreement with the present experimental optical band gap energy (3.4 eV).

1.4. CONCLUSIONS

Highly conductive and transparent CSO thin films have been grown on glass and

single-crystal MgO(100) substrates at 400 $^{\circ}$C by an MOCVD process. XRD data reveal that all of these as-deposited CSO films are phase-pure and highly crystalline, with features assignable to the cubic CdO-type crystal structure. CdO lattice dimensions are found to contract with the introduction of Sc^{3+}, in agreement with the FLAPW calculations. However, the observed lattice shrinkage is to some degree compensated by an expansion mechanism, which, based on our band structure calculations for Ga-, Sc-, In-, and Y-doped CdO, originates from the antibonding character of the conduction band formed from Cd 5s and O 2p states. Thin film conductivities as high as 6,000 S/cm are obtained on glass substrates at 1.2 % Sc doping. Compared to In-doped CdO, the CSO films on glass exhibit lower carrier mobilities and concentrations, due to the lack of energetically comparable Sc s states that can hybridize with the Cd 5s conduction band and the lower dispersion of this s-type band – as revealed by first-principles FLAPW electronic band structure calculations. CSO thin films on MgO(100) with a maximum conductivity of 18,100 S/cm are obtained at a Sc doping level of ~1.8 atom %, which is to date the most conductive transparent conducting oxide material grown by MOCVD. These epitaxial films grown on MgO(100) exhibit a biaxial, highly textured microstructure, leading to higher doping efficiency than on glass and with fewer scattering centers. This is likely responsible for the higher conductivity compared to the films on glass. All of these MOCVD-derived thin films exhibit good optical transparency, with an average transmittance $\geq$ 80% in the visible range. Sc doping widens the band gap from 2.7 to 3.4 eV via a Burstein-Moss band-filling shift, in agreement with our sX-LDA calculations. The high electrical conductivity and optical transparency render

MOCVD-derived CSO thin films attractive candidates for next-generation transparent electrodes for a variety of optoelectronic devices.
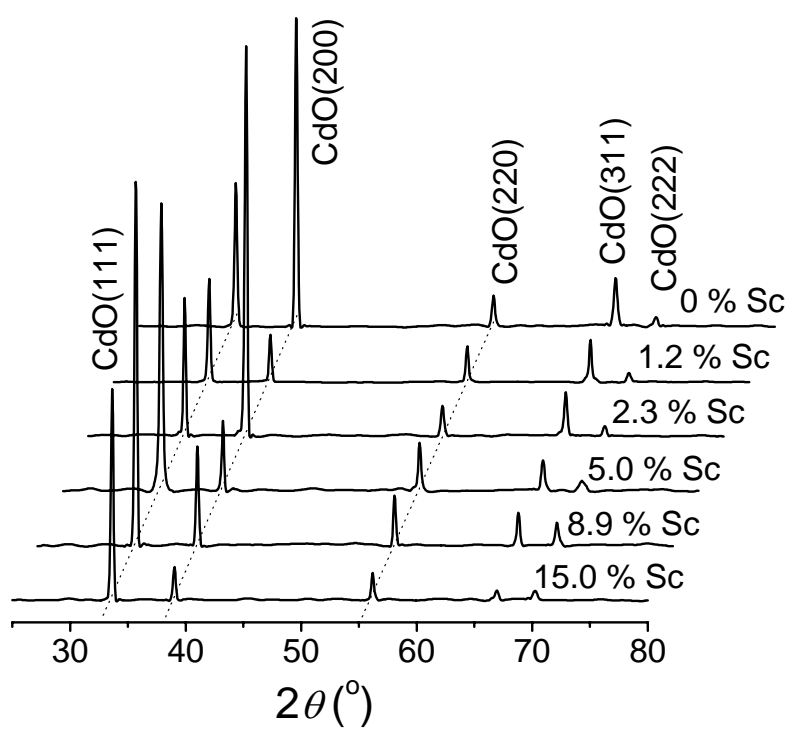
Figure 1.1. θ-2θ x-ray diffractograms of CSO thin films grown on glass at 400°C

by MOCVD as a function of Sc doping level (given in atom %)
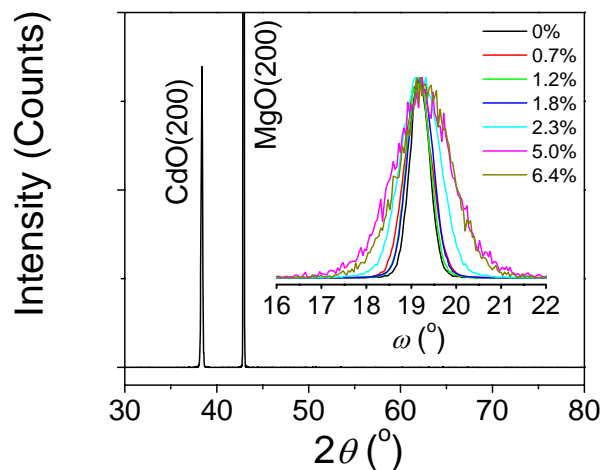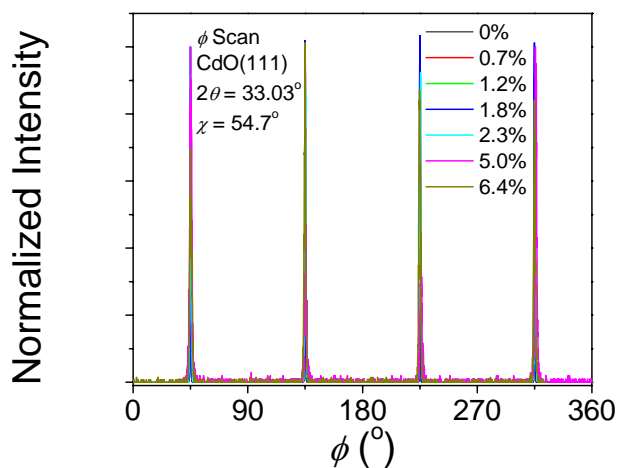
Figure 1.2. XRD texture analyses of CSO thin films grown on MgO(100) by MOCVD as a function of Sc doping level: A) θ-2θ x-ray diffractograms, (inset: rocking curves measured on the CdO(200) XRD peak); B) In-plane ϕ scans measured on the CdO(111) XRD peak with χ = 54.7. Sc doping level is given in atom %
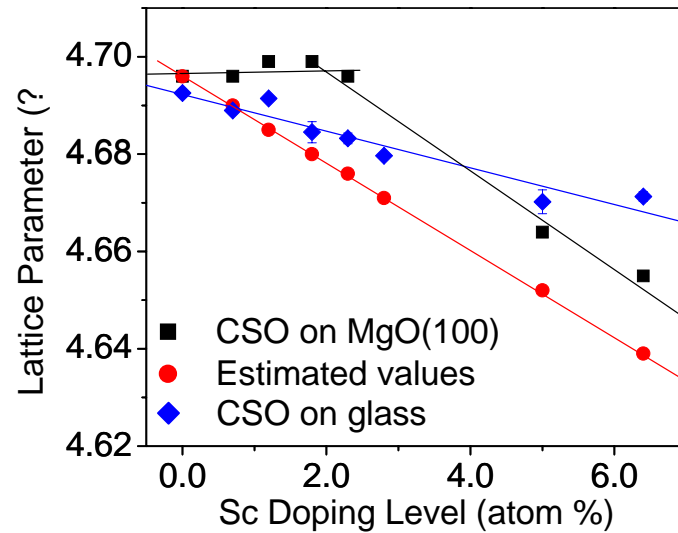
Figure 1.3. Lattice parameter changes as a function of Sc doping level for CSO thin films. Estimated Vegard's law lattice parameter values are calculated according to the following equation:

$$a_{estimated} = a_{CdO} \times \frac{r_{Cd} \times Cd\% + r_{Sc} \times Sc\%}{r_{Cd}}$$

Where a_{CdO} is the CdO lattice parameter (4.696 Å), r_{Cd} is the six-coordinate ionic radius of Cd, Cd% is the Cd atomic percentage, r_{Sc} is the six-coordinate ionic radius of Sc, and Sc% is the Sc atomic percentage (Cd% +Sc% = 1). Lines through the data points are drawn as a guide to the eye
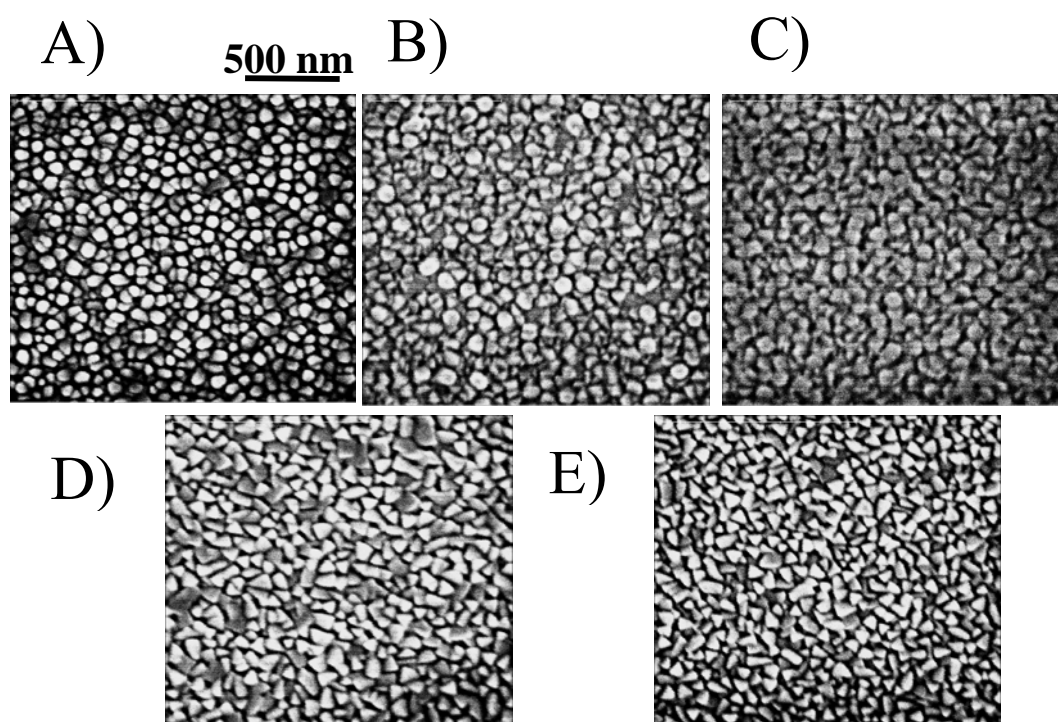
Figure 1.4. SEM images of CSO thin films on glass as a function of Sc doping level (given in atom %): A) 0.0 %; B) 1.2 %; C) 2.3 %; D) 5.0 %; E) 6.4 %

A)

B)
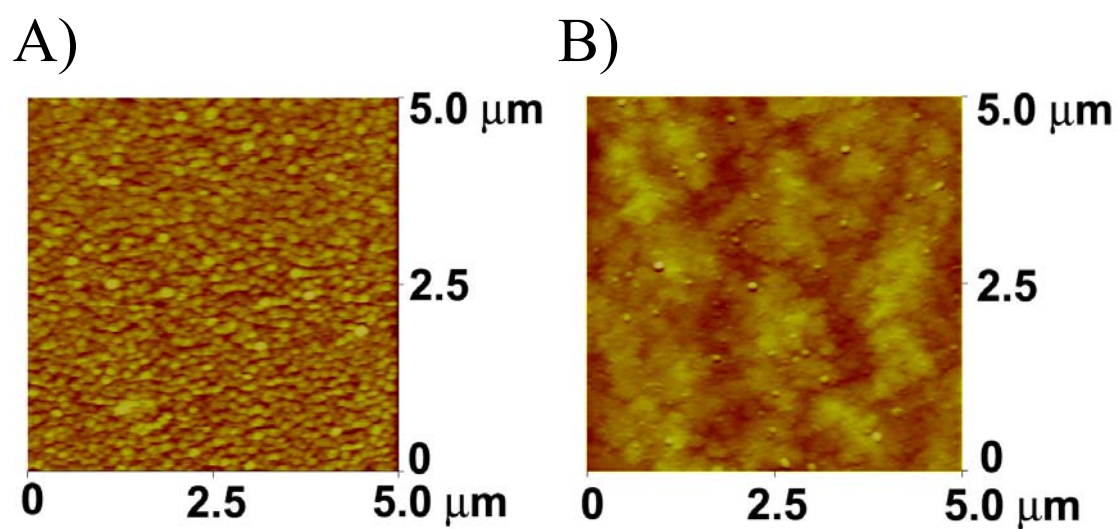
Figure 1.5.   AFM images of 2.3 atom % Sc-doped CdO thin films: A) on glass;

B) on MgO(100)
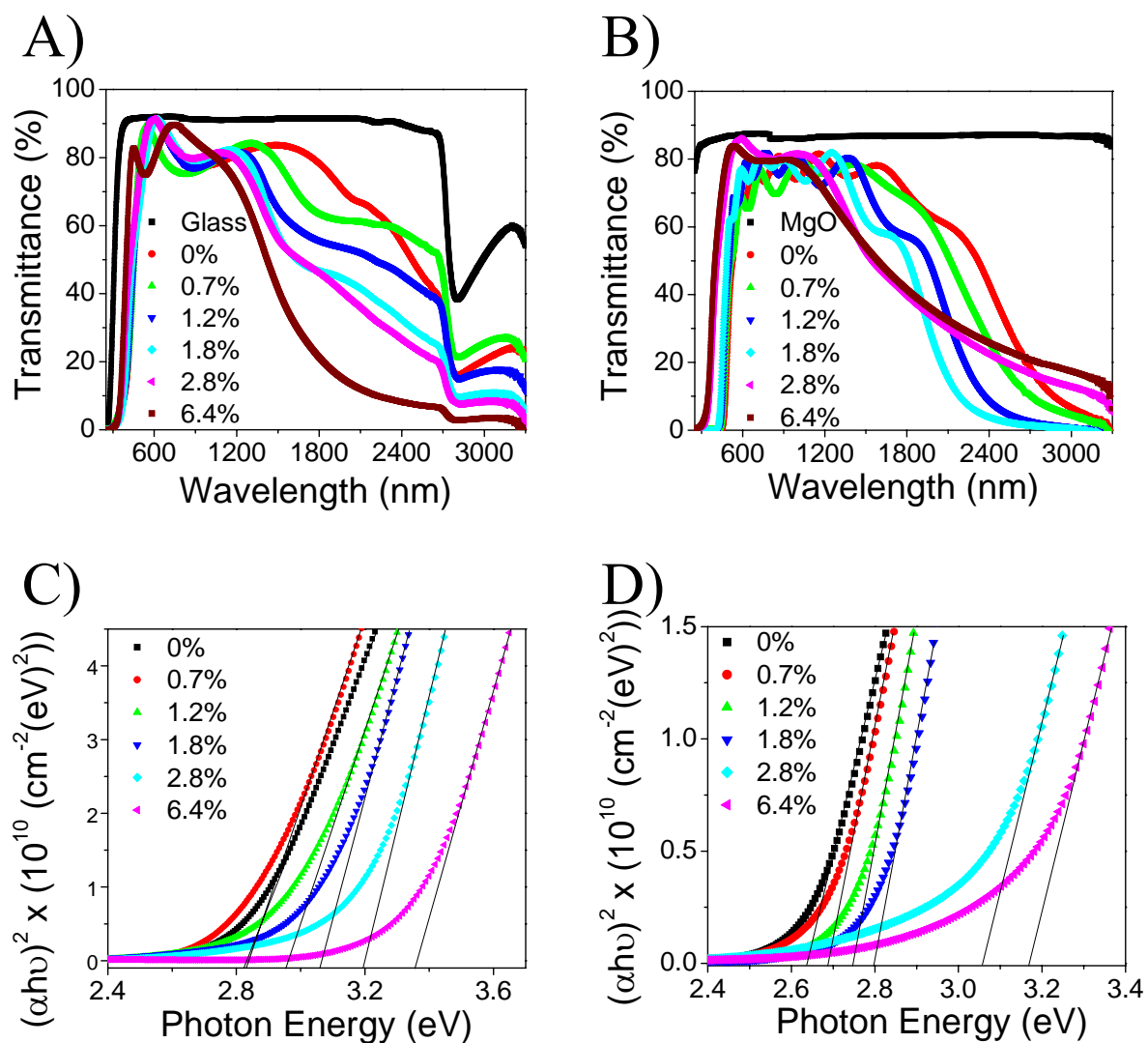
Figure 1.6. Optical characterization of CSO thin films as a function of Sc doping: A) Optical transmission spectra of CSO on glass; B) Optical transmission spectra of CSO on MgO(100); C) Band gap estimations of CSO on glass; D) Band gap estimations of CSO on MgO (100). Sc doping levels are given in atom %
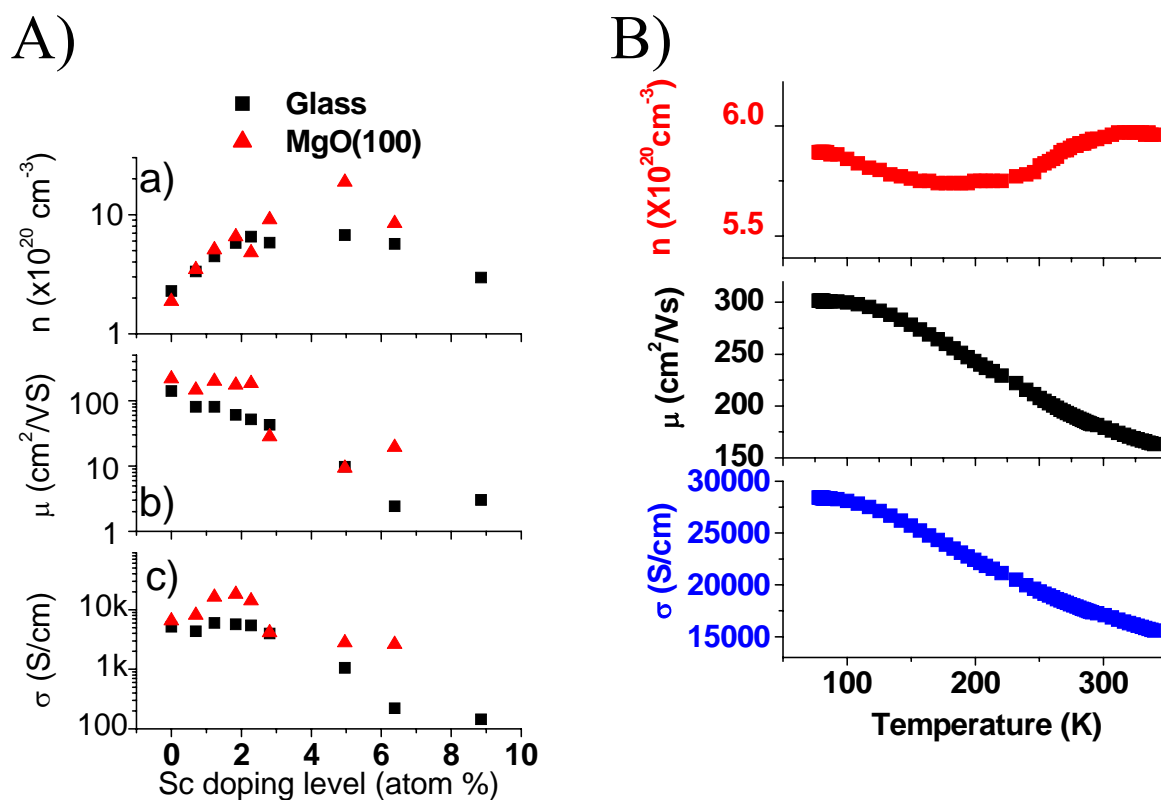
Figure 1.7. A) Room temperature four-probe charge transport measurements for CSO thin films on glass and MgO(100): a) carrier concentration, b) mobility, c) conductivity. B) Variable temperature conductivity and Hall effect measurements for 1.8% CSO thin film on MgO(100)
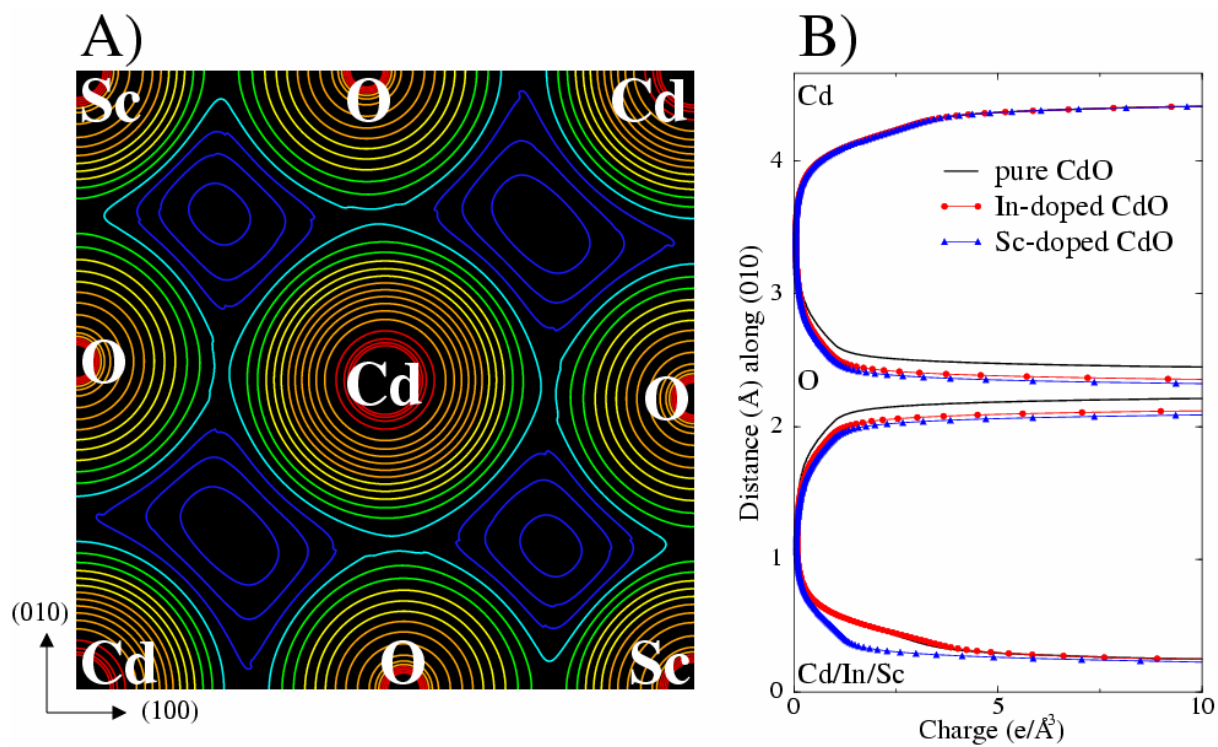
Figure 1.8. A) Calculated charge density distribution for 12.5 atom % Sc-doped CdO in the *ab* plane. B) Comparison of the charge density along (010) for pure and Sc (or In) doped cases. Results for pure CdO and 12.5 atom % In-doped CdO obtained from additional calculations
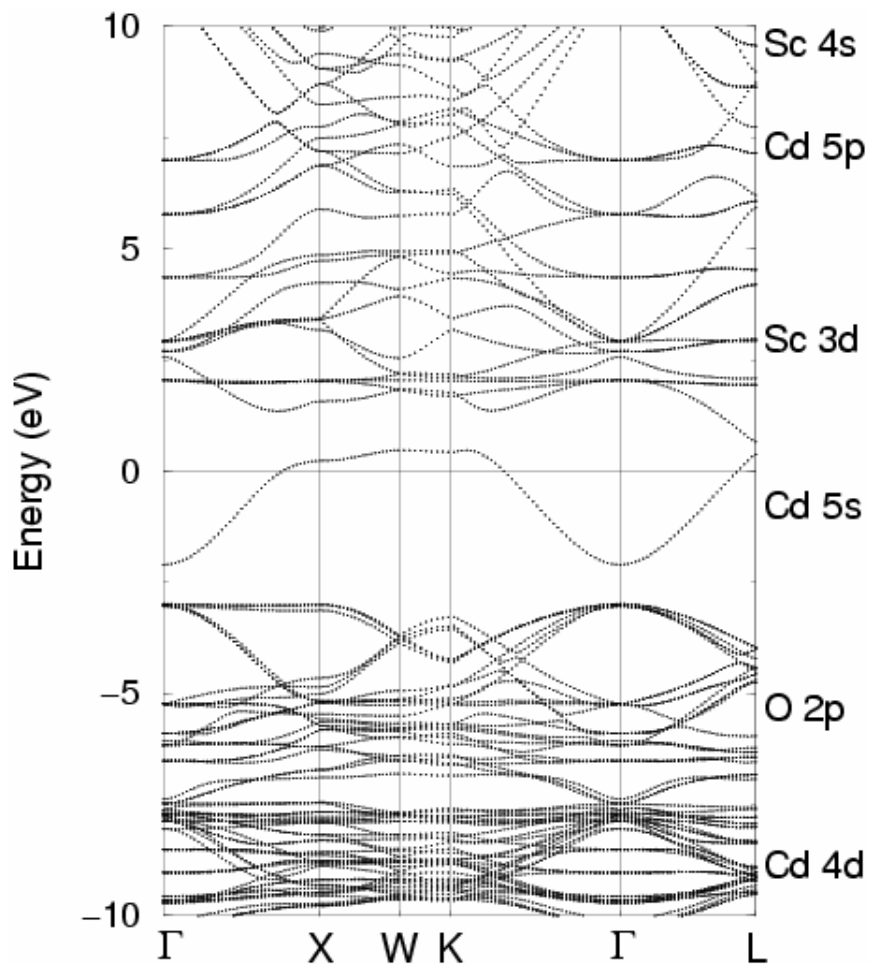
Figure 1.9. Calculated sX-LDA band structure for 12.5 atom % Sc-doped CdO along the high symmetry directions in the Brillouin zone. The origin of the energy is taken at the Fermi level; the electronic states are labeled

CHAPTER TWO

CdO as the Archetypical Transparent Conducting Oxide. Systematics of Dopant Ionic Radius and Electronic Structure Effects on Charge Transport and Band Structure

2.1. INTRODUCTION

Transparent conducting oxides (TCOs) have attracted increasing attention over the last two decades as critical components of flat panel displays, solar cells, and low-emissivity windows.[1,2] At present, tin-doped indium oxide (ITO), with a typical electrical conductivity of $3\text{-}5\times10^3$ S/cm and 85-90 % transparency in the visible region, is employed on a huge scale as a transparent electrode in many display technologies. However, there are several drawbacks that cloud its future applicability: (1) the limited availability and high cost of indium; (2) the relatively low conductivity (not suitable for large-area displays); (3) significant optical absorption in the blue-green region (not suitable for many full-color displays); and (4) chemical instability in certain device structures (e.g., corrosion in organic light-emitting diode (OLED) devices). In view of these issues, intense research has been focused on understanding fundamental TCO crystal structure–film microstructure-electronic structure–charge transport–optical transparency relationships and on searching for ITO alternatives that are less expensive and possess comparable or higher conductivity and/or wider optical transparency windows.[1,3]

Recently, CdO-based TCOs have been of interest due to their relatively simple crystal structures, high carrier mobilities, and sometimes nearly metallic conductivities.[1,4,5,6,7] Epitaxial growth of Sn-doped CdO thin films on MgO(111) by pulsed laser deposition (PLD) has achieved impressive mobilities and conductivities as high as 607 $cm^2/V{\cdot}s$ and 42,000 S/cm, respectively,

rendering them the most conductive TCO thin films with the highest carrier mobility discovered to date.[6] In addition, Cd_2SnO_4, $CdIn_2O_4$, and CdO-ZnO thin films have been fabricated with impressive conductivities and good optical transparencies for photovoltaic applications.[2] Although the band gap of bulk CdO is only 2.3 eV,[8] leading to relatively poor optical transparency in the short wavelength range, aliovalent metal doping offers the possibility of tuning the electronic structure and the optical band gap through a carrier density dependent Burstein-Moss shift.[5,9] For all these reasons, CdO with a simple cubic rock-salt crystal structure and small conduction electron effective mass represents an ideal model material in which to study the effects of doping on TCO band structure, crystal chemistry, and charge transport.

Various deposition techniques such as reactive evaporation,[10] solution growth,[11] spray pyrolysis,[12] sputtering,[13] PLD,[6] and MOCVD [5,7,14] have been employed to grow CdO and CdO-based thin films. For device fabrication, chemical vapor deposition offers many attractive features such as in-situ growth under a variety of atmospheres, low cost equipment, amenability to large area coverage with high throughput, conformal coverage, easy control of growth chemistry, and the possibility of creating metastable phases.[15] In previous work from this laboratory, undoped and doped CdO thin films were successfully grown by MOCVD using optimized Cd precursors.[5] In-doped CdO thin films grown on glass by MOCVD exibit conductivities as high as 16,800 S/cm.[5b] In addition, recent studies of Sc-doped CdO thin films reveal that Sc doping significantly contracts the CdO lattice parameter due to its smaller six-coordinate ionic radius, 0.89 Å, vs. 1.09 Å for Cd^{2+}.[16]   Compared to In-doped CdO films,

Sc-doped CdO films exhibit appreciably lower carrier mobilities and concentrations due to the lack of hybridization between the Cd 5s conduction band and Sc 4s states.[5e] Yttrium(III) with a six-coordinate ionic radius of 1.04 Å, which is very close to that of Cd, 1.09 Å, has been suggested as an efficient *n*-type dopant in the case of bulk CdO materials.[17,18] It has been reported that for bulk CdO, light Y doping (1-1.5 atom %) increases the carrier density and thus results in lower resistivities in CYO and Cd_2SnO_4 with respect to the undoped analogues. However, CYO thin films have never been prepared and studied.

To further investigate dopant ion size and electronic structure effects on the charge transport properties and electronic band structures of CdO-based TCOs, a series of Y-doped CdO (CYO) thin films has been grown on both amorphous glass and single-crystal MgO(100) substrates by MOCVD, and their electrical and optical properties characterized and compared with those of In- and Sc-doped CdO thin films. It will be seen that phase-pure CYO thin films with conductivities of 8,540 S/cm and 17,800 S/cm on glass and MgO(100), respectively, are obtained at an optimum Y-doping level of 1.2~1.3 %. To better understand these trends, we report first-principles full potential linear augmented plane wave (FLAPW) electronic band structure calculations within the screened exchange local density approximation (sX-LDA) to systematically compare the structure, electronic, and optical properties of the In-, Sc-, and Y-doped CdO series. Finally, clues for optimizing TCO optical and electrical properties are elucidated from these experimental and theoretical results.

2.2. EXPERIMENTAL

2.2.1. MOCVD Precursors and Thin Film Growth

CdO-based thin film growth was carried out in the previously described horizontal, cold-wall MOCVD reactor.[19] The volatile metal-organic Cd precursor $Cd(hfa)_2(N,N'-DE-N,N'-DMEDA)$(**1**) (hfa = hexafluoro-acetylacetonate, N,N-DE-N',N'-DMEDA = N,N-diethyl-N',N'-dimethyl-ethyldnediamine), was prepared from high-purity $Cd(NO_3)_2 \cdot 4H_2O$ (99.999 %, Aldrich) as described previously [5d] and was triply vacuum-sublimed. $Y(dpm)_3$ (**2**) (dpm = dipivaloymethanate) was prepared from $Y(NO_3)_3 \cdot 4H_2O$ (99.999 %, Aldrich) by a literature procedure.[20] For pure CdO and Y-doped CdO thin film growth, precursor temperature/Ar carrier gas flow rates were optimized by experimentation at: $Cd(hfa)_2(N,N-DE-N',N'-DMEDA)$, 85 ^{o}C / 18 sccm; $Y(dpm)_3$, 90-105 °C / 10 sccm. The O_2 oxidizing gas was introduced at 400 sccm by bubbling through distilled water. A system operating pressure of 4.2±0.1 Torr and a substrate temperature of 410 °C established by experimentation were maintained during the thin film deposition. Corning 1737F glass and polished MgO(100) substrates were purchased from Precision Glass and Optics and MTI Corporation, respectively. Both the glass and the MgO(100) substrate surfaces were cleaned with acetone prior to the film deposition, and placed side-by-side on the SiC-coated MOCVD susceptor for simultaneous growth experiments.

2.2.2. Film Physical Characterization Measurements

Composition analyses were carried out using inductively coupled plasma atomic emission spectrometry (ICP-AES). Optical transparency measurements were carried out with a Cary 500 UV-Vis-NIR spectrophotometer. Film thicknesses were measured with a Tencor P-10 profilometer after etching a step in the film using 5 % HCl solution. X-ray diffraction θ-2θ scans of CdO films on glass were obtained with a Rigaku DMAX-A powder diffractometer using Ni-filtered Cu K_α radiation, and were calibrated in situ with polycrystalline silicon. Rocking curves and ϕ scans of the epitaxial thin films on MgO(100) substrates were obtained on a home-built Rigaku four-circle diffractometer with detector-selected Cu K_α radiation. Film surface morphology was examined using a Digital Instruments Nanoscope III atomic force microscope (AFM) operating in the contact mode. Film microstructure was imaged on a Hitachi S4500 FE scanning electron microscope (SEM). Four-probe charge transport data were collected on Bio-Rad HL5500 Hall-effect measurement system at ambient temperature. Variable-temperature Hall effect and 4-probe conductivity data were collected between 77 and 340 K using instrumentation described previously.[21]

2.2.3. Theoretical Methods

First-principles electronic band structure calculations on 12.5 atom % In-, Y-, and Sc-doped CdO were performed using the highly precise all-electron full-potential linearized augmented plane wave (FLAPW) method [22] that has no shape approximation for the potential

and charge density. The exchange-correlation energies were treated via the local density approximation (LDA). Cut-offs of the plane-wave basis (14.4 Ry) and potential representation (81.0 Ry), and expansion in terms of spherical harmonics with $l \leq 8$ inside the muffin-tin spheres were used. The equilibrium relaxed geometries of the crystal structures were determined via total energy and atomic forces minimization for the lattice parameter a and the internal atomic positions. Furthermore, to determine accurately the excited state band structures of In-, Y-, and Sc-doped CdO, we employed the self-consistent screened-exchange local density approximation (sX-LDA) [23] which is known to provide a considerably improved description of the optical properties as compared to the LDA.[22] Cut-off parameters of 10.24 Ry in the wave vectors and $l \leq$ 3 inside the muffin-tin spheres were used. Summations over the Brillouin zone were carried out using 10 special k points in the irreducible wedge.

2.3. RESULTS AND DISCUSSION

We first describe Y-doped CdO (CYO) thin film growth by an efficient MOCVD process. Then, CYO film composition, morphology, microstructure, and epitaxy are characterized as a function of doping level using a broad array of complementary physical techniques. In addition, film optical and electrical properties are investigated and compared with those of the In-, and Sc-doped CdO analogues grown by the same technique. Finally, first-principles full potential linear augmented plane wave (FLAPW) electronic band structure calculations within the

screened exchange local density approximation (sX-LDA) are carried out to compare the structure, electronic, and optical properties of the In-, Sc-, and Y-doped CdO systems.

2.3.1. Film Growth

A series of conductive CYO thin films was grown on 1737F glass and single crystal MgO(100) at 410 °C and under a 400 sccm O_2 flow rate for 2 hr by MOCVD. The growth rates of the film are ~1.5 nm/min on glass, and ~ 3.0 nm/min on MgO(100), respectively, which are similar to those established for In-,[24] and Sc-doped CdO.[5e] The Y doping percentage can be varied from 0 % to 4.2 % by varying the Y precursor reservoir temperature.

2.3.2. Film Composition, Morphology, Microstructure, and Epitaxy

X-ray diffraction θ-2θ scans were carried out from $2\theta = 25^o$ to 80°. Figure 1A shows XRD data as a function of Y doping level. As can be seen from the figure, all of the films with Y doping levels up to 4.2 % are phase-pure, with a highly crystalline fcc CdO structure. No Y_2O_3 or other phases are detected by XRD, indicating Y^{3+} substitutes for the Cd^{2+} in the lattice instead of forming a new phase. This is further evidenced by the fact that the carrier concentration increases progressively with increased Y doping level (see below). It is clear that the presently determined solubility of Y in CdO thin films, ~ 4.2 %, is somewhat greater than possible in the CdO bulk material, 3.5%.[17,18] Furthermore, note that at low doping levels (Y $\leq$ 2.4 %), films on glass grow preferentially with the (*h00*) planes parallel to the surface; while at higher doping

levels (Y > 2.4 %), (111) reflections dominate. At present, the reason for the change of preferred

growth orientation is not immediately evident.

Using polycrystalline silicon as an internal calibration reference, the precise lattice

parameters of the MOCVD-derived CYO thins films on glass were determined (Figure 1B). It is

found that the lattice parameters are essentially invariant with increasing Y doping level. Note

that with the introduction of Y, the lattice dimensions are not expected to change greatly or

should shrink slightly, if Y^{3+} ions replace Cd^{2+} in the lattice instead of forming a new phase,

since six-coordinate Y^{3+} with an ionic radius of 1.04 Å is slightly smaller than Cd^{2+} (1.09 Å).[16]

In addition, the Y^{3+}-induced contraction may be counteracted by an antibonding expansion

mechanism (see theoretical discussion below). On the other hand, In^{3+} and Sc^{3+} dopants, having

smaller six-coordinate ionic radii of 0.94 and 0.89 Å, respectively, shrink the lattice

monotonically with increases in doping level.[5b,e] However, the shrinkages caused by progressive

In and Sc doping are not as large as estimated from simple Vegard's law considerations, likely

due to compensation by the antibonding character of the conduction band formed from Cd 5s and

O 2p states (see theoretical discussion).[5e,24,25]

In contrast to the above results for growth on amorphous glass substrates, all CYO thin

films grown on MgO(100) exhibit a highly (200) textured microstructure at all doping levels less

than 4.2 %. The texture of the thin films is shown in Figure 2. As can be seen from Figure 2A,

the rocking curves of the films show good out-of-plane alignment. The

full-width-at-half-maximum (FWHM) increases from 0.5^{o} for pure CdO films to 1.0^{o} at 3.3 atom

% Y doping, and to 3.5° at 4.2 atom % Y-doping, indicating that the crystallinity decreases with the increase in Y doping. The in-plane orientation was investigated by ϕ scans of the CdO (111) reflection at $\chi = 54.7°$, and data are shown in Figure 2B. The clear four-fold rotational symmetry of the CdO (111) reflections together with the small FWHMs (0.8° for pure CdO, 1.2° for CYO at 3.3 % Y doping) reveal excellent in-plane orientation of the films. The orientation relations between the CYO thin films and the MgO(100) substrates is therefore CdO(100)‖MgO(100).

SEM surface images in Figure 3 show that the as-deposited CYO thin films grown on glass are densely packed with a heavily grained structure. At low Y doping levels ($\leq$ 1.5 %), films on glass and MgO(100) are all very uniform with rounded grains in plan view. With the Y doping increased to 2.4 and 4.2 %, the grains of the films on glass are largely triangular in shape, suggesting that the (111) planes are parallel to the surface, which agrees well with the XRD analysis alluded to above. Furthermore, the SEM images reveal that the grain size decreases with increased Y-doping level, similar to the AFM images discussed below. As for the epitaxial films on MgO(100), the films with doping levels $\leq$ 1.5 % are featureless (single-grained) under SEM and found to be very smooth and uniform under AFM. As the Y doping level is increased to $\geq$ 2.4 %, a grained structure is clearly visible. Contact-mode AFM images of the CYO thin films are shown in Figure 4. AFM images reveal that all the thin films on glass are uniform and smooth, with root-mean-square (RMS) roughnesses of 5-7 nm over a 5 μm × 5 μm area (Figures 4A, 4C, and 4E). Similar to the SEM observations, the AFM images show that the grain size of the films decreases with increasing Y doping levels. As for the CYO films grown on MgO(100),

the surface roughness of the films is strongly dependent on the doping level. The RMS roughness

is found to be 1~2 nm when the doping level is $\leq$ 1.5 % (Fig. 4B, 4D), and 4~7 nm when the

doping level is >1.5 % (Fig. 4F).

2.3.3. Film Optical and Electrical Properties

All the as-grown CdO films are light-yellow to the eye but highly transparent. The color

becomes lighter with increased Y-doping as the band edge shifts to higher energies. Optical

transmission spectra of CYO thin films grown on glass are shown in Figure 5A. For CYO thin

films with thicknesses of ~200 nm, the average transmittance at 550 nm is ~ 85 %. With an

increase of Y doping level, the band edges are found to be dramatically blue–shifted, doubtless

due to the Burstein-Moss effect.[9] Simultaneously, the plasma edges shift to the blue, owing to the

increase of free carrier concentration with increased doping level. Band gap estimates were

derived from the optical transmission spectra by extrapolating the linear portion of the plot of

$(\alpha h\nu)^2$ vs. $h\nu$ to $\alpha = 0$ (Figure 5B). It is found that the band gap increases from 2.86 eV to 3.27

eV with an increase in Y doping from 0 % to 4.2 %.

As in other ailovalent metal-doped CdO materials investigated to date, all of the Y-doped

CdO film samples exhibit n-type conductivity as determined by negative Hall coefficients.

Figure 6 shows the temperature dependence of thin film charge transport properties for a 1.3

atom % CYO film on MgO (100), which achieves the highest observed conductivity of 17,800

S/cm. Similar to In- and Sc-doped CdO,[5b,e] the mobilities and conductivities of CYO films are

independent of temperature in the low temperature region (<100 K), suggesting that neutral impurity scattering (NIS) and /or ionized impurity scattering (IIS) processes are dominant (see below). In the high temperature region (>100 K), the mobility and conductivity decrease with increasing temperature, suggesting that lattice vibration scattering (LVS), which is temperature-dependent, has now become an important scattering contributor.

Electrical conductivity, mobility, and carrier concentration data for as-grown CdO thin films as a function of Y, In, and Sc doping levels are compared in Figure 7. For the present Y-doped CdO films, with the increase of Y doping, the carrier concentration increases from 2.3×10^{20} cm^{-3} for pure CdO thin films on glass to 7.0×10^{20} cm^{-3} at ~2.4 % Y doping. The mobility, however, drops precipitously with increased Y doping. It is clear from these data that Y^{3+} ions behave as effective dopants by replacing Cd^{2+} sites in the lattice and donating electrons to act as charge carriers. However, at doping levels greater than 2.4 %, the carrier density plateaus and the mobilities decline substantially, indicating that some of the Y dopant sites may not readily be ionized and/or do not contribute to the mobile charge carriers. In addition, excess Y doping appears to degrade the thin film crystallinity and increase carrier scattering, thereby decreasing carrier mobility and conductivity. Compared with In and Sc doping, much less Y can be effectively doped into the CdO lattice. Thin films with maximum conductivities of 8,540 S/cm and 17,800 S/cm on glass and MgO(100), respectively, are obtained at 1.2~1.3 % Y doping. Compared with films on glass, CYO films on MgO(100), at the same doping level, exhibit similar doping level-dependent trends but exhibit much greater carrier concentrations and

mobilities (Figure 7), indicating that the epitaxial films possess fewer scattering centers and higher doping efficiency due to their highly textured microstructure/enhanced crystalline perfection, similar to behavior found for epitaxial CdO on MgO(100)[5d] and epitaxial ITO on single-crystal YSZ.[26] In addition, the comparison of charge transport properties for In-, Y-, and Sc-doped CdO given in Figure 7 shows that the carrier mobilities and doping efficiencies decrease in the order In > Y > Sc.

2.3.4 Band Structure Calculations

The total energy FLAPW method was used to carry out full optimization of the CYO crystal structure (both the lattice and internal parameters were optimized) at 12.5 atom % Y doping. We find that the CYO lattice parameter, $a = 4.67$ Å, is slightly larger than that of pure CdO (4.66 Å, as obtained from a separate calculation), despite the fact that the six-coordinate ionic radius of Y^{3+} (1.04 Å) is somewhat smaller than that of Cd^{2+} (1.09 Å). This finding can be explained by comparison of the calculated structural and electronic properties of In-, Y-, and Sc-doped CdO. In Table 1, we present the LDA-optimized lattice parameters and relaxed distances between the Cd or X (X = In, Y, or Sc) atom and its nearest O neighbors, D_{Cd-O} and D_{X-O}, for In-, Y-, and Sc-doped CdO. It can be seen that the calculated change in the lattice parameter for different dopants correlates well with their ionic radii, namely, Y^{3+} (1.04 Å) > In^{3+} (0.94 Å) > Sc^{3+} (0.89 Å). Furthermore, it is found that smaller dopant ionic radii result in weaker Cd 5s – O 2p hybridization due to relaxation of the oxide anions around the dopant cations. Therefore, any

shrinkage in the lattice parameter due to the larger Y^{3+} ion is well compensated by the aforementioned antibonding expansion mechanism, in contrast to Sc-doped CdO where the lattice is significantly compressed due to the very much smaller ionic radius of Sc^{3+}, hence again inducing diminished s-p hybridization between the Cd 5s and O 2p orbitals. These results are in good agreement with the experimental findings reported above and with previous structural results for the In-, and Y-doped CdO bulk materials.[17,27]

The band structure of CYO at 12.5 atom % Y doping calculated within the sX-LDA formalism is shown in Figure 8. Despite a rather small (indirect) band gap of ~ 1eV in pure CdO,[5c] the Y doping results in a Burstein-Moss shift which significantly widens the optical transparency window so that the energies of the intense inter-band transitions from the valence band are above the visible range in energy: the calculated sX-LDA band gap energies, E_g, (cf., Table 1) which determine the optical transparency of CYO are found to be 3.38, 4.04, and 4.17 eV in the [100], [110], and [111] directions, respectively. The minimum band gap value is in good agreement with the present experimental result, 3.27 eV. As expected, LDA alone is found to underestimate the band gap energies, yielding 2.51, 3.13, and 3.17 eV in the [100], [110], and [111] directions, respectively. We next compare the sX-LDA results for CYO with those for In- and Sc-doped CdO obtained at the same doping level of 12.5 atom %. In both cases, smaller band gap energies are found, namely, 3.03, 3.68, and 3.83 eV for In doping and 3.02, 3.65, and 3.76 eV for Sc doping in [100], [110], and [111] directions, respectively. This result correlates well with the larger calculated distances between the Cd atom and its neighboring O atoms in

In-(2.42 Å) and Sc-(2.45 Å) doped CdO as compared to those in CYO (2.39 Å). Thus, we conclude that a larger ionic radius dopant ion results in a larger optical band gap. More detailed investigations of the optical properties of the In-, Y-, and Sc- doped CdO, including the calculations of the transition matrix elements, will be published elsewhere.[25]

Similar to the cases of In- and Sc- doped CdO,[5b,c,e] the highly dispersed CYO single conduction band, derived mainly from the 5s states of Cd, crosses the Fermi level in the [100] (Δ), [110] (Λ) and [111] (Σ) directions (cf., Figure 8). However, in marked contrast to the case of In doping, the Y 5s and Sc 4s states are found to lie high in the conduction band (at ~ 8.0 and ~9.5 eV, respectively) and thus do not hybridize with the Cd 5s states. Therefore, the uniform electronic charge density distribution associated with the energy-compatible s-orbital of the In ion, is not possible in the Y and Sc cases where the d-orbitals of the dopant ions hybridize only with the p-orbitals of the nearest oxygen neighbors, cf. Figure 9. Consequently, we find that the relative contributions from the oxygen neighbors of the dopant ions to the conduction band, calculated within the energy window from 0.027 eV below the Fermi level, decrease significantly in the order In > Y > Sc (namely, 24 %, 22 %, and 12 % for the In-, Y-, and Sc-doped CdO, respectively), resulting in charge redistribution and its localization on the Cd ions which contribute 38 %, 39 %, and 48 % for the In-, Y-, and Sc-doped CdO, respectively. A comparison of the dispersion of the free-electron-like band for In-, Y-, and Sc-doped CdO, given in Figure 10, shows that the width of the band, ΔE (Table 1), significantly narrows in the order In > Y > Sc. This can be explained by the fact that the width of the dispersed band is strongly

affected by the presence of the Y 4d or Sc 3d states near the bottom of the conduction band

which lies at 3.4 eV and at 2.0 eV for Y- and Sc-doped CdO, respectively, in contrast to the In

case, where the 4d states are fully occupied and lie at −15 eV. Importantly, this dependence of

the band dispersion on the dopant identity suggests a decrease in the conductivity, σ, for the

above sequence. The conductivity can be expressed as in equation (1):

$$\sigma(\varepsilon) = e^2 \sum_{k} N(\varepsilon) v_k^2(\varepsilon) \tau(\varepsilon) \qquad (1)$$

where e = the electron charge, k = the wave vector, ε = the band energy, $N(\varepsilon)$ = the density of

states, $v_k(\varepsilon)$ = the group velocity, and $\tau(\varepsilon)$ = the relaxation time. Assuming $\tau(\varepsilon)$ to be similar for

Y-, In-, and Sc-doped CdO, we can calculate the electron velocities, v, at the Fermi level in the

(Δ) [100], (Λ) [110], and (Σ) [111] directions (Table 1). It is found that despite the increase in the

density of states at the Fermi level, $N(E_F)$ (Table 1), associated with the lower dispersion of the

single band, the electron velocities decrease significantly in the order In > Y > Sc, leading to a

pronounced decrease of the conductivity for this sequence. These findings are in excellent

agreement with experimental observations on the carrier mobility and conductivity reported

above and in previous studies.[5e] Finally, note that for all dopants considered, the largest velocity

is in the [100] (Δ) direction, while considerably smaller values are obtained for the [110] (Λ) and

[111] (Σ) directions.

2.4. CONCLUSIONS

Highly conductive and transparent CYO thin films have been grown on glass and single crystal MgO(100) substrates at 410 ^{o}C by low pressure MOCVD. The as-deposited CYO thin films exhibit good optical transparency, with an average transmittance of 85 % in the visible region. As in the cases of In and Sc doping, Y doping significantly increases the electrical conductivity and widens the optical band gap. Thin films with maximum conductivities of 8,540 S/cm and 17,800 S/cm on glass and MgO(100), respectively, are obtained at a Y doping level of 1.2~1.3 %. Y doping widens the band gap from 2.86 to 3.27 eV via a Burstein-Moss (B-M) shift. Epitaxial films grown on MgO(100) also exhibit a biaxial, highly textured microstructure, leading to higher doping efficiency and fewer scattering centers, which is suggested to be responsible for the higher conductivity vs. the films on glass. Both experimental and theoretical results reveal that dopant ion size and electronic structure have a significant influence on the CdO-based TCO crystal and band structures, as well as on the optical and electrical properties. First, In^{3+} (0.94 Å) and Sc^{3+}(0.89 Å), with smaller ion sizes than that of Cd^{2+}(1.09 Å), shrink the lattice parameters; while Y(1.04 Å), with similar ion size to that of Cd^{2+}, does not significantly alter the lattice parameter.   Second, in marked contrast to In-doped CdO, in the cases of Y and Sc doping, the Cd 5s states do not hybridize significantly with Y 5s and Sc 4s states, respectively. Third, the presence of the "d states" of Y and Sc significantly affects the dispersion of the single band which crosses the Fermi level, resulting in lower mobility as compared to In-doped CdO,

which agrees well with experimental observation.

Based on the results of present studies, it can be seen that CdO-based TCO films generally exhibit higher carrier mobility than that of In_2O_3-, ZnO-, and SnO_2-based TCO materials, which can be ascribed to CdO's simple cubic crystal structure, and broadly dispersed, free electron-like Cd 5s-based conduction band. In the doping studies, it is found that the smaller the dopant size, the higher the dopant solubility in the CdO matrix. However, the doping efficiency is strongly dependent on the degree of orbital hybridization between the dopant orbital and Cd 5s states. Based on the calculation results,[25] we find that dopant ions whose s-orbital states are empty and close to the Cd 5s state in energy, such as Sn^{4+} and Sb^{5+}, should be more effective than those with empty d orbitals, such as Zr^{4+} and Nb^{5+}. These implications should be applicable to other doped TCO materials as well and are currently under investigation. In conclusion, we find that dopant ion size and electronic structure have substantial influence on the CdO crystal and band structure, especially on the energetic position and width of the highly dispersed conduction band, which provide necessary conditions for creating transparent conducting behavior with doping.

Dopant	In	Y	Sc
a, Å	4.66	4.67	4.63
D_{X-O}, Å	2.24	2.28	2.18
D_{Cd-O}, Å	2.42	2.39	2.45
$E_g(\Delta)$, eV	3.03	3.38	3.02
$E_g(\Lambda)$, eV	3.68	4.04	3.65
$E_g(\Sigma)$, eV	3.83	4.17	3.76
ΔE, eV	3.91	3.36	2.57
$v(\Delta)$, $\times 10^5$ m/s	0.42	0.36	0.19
$v(\Lambda)$, $\times 10^5$ m/s	0.23	0.21	0.17
$v(\Sigma)$, $\times 10^5$ m/s	0.12	0.12	0.10
$N(E_F)$	1.16	1.34	2.00

Table 2.1. Calculated optimized lattice parameters, a; relaxed distances between the Cd (X = In, Y or Sc) atom and its nearest O neighbors, D_{Cd-O} (D_{X-O}); optical band gap values, E_g, in the (Δ) [100], (Λ) [110], and (Σ) [111] directions; width of the single dispersed band, ΔE; electron velocities, v, at the Fermi level in the (Δ) [100], (Λ) [110], and (Σ) [111] directions; and density of states at the Fermi level, $N(E_F)$, for In-, Y-, and Sc-doped CdO.

(A)

(B)
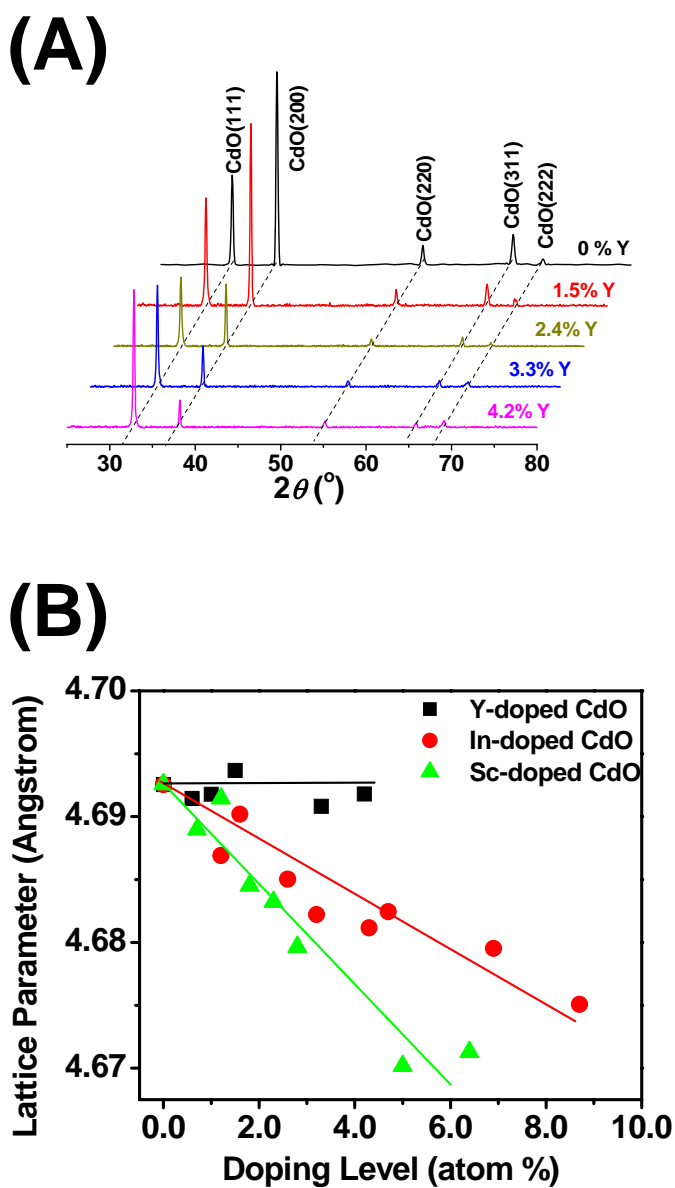
Figure 2.1. (A) θ-2θ X-ray diffractograms of CYO thin films grown on glass at 410°C by MOCVD as a function of Y doping level (given in atom %). (B) Lattice parameter changes as a function of dopant size and doping level for Y-, In-, and Sc-doped CdO thin films grown on glass. Lines through the data points are drawn as a guide to the eye
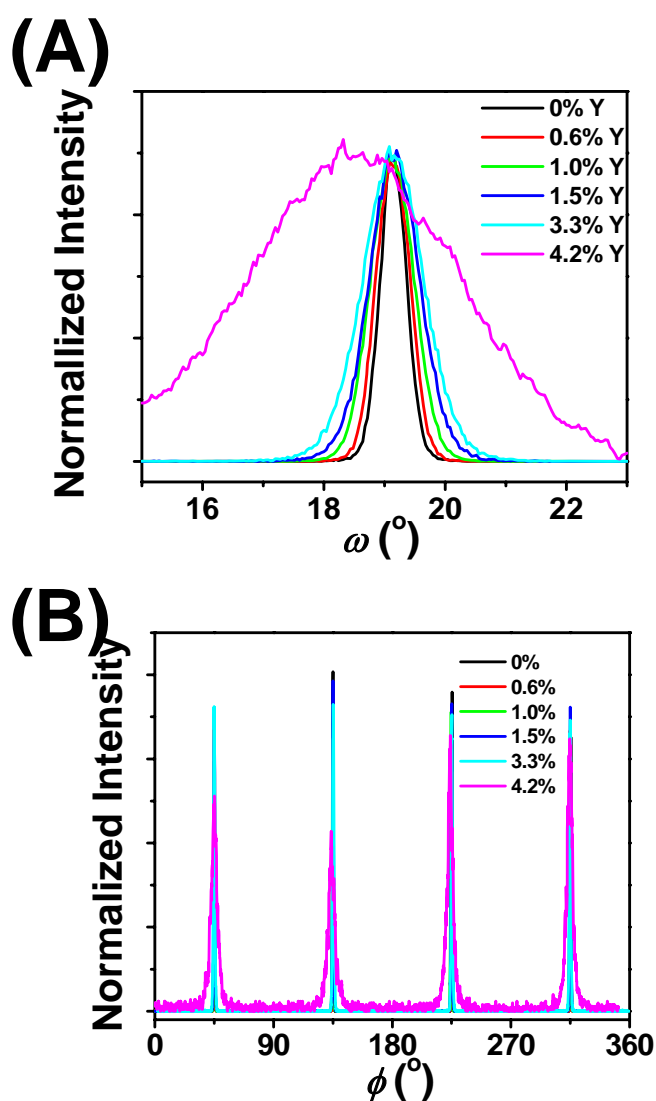
Figure 2.2. XRD texture analyses of CYO thin films grown on single-crystal MgO(100) as a function of Y doping level: (A) rocking curves measured on the CdO(200) XRD peak; (B) in-plane ϕ scans measured on the CdO (111) XRD peak with $\chi = 54.7$. Y doping level given in atom %
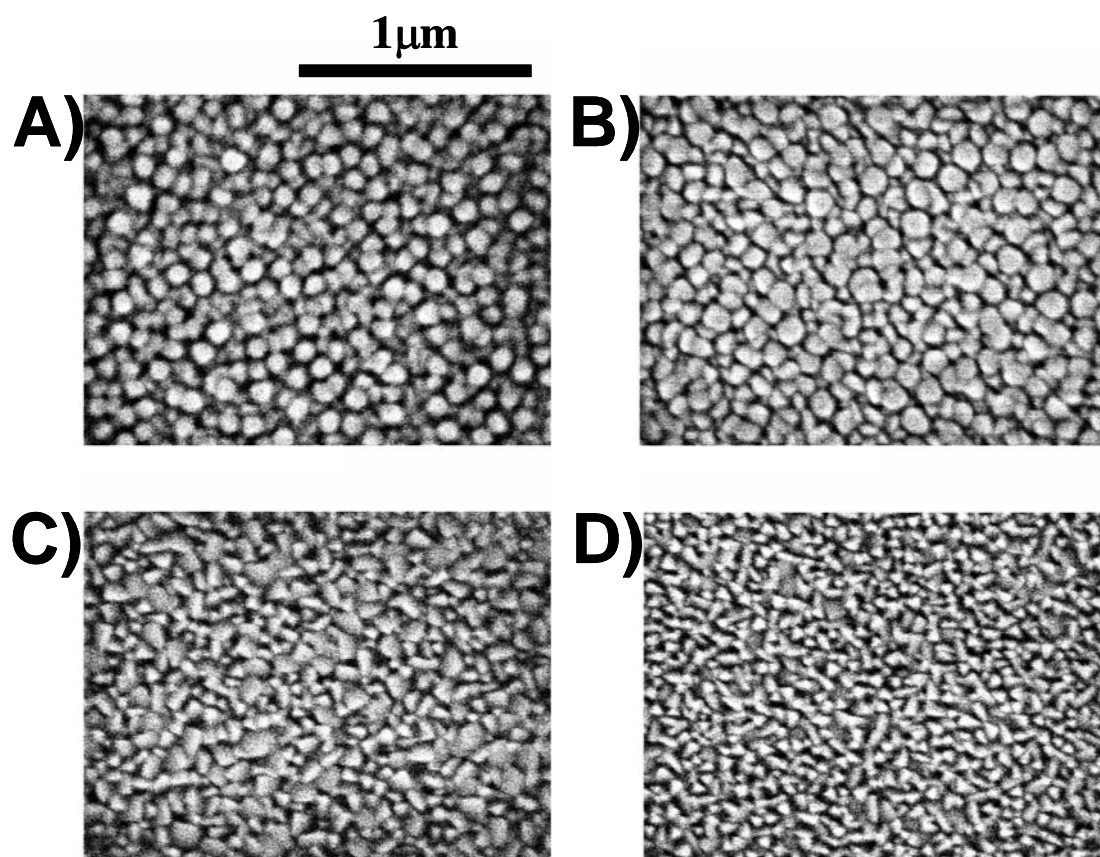
Figure 2.3. SEM images of CYO thin films on glass as a function of Y-doping (given in atom %). (A) 0.6 %; (B) 1.5 %; (C) 2.4 %; (D) 4.2 %
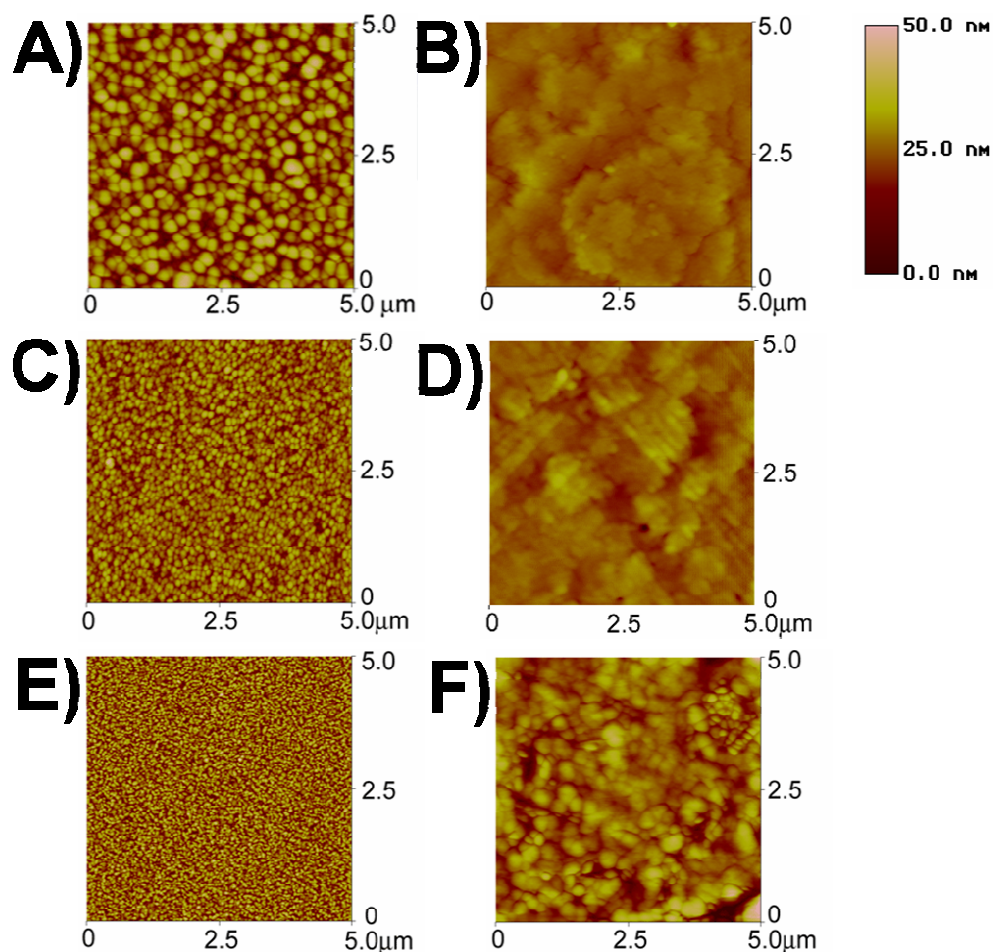
Figure 2.4. AFM images of CYO thin films as a function of Y-doping level (given in atom %): (A) 0.6 % Y-doped CdO on glass, RMS roughness = 7.2 nm; (B) 0.6 % Y-doped CdO on MgO(100); RMS roughness = 1.9 nm (C) 1.5 % Y-doped CdO on glass; RMS roughness = 5.1 nm (D) 1.5 % Y-doped CdO MgO(100); RMS roughness = 1.1 nm (E) 2.4 % Y-doped CdO on glass; RMS roughness = 6.9 nm (F) 2.4 % Y-doped CdO on MgO(100), RMS roughness = 5.7 nm
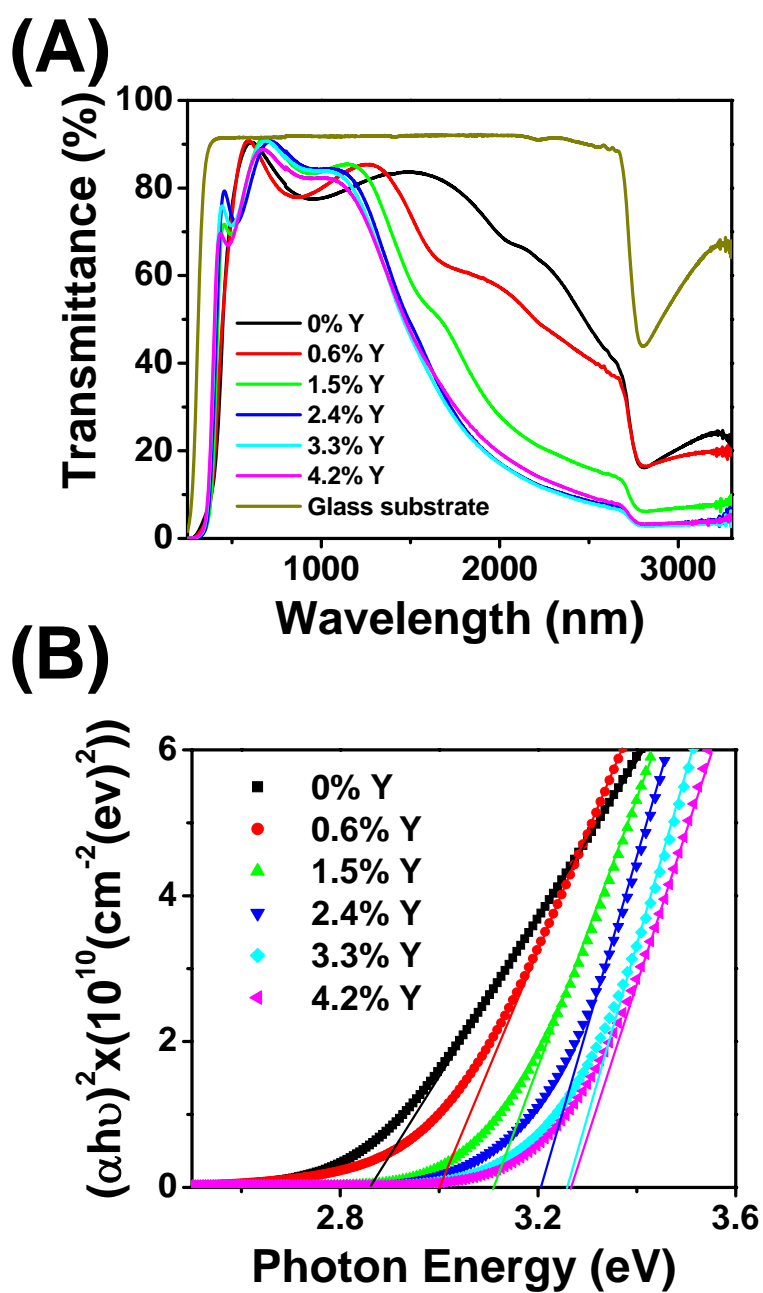
Figure 2.5. Optical characterization of MOCVD-derived CYO thin films grown on glass as a function of Y-doping: (A) optical transmission spectra; (B) band gap estimations
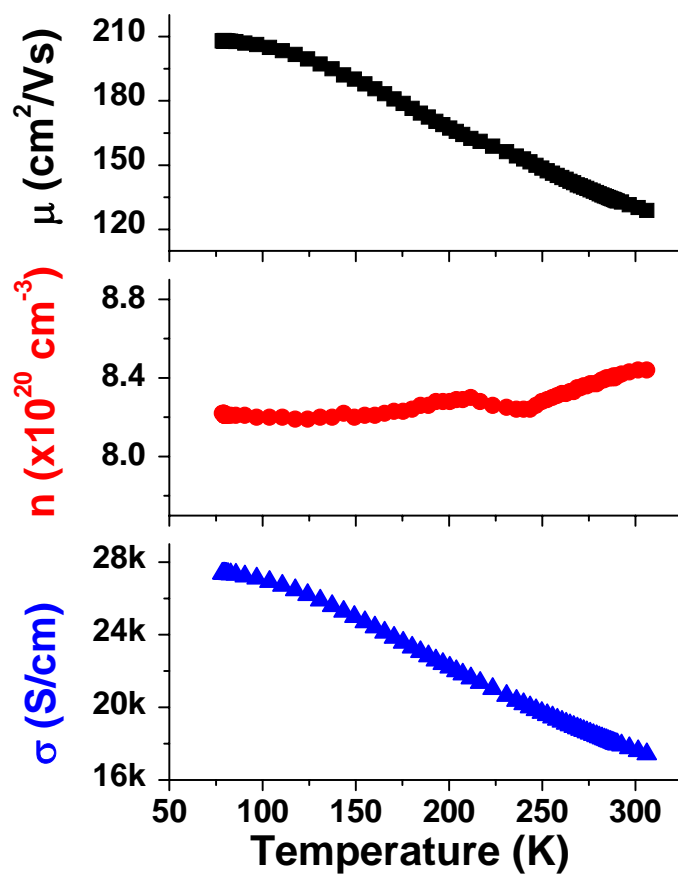
Figure 2.6. Variable temperature electrical conductivity and Hall effect measurements for 1.3 atom % Y-doped CdO thin film on MgO(100): carrier mobility (■), Carrier concentration (●), and electrical conductivity (▲)
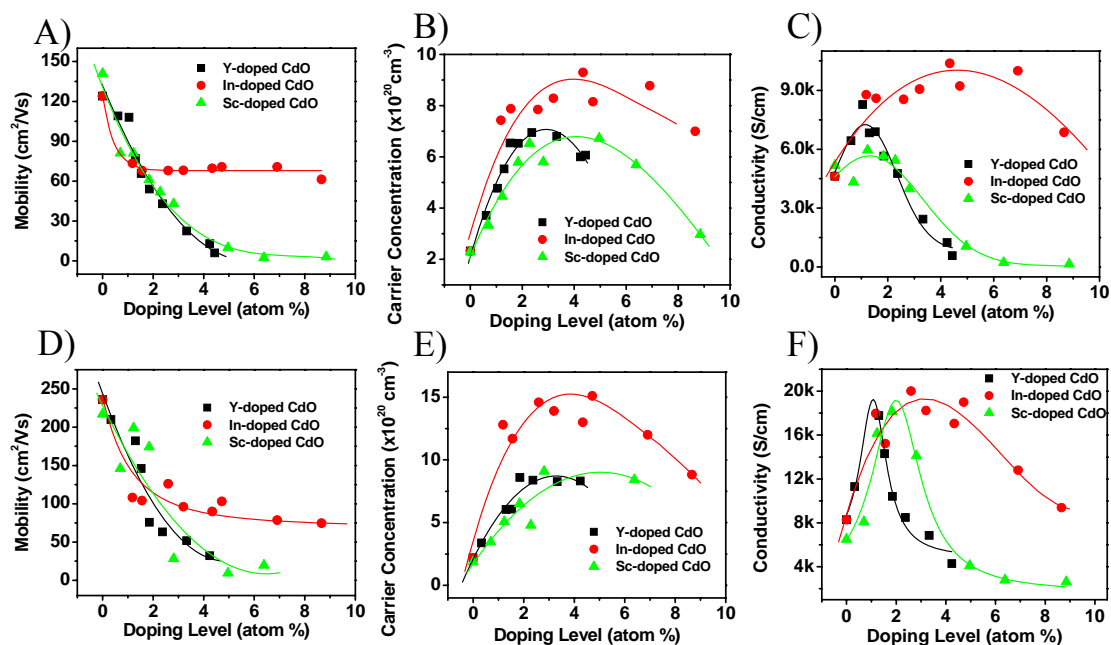
Figure 2.7. Room temperature four-probe charge transport measurements for Y-, In-, and Sc-doped CdO thin films on glass: (A) carrier concentration, (B) mobility, (C) conductivity; and on MgO(100): (D) carrier concentration, (E) mobility, (F) electrical conductivity, respectively. Lines are a guide to the eyes
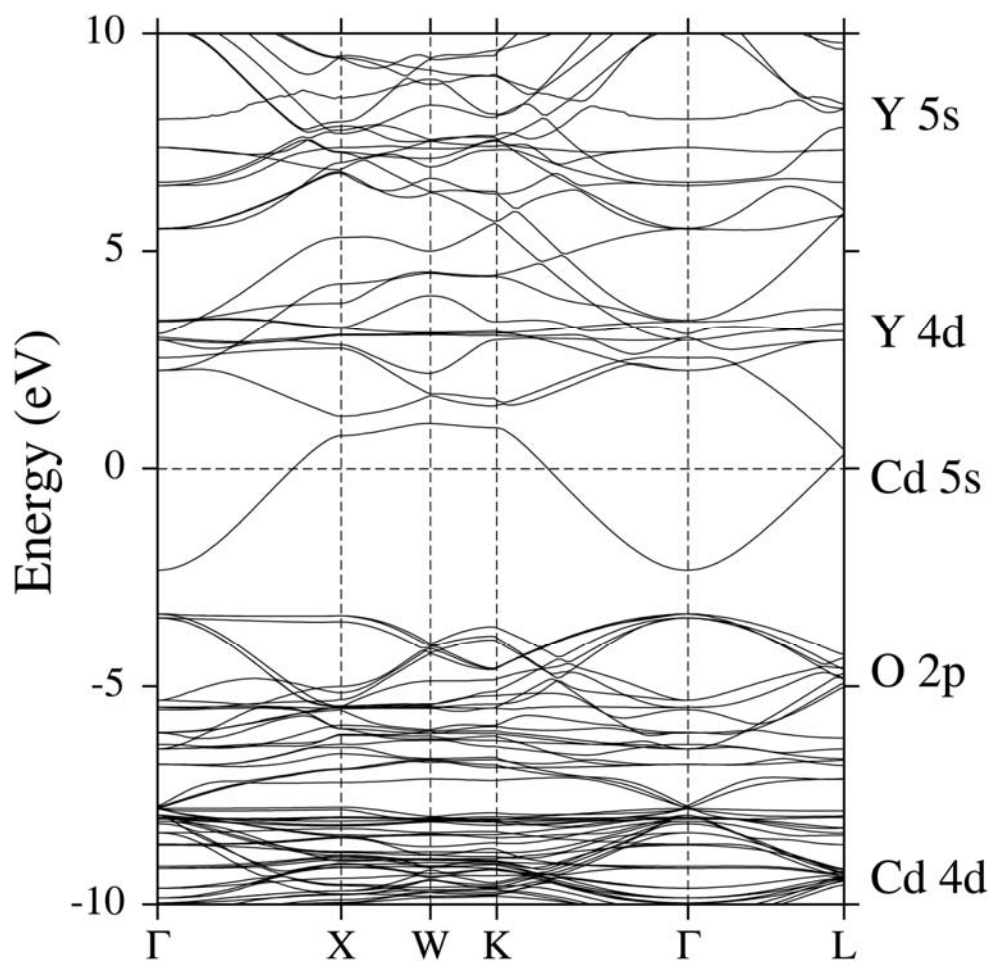
Figure 2.8. Band structure of 12.5 atom % Y-doped CdO calculated within the sX-LDA formalism along the high symmetry directions in the Brillouin zone. The origin of the energy is taken at the Fermi level
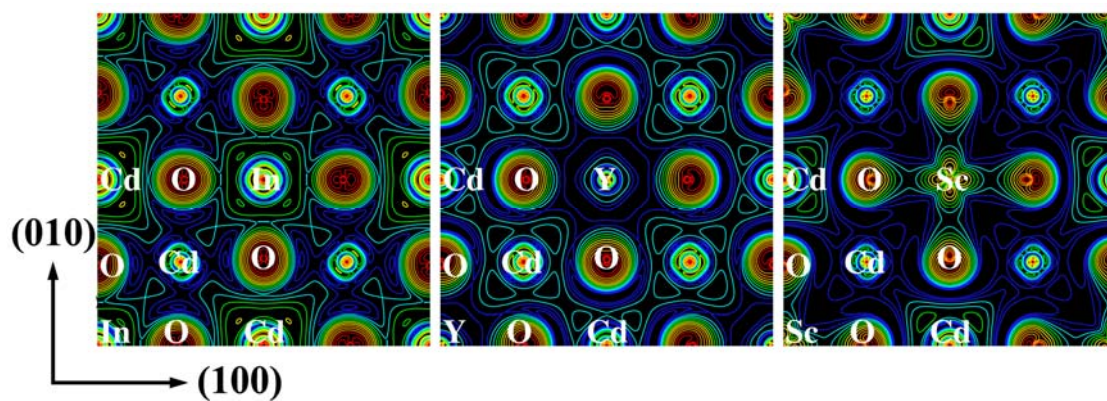
Figure 2.9. Calculated charge density distribution in the *ab* plane within the energy window of 0.027 eV below the Fermi level for the In-, Y-, and Sc-doped CdO. Atoms within one unit cell are labeled
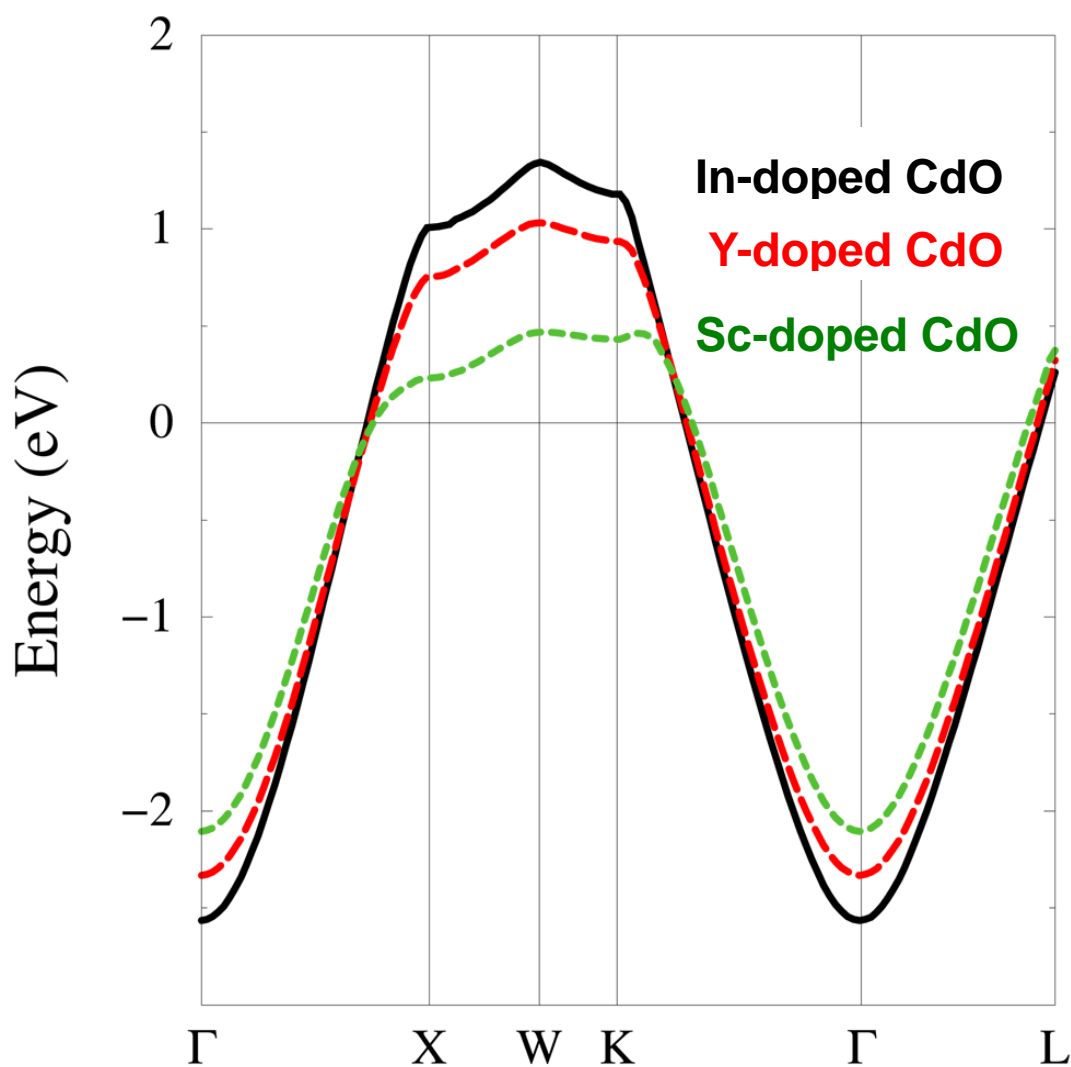
Figure 2.10. Comparison of the single band dispersion of 12.5 atom % In-doped CdO (solid line), Y-doped CdO (dashed line), and Sc-doped CdO (dotted line) calculated within the sX-LDA formalism. The origin of the energy is taken at the Fermi level

CHAPTER THREE

Tuning the Properties of Transparent Oxide Conductors. Dopant Ion Size and Electronic Structure Effects on CdO-Based Transparent Conducting Oxides. Ga- and In – Doped CdO Thin Films Grown by MOCVD

3.1. INTRODUCTION

Transparent conducting oxides (TCOs) gained significant attention over the last two decades, serving as key components in opto-electronic devices such as flat panel displays (FPDs), organic light-emitting diodes (OLEDs), photovoltaics, solar cells, optical waveguides and energy-efficient windows.[1-13] Currently, tin-doped indium oxide (ITO), with a typical electrical conductivity of 3-5$\times$ 10^3 S/cm and 85-90 % transparency in the visible region, is employed on a huge scale as a transparent electrode in many display technologies. However, there are several important limitations that cloud its future applicability: (1) limited availability and high cost of indium; (2) relatively low conductivity (not suitable for large-area displays); (3) significant optical absorption in the blue-green region (not suitable for many full-color displays); and (4) chemical instability in certain device structures (e.g., corrosion in OLEDs). In view of these issues, intense research has focused on understanding fundamental TCO crystal structure-film microstructure- electronic structure-charge transport-optical transparency relationships and on searching for ITO alternatives that are less expensive and possess comparable or higher conductivity and/or wider optical transparency windows.[3, 5, 9, 10, 12, 14-20]

Recently, CdO-based TCOs have received much attention due to their exceptional carrier mobilities, nearly metallic conductivities, and relatively simple crystal structures.[11, 21-28] Sn doping of CdO thin films grown epitaxially on MgO(111) by pulsed laser deposition (PLD) achieves thin film mobilities and conductivities as high as 607 cm^2/V·s and 42,000 S/cm,

respectively, rendering them the most conductive TCO thin films with the highest carrier mobilities reported to date.[26] Although the optical band gap of pure bulk CdO is only 2.3 eV,[29] leading to relatively poor optical transparency in the short wavelength range, aliovalent metal doping offers the possibility of tuning the electronic structure and the optical band gap through a carrier concentration-dependent Burstein-Moss (B-M) energy level shift.[30, 31] CdO, with a simple cubic rock salt structure, broadly dispersed s-like conduction bands, and a small carrier effective mass, is considered to be an ideal model material in which to study the effects of doping on TCO band structure, crystal chemistry, and charge transport.

Various deposition techniques, such as reactive evaporation,[32, 33] solution growth,[34] spray pyrolysis,[35, 36] sputtering,[37-40] PLD,[26] and MOCVD,[23, 25, 27, 28, 41-44] have been employed to grow CdO and CdO-based thin films. For device fabrication, chemical vapor deposition offers many attractive features, such as in situ growth under a variety of atmospheres, low-cost equipment, amenability to large area coverage with high throughput, conformal coverage, easy control of growth chemistry, and the possibility of creating metastable phases.[45]

In previous work from this laboratory, undoped and doped CdO thin films were successfully grown by MOCVD using optimized metal-organic Cd precursors.[23, 25, 27, 44] In-doped CdO thin films grown on glass by MOCVD exhibit conductivities as high as 16,800 S/cm. It was found that In-doping dramatically alters the CdO band structure by extensive mixing of In 5s and Cd 5s states, also yielding a hybridization gap in the conduction band.[44] Sc^{3+}, Y^{3+} with six-coordinate ionic radii of 0.89 Å and 1.04 Å respectively, were employed to test the dopant

size effects.[23, 27] Furthermore, compared with In^{3+} and Sn^{4+}, Sc^{3+} and Y^{3+} do not have

energetically comparable s states that can hybridize with the Cd 5s states in the conduction band.

Thus, these experiments also strove to assess the role of these s states. It was found that thin film

conductivities as high as 6,000 S/cm, and 8,540 S/cm are obtained on glass substrates at 1.2 %

Sc and 1.2 % Y doping, respectively. Compared to In-doped CdO, the Sc- and Y-doped CdO

(CSO, CYO) thin films on glass exhibit lower carrier mobilities and carrier concentrations, due

to the lack of energetically comparable s states that can hybridize with the Cd 5s conduction

band and the resulting lower dispersion of this s-type band – as revealed by first-principles

FLAPW electronic band structure calculations.[23, 27, 46] CSO and CYO thin films on MgO(100)

with a maximum conductivity of 18,100 S/cm and 17,800 S/cm are obtained at a Sc doping level

of ~1.8 % and Y doping level of 1.3 %, respectively, which are to date the most conductive

transparent conducting oxide materials grown by MOCVD. All of these MOCVD-derived thin

films exhibit good optical transparency, with an average transmittance > 80 % in the visible

range. Sc, Y doping effectively widens the band gap from 2.7 to 3.4 eV via a Burstein-Moss

band-filling shift, in agreement with our sX-LDA calculations.[23, 27, 46] Our continued interest in

CdO-based TCOs focuses on understanding crystal structure-charge transport relationships by

further doping CdO with a wide variety of dopants which simultaneously: (1) offer controlled

lattice parameter excursions via varying the ionic radius; (2) offer varying degrees of orbital

overlap between the Cd^{2+} conduction band states and the dopant ions. Hence Ga^{3+}, with a much

smaller ionic radius than In^{3+} (0.76 Å vs. 0.94 Å) , and fully occupied 3d orbitals (unlike $Sc^{3+}$and

Y^{3+}), represents an ideal probe ion to examine dopant radius size effects; furthermore, In^{3+}, which was previously found to be the optimum dopant for CdO thin films on amorphous glass substrates and is theoretically predicted to be an ideal doping candidate,[27, 44] has never before been grown epitaxially on single crystal substrates.

In this contribution, we report the growth of Ga- and In-doped CdO (CGO, CIO) thin films on amorphous glass and single crystal MgO(100) substrates by MOCVD. The CGO, CIO thin film phase structure, microstructure, electrical, and optical properties are investigated in detail as a function of doping level and growth parameters and are compared with CSO and CYO thin films. It will be seen that phase-pure CGO and CIO thin films exhibit conductivities of 11,500 S/cm and 20,000 S/cm, respectively, at Ga and In doping levels of 1.6 % and 2.6 %, respectively. All the as-deposited TCO thin films exhibit good visible region transparency, with an average transmittance > 80 %.

3.2. EXPERIMENTAL

3.2.1 MOCVD Precursors and Thin Film Growth

CdO-based thin film growth was carried out in the previously described horizontal, cold-wall MOCVD reactor.[47] The volatile metal-organic Cd precursor $Cd(hfa)_2$(N,N-DE-N',N'-DMEDA) (**1**) (hfa = hexafluoroacetylacetonate, N,N-DE-N',N'-DMEDA = N,N- diethyl-N',N'- dimethyl - ethyldnediamine) was prepared from

high-purity $Cd(NO_3)_2 \cdot 4H_2O$ (99.999 %, Aldrich), and was triply vacuum-sublimed.[25] $Ga(dpm)_3$

(**2**), and $In(dpm)_3$ (**3**) (dpm = dipivaloymethanate) were prepared from $Ga(NO_3)_3 \cdot 4H_2O$ (99.999

%, Alfa Aesar) and $In(NO_3)_3$ (99.999 %, Alfa Aesar) by literature procedures.[48-50]

1   **2**   **3**
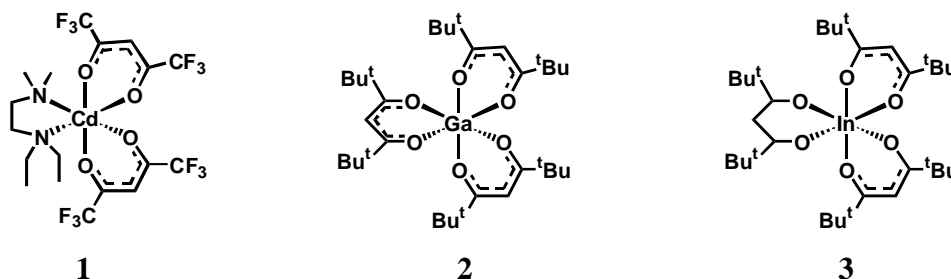
For Ga-, and In-doped CdO thin film growth, the precursor reservoir temperatures/Ar carrier gas

flow rates were optimized at: $Cd(hfa)_2$(N,N'-DE-N,N'-DMEDA), 85°C /15 sccm; $Ga(dpm)_3$,

92°C/6-40 sccm; $In(dpm)_3$ 94-95°C/5-20 sccm. The O_2 oxidizing gas was introduced upstream at

400 sccm after bubbling through distilled water. A system operating pressure of 4.0 ± 0.1 Torr

and a substrate temperature of 400°C was maintained during the thin film deposition. Corning

1737F glass and polished single-crystal MgO(100) ($a = 4.216$ Å) substrates were purchased from

Precision Glass and Optics and MTI Corporation, respectively. Both the glass and the MgO(100)

substrate surfaces were cleaned with acetone prior to the film deposition, and were placed

side-by-side on a SiC-coated susceptor in the growth reactor for simultaneous growth

experiments.

3.2.2 Film Physical Characterization Measurements

Composition analyses of the present films were carried out using inductively coupled

plasma atomic emission spectrometry (ICP-AES). Optical transparency measurements were carried out in the range of 300 – 3300 nm with a Cary 500 UV-Vis-NIR spectrophotometer. Film thicknesses were measured using a Tencor P-10 profilometer after etching a step in the film using 5 % HCl solution. X-ray diffraction θ-2θ scans of CdO films on glass were obtained with a Rigaku DMAX-A powder diffractometer using Ni-filtered Cu K_α radiation. Rocking curves and ϕ scans of the epitaxial thin films on MgO(100) substrates were obtained on a home-built Rigaku four-circle diffractometer with detector-selected Cu K_α radiation. Film surface morphology was imaged using a Digital Instruments Nanoscope III atomic force microscope (AFM) operating in the contact mode. Film microstructure was imaged on a Hitachi S4500 FE scanning electron microscope (SEM). Transmission electron microscopy (TEM) images, and selected area electron diffraction (SAED) patterns were obtained using a Hitachi 2000 microscope operating at 200 keV. Cross-sectional samples were prepared by mechanical grinding, dimpling and ion milling. Ambient-temperature four-probe charge transport data were acquired on a Bio-Rad HL5500 Hall-effect measurement system. Variable-temperature Hall effect and 4-probe conductivity data were collected between 4K and 330K and used instrumentation described previously.[51]

3.3 RESULTS AND DISCUSSION

We first describe CGO and CIO thin film growth by an efficient MOCVD process. Then, CGO and CIO film composition, morphology, microstructure, and epitaxy are characterized as a

function of doping level using a broad array of complementary physical techniques. In addition, film optical and electrical properties are investigated and compared with those of the Sc-, and Y-doped CdO analogues grown by the same technique. In doing so, we demonstrate the tunability of the CdO-based TCO materials by varying the dopants and substrates to achieve optimized transparent conductor properties.

3.3.1. Film Growth

A series of conductive CGO and CIO thin films was grown on 1737F glass and single crystal MgO(100) at 410 °C and under a 400 sccm O_2 flow rate for 2 hr by MOCVD. The growth rates of the films are ~1-2 nm/min on glass, and ~ 1.5-2.5 nm/min on MgO(100), respectively, which are similar to those established for Sc-, and Y-doped CdO. The Ga and In doping levels can be varied from 0 % - 6.0 % and 0 % - 6.9 %, respectively, by varying the Ga and In precursor reservoir temperatures and Ar carrier gas flow rates.

3.3.2. Film Composition, Morphology, Microstructure, and Epitaxy

X-ray diffraction θ-2θ scans were carried out from $2\theta = 25^o$ to 75°. Figure 1 shows XRD data as a function of Ga (1A) and In (1B) doping level. As can be seen from the figures, all of the films with Ga and In doping levels up to 6.0 % and 6.9 % are phase-pure, with a highly crystalline fcc CdO structure. No Ga_2O_3, In_2O_3, or other phases are detected by XRD, indicating Ga^{3+} and In^{3+} substitutes for the Cd^{2+} in the lattice instead of forming a new phase.

Using polycrystalline silicon as an internal calibration reference, the precise lattice parameters of the MOCVD-derived CGO and CIO thin films on glass were determined, and are also compared with the results of Sc and Y doping in Figure 2. It is found that the lattice parameters are gradually compressed with increasing Ga and In doping levels. Note that with the introduction of Ga, the lattice dimensions are not decreased as much as expected, based purely on Vegard's law dopant radius considerations, since six-coordinate Ga^{3+} with an ionic radius of 0.76 Å is far smaller than Cd^{2+} (1.09 Å). This suggests that the Ga doping efficiency is lower than for In, Sc, and Y, even though no new phase is formed. This is trend further supported by the observation that the carrier concentration increases only slightly with increased Ga doping levels (see below). In marked contrast, In^{3+}, having a six-coordinate ionic radius of 0.94 Å (more comparable to that of Cd^{2+}), compresses the lattice monotonically with increased doping levels, and the carrier concentration increases with In doping is consistent with significantly greater doping efficiency. Note, however, that even the significant lattice contractions caused by progressive In doping fall below those estimated from simple Vegard's law considerations (Figure 2). This effect is likely due to compensation by the antibonding character of the conduction band formed from the Cd 5s and O 2p states as discussed elsewhere.[23, 46]

In contrast to the above results for growth on amorphous glass substrates, all CGO and CIO thin films grown on MgO(100) exhibit a highly (200) textured microstructure. The texture of the thin films is shown in Figures 3 and 4. As can be seen from Figure 3, the rocking curves of the films show good out-of-plane alignment. The full-width-at-half-maximum (FWHM)

increases from 0.5^o for pure CdO films to 1.0^o and 1.0^o at 2.4 % Ga and 2.6 % In doping, respectively, and to 1.8^o and 1.4^o at 6.0 % Ga and 6.9 % In doping, respectively, indicating that the crystallinity decreases with increased Ga and In doping. Note that the In-doped CdO thin films have the greatest crystallinity among the four dopants studied. In-plane orientation was investigated by ϕ-scans of the CdO (111) reflection at $\chi = 54.7^o$, and data are shown in Figure 4. The clear four-fold rotational symmetry of the CdO (111) reflections together with the small FWHMs (0.5^o for pure CdO, 1.2^o for CGO at 2.4 % Ga doping, 1.1^o for CIO at 2.6 % In doping) reveal excellent in-plane orientation of the films. The orientation relations between the CGO and CIO thin films and the MgO(100) substrates are therefore CdO(100)‖MgO(100).

TEM images and SAED patterns of 1.6 % Ga-doped CdO films grown on MgO(100) are shown in Figure 5. The SAED pattern of the film indicates that the CdO grains retain the biaxial (in-plane and out-of-plane) texture of the single crystal substrate. Figure 5B shows that the Ga-doped CdO thin film grow epitaxially with a highly textured crystallinity. The dark shadow an the interface of the TEM cross-section indicates that most of the strain from the mismatch of the lattice ($a_{MgO} = 4.216$ Å, ~10 % smaller than $a_{CdO} = 4.696$ Å) has relaxed at or near the interface.

SEM surface images in Figures 6 and 7 show that the as-deposited CGO and CIO thin films grown on glass are densely packed with heavily grained structures. At low Ga and In doping levels ($\leq$ 3.2-3.3 %), films on glass are all very uniform with rounded grains in plan view. With the Ga and In doping increased to 4.9 % and 4.3 %, respectively, and higher, the grains of the

films on glass are largely triangular in shape, suggesting that the (111) planes are parallel to the surface, which agrees well with the XRD analysis and is similar to trends observed in Sc and Y doping.[23, 27] As for the epitaxial films on MgO(100), the films with Ga doping levels ≤ 1.6 % are featureless (single-grained) by SEM and are found to be very smooth and uniform by AFM. As the Ga doping level is increased to ≥ 3.3 %, a grained structure is clearly visible; the films with In doping are smoother and featureless up to 4.3 % doing (single-grained) by SEM, and confirmed to be very smooth and uniform by AFM. Contact-mode AFM images of the CGO and CIO thin films are shown in Figure 8. The data reveal that the CIO thin films on glass are very uniform and smooth, with root-mean-square (RMS) roughnesses of 2.5-3.5 nm over a 5 μm × 5 μm area (Figure 8B), while the CGO thin films are somewhat rougher, exhibiting root-mean-square (RMS) roughnesses of 7-9 nm over a 5 μm × 5 μm area (Figure 8A). Regarding the CGO and CIO films grown on MgO(100), the surface roughnesses of the films are smoother than those grown on glass, also similar to the Sc- and Y-doped CdO series.[23, 27] The RMS roughness is found to be 1~3 nm for In-doped CdO (Figure 8D), and 5~7 nm for Ga-doped Cd (Figure 8C).

3.3.3. Film Optical and Electrical Properties

All of the as-grown CdO films are light-yellow to the eye but highly transparent. The color becomes lighter with increased Ga and In doping as the band edge shifts to higher energies.

Optical transmission spectra of CGO and CIO thin films grown on glass are shown in Figure 9. For CGO and CIO thin films with thicknesses of ~200 nm, the average transmittance at 550 nm is ~ 85 %. With an increase of Ga and In doping level, the band edges are found to be dramatically blue–shifted, doubtless due to the Burstein-Moss effect. Simultaneously, the plasma edges shift to the blue, owing to the increase in free carrier concentration with increased doping level. Band gap estimates were derived from the optical transmission spectra by extrapolating the linear portion of the plot of $(\alpha h\nu)^2$ vs. $h\nu$ to $\alpha = 0$ (Figure 10). It is found that the band gap increases from 2.85 eV to 3.08 eV with an increase in Ga doping from 0 % to 6.0 %; and to 3.18 eV with increases in In doping from 0 % to 6.9 %.

As in other ailovalent metal-doped CdO materials investigated to date, all of the Ga- and In-doped CdO film samples exhibit n-type conductivity as determined by negative Hall coefficients. Figure 11 shows the temperature dependence of thin film charge transport properties for a 2.7 atom % CGO film on MgO (100). Similar to Y- and Sc-doped CdO,[23, 27] the mobilities and conductivities of CGO films are essentially independent of temperature in the low temperature region (< 100 K), suggesting that neutral impurity scattering (NIS) and/or ionized impurity scattering (IIS) processes are dominant.[25, 52-55] In the high temperature region (> 100 K), the mobility and conductivity decrease with increasing temperature, suggesting that lattice vibration scattering (LVS), which is temperature-dependent, has now become an important scattering contributor.[56-58] The importance of grain boundary scattering (GBS) is an incompletely resolved mechanistic issue in most CdO-based TCOs. It has been argued that GBS is

insignificant for highly degenerate TCOs because the carrier mean-free-paths (determined optically) are typically much smaller than the grain sizes of typical films.[25, 52, 57-60]

Electrical conductivity, mobility, and carrier concentration data for as-grown CdO thin films as a function of Ga and In doping level are plotted, Data for Y- and Sc-doped thin films are also compared in Figures 12-14. For the present In-doped CdO films, with an increase in In doping, the carrier concentration increases from 2.3×10^{20} cm^{-3} for pure CdO thin films on glass to 9.3 $\times 10^{20}$ cm^{-3} at ~ 4.3 % In doping, while for the Ga-doped CdO thin films, the carrier concentration increases only marginally to 4.4×10^{20} cm^{-3} at 4.9 % Ga doping. The GCO mobility, however, drops precipitously with increased Ga doping. However, in the case of In doping, due to the more effective overlap of the In and Cd 5s orbitals, the mobility falls at a far slower rate compared to the mobility in Y-, Sc-, and Ga- doped CdO. It is clear from these data that M^{3+} (M = Ga, In, Sc and Y) ions behave as effective dopants by replacing Cd^{2+} sites in the lattice and donating electrons to act as charge carriers. However, at certain doping levels (2-5 %), the carrier density plateaus and the mobilities decline substantially, indicating that some of the M dopant sites may not be readily ionized and/or do not contribute to the mobile charge carriers. In addition, excess M doping appears to degrade the thin film crystallinity and increase carrier scattering, thereby decreasing carrier mobility and conductivity. Compared with In doping, much less Ga can be effectively doped into the CdO lattice. Thin films with maximum conductivities of 10,400 S/cm and 20,000 S/cm on glass and MgO(100), respectively, are obtained at 4.3 % and 2.6 % In doping. Compared with films on glass, CIO films on MgO(100), at the same doping

level, exhibit similar doping level-dependent trends but exhibit much greater carrier concentrations and mobilities, indicating that the epitaxial films possess fewer scattering centers and higher doping efficiency due to their highly textured microstructure/enhanced crystalline perfection, similar to behavior found for epitaxial CdO on MgO(100) and epitaxial ITO on single-crystal YSZ.[61] In the contrasting case of Ga doping, which exhibits much lower doping efficiency, the conductivity of the doped thin films on glass falls with increasing Ga doping levels and essentially never achieves the pure CdO level. CGO films grown on MgO(100), with the contribution of epitaxial effects, exhibit higher doping efficiency, and a maximum conductivity of 11,500 S/cm is achieved at a 1.6 % doping level. In addition, comparison of the charge transport properties for Ga-, In-, Y-, and Sc-doped CdO given in Figures 12-14 shows that carrier mobilities and doping efficiencies decrease in the order In > Y > Sc >Ga.

3.4.   CONCLUSIONS

Highly conductive and transparent CGO and CIO thin films have been grown on glass and single crystal MgO(100) substrates at 410 ^{o}C by low-pressure MOCVD. As-deposited CGO and CIO thin films exhibit good optical transparency, with an average transmittance of 85 % in the visible region. As in the cases of Y and Sc doping, In doping significantly increases the electrical conductivity and widens the optical band gap. In contrast, for Ga doping, due to the small ionic radius and lack of s orbital overlap with Cd 5s states, the electrical conductivity and optical band

gap are increased only modestly. Thin films with maximum conductivities of 10,400 S/cm and 20,000 S/cm on glass and MgO(100), respectively, are obtained at In doping levels of 4.3 %. and 2.6 %. Ga doping, however, only increases the conductivity to 11,500 at 1.6 % Ga doping on MgO (100) substrates, and doping of Ga on glass substrates does not increase the conductivity significantly. In and Ga doping widens the band gap from 2.85 to 3.18 eV and 3.08 eV, respectively, via a Burstein-Moss (B-M) shift. Epitaxial films grown on MgO(100) also exhibit a biaxial, highly textured microstructure, leading to higher doping efficiency and fewer scattering centers, which is suggested to be responsible for the higher conductivity vs. the films on glass.[25] Experimental results reveal that dopant ion size and electronic structure have a significant influence on the CdO-based TCO crystal and band structures, as well as on the optical and electrical properties. First, Ga^{3+} (0.76 Å), In^{3+} (0.94 Å) and Sc^{3+} (0.89 Å), with smaller ion sizes than that of Cd^{2+} (1.09 Å), compress the lattice parameters, while Y(1.04 Å), with an ion size similar to that of Cd^{2+}, does not significantly alter the lattice parameter. Ga(0.76 Å), with the smallest radius among the four dopants, only compresses the lattice slightly and exhibits low doping efficiency. Second, in marked contrast to In-doped CdO, in the cases of Ga doping, the Cd 5s states do not hybridize significantly with Ga 4s states due to an energy level mismatch. Third, the presence of the "d states" of Y and Sc significantly affects the dispersion of the single band which crosses the Fermi level, resulting in lower mobility as compared to In-doped CdO. While Ga has fully filled d states, because of its much smaller ionic radius and lack of significant overlap with the Cd 5s states, cannot effectively replace Cd^{2+} and contribute carriers

proportionately to the doping. Thus, it exhibits the lowest doping efficiency and poorest electrical properties, in agreement with the theoretical calculations.

Based on the results of the present studies, it can be seen that CdO-based TCO films generally exhibit higher carrier mobilities than do those of In_2O_3-, ZnO-, and SnO_2-based TCO materials. This can be ascribed to the simple CdO cubic crystal structure, broadly dispersed, free electron-like Cd 5s-based conduction band, and low carrier effective masses. In the doping studies, it is found that doping efficiency is strongly dependent on the degree of orbital hybridization between the dopant orbital and Cd 5s states. In conclusion, we find that dopant ion size and electronic structure have substantial influence on the CdO crystal and band structure, especially on the energetic position and width of the highly dispersed conduction band, which provide the necessary conditions for optimizing transparent conducting behavior with doping.

A)

B)
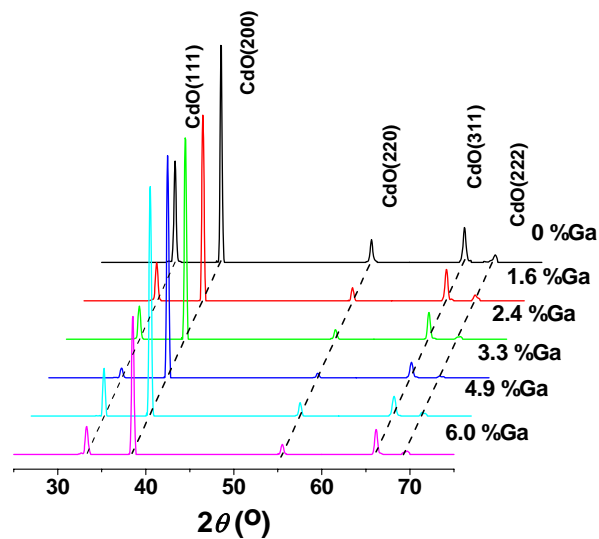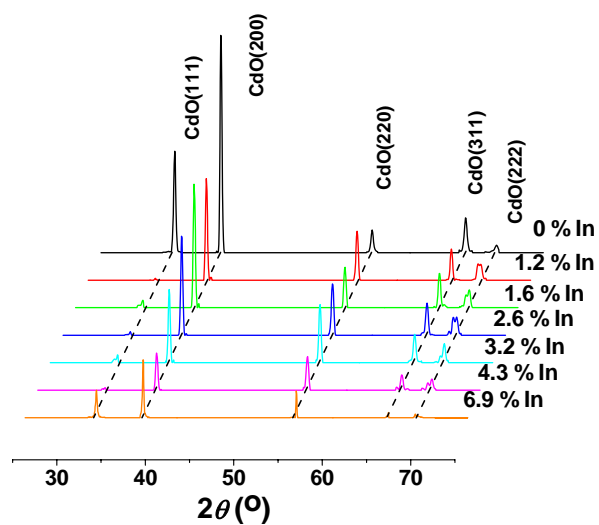
Figure 3.1. *θ-2θ* X-ray diffractograms of CGO (A) and CIO (B) thin films grown on glass at 410°C by MOCVD as a function of Ga and In doping level (given in atom %)
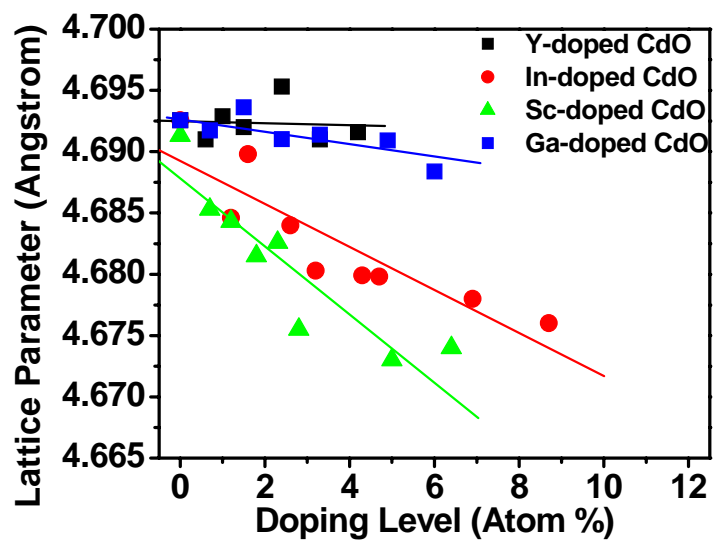
Figure 3.2.   Lattice parameter changes as a function of dopant size and doping

level for Ga-, In-, Sc-, and Y-doped CdO thin films grown on glass.

Lines through the data points are drawn as a guide to the eye

A)
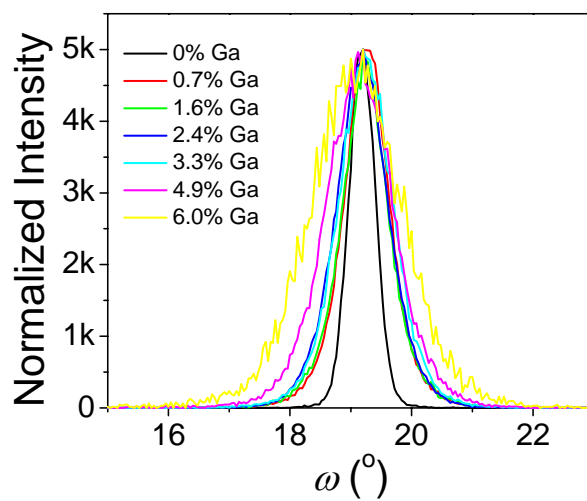
B)
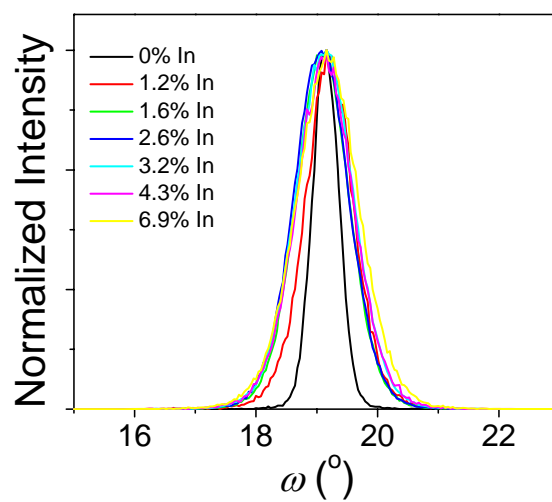
Figure 3.3. XRD texture analyses of CGO (A) and CIO (B) thin films grown on single-crystal MgO(100) as a function of Ga and In doping level; rocking curves measured on the CdO(200) XRD peak

A)
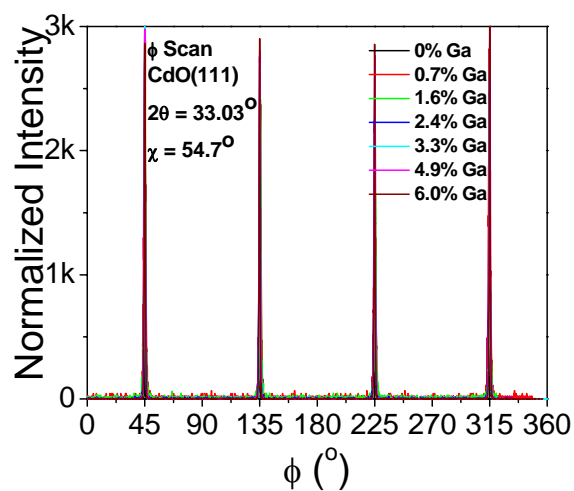
B)
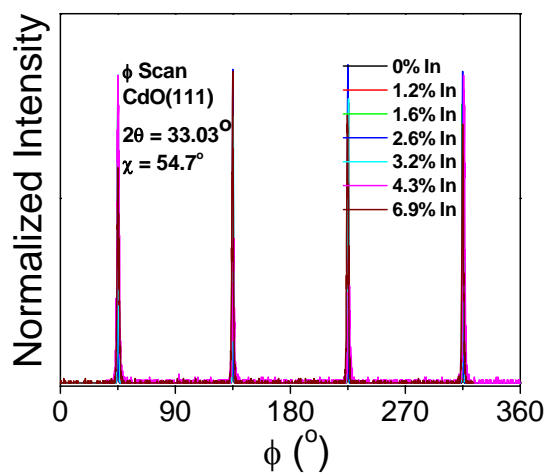
Figure 3.4. XRD texture analyses of CGO (A) and CIO (B) thin films grown on single-crystal MgO(100) as a function of Ga and In doping level: in-plane ϕ scans measured on the CdO (111) XRD peak with χ = 54.7. Ga and In doping level given in atom %

A)

B)
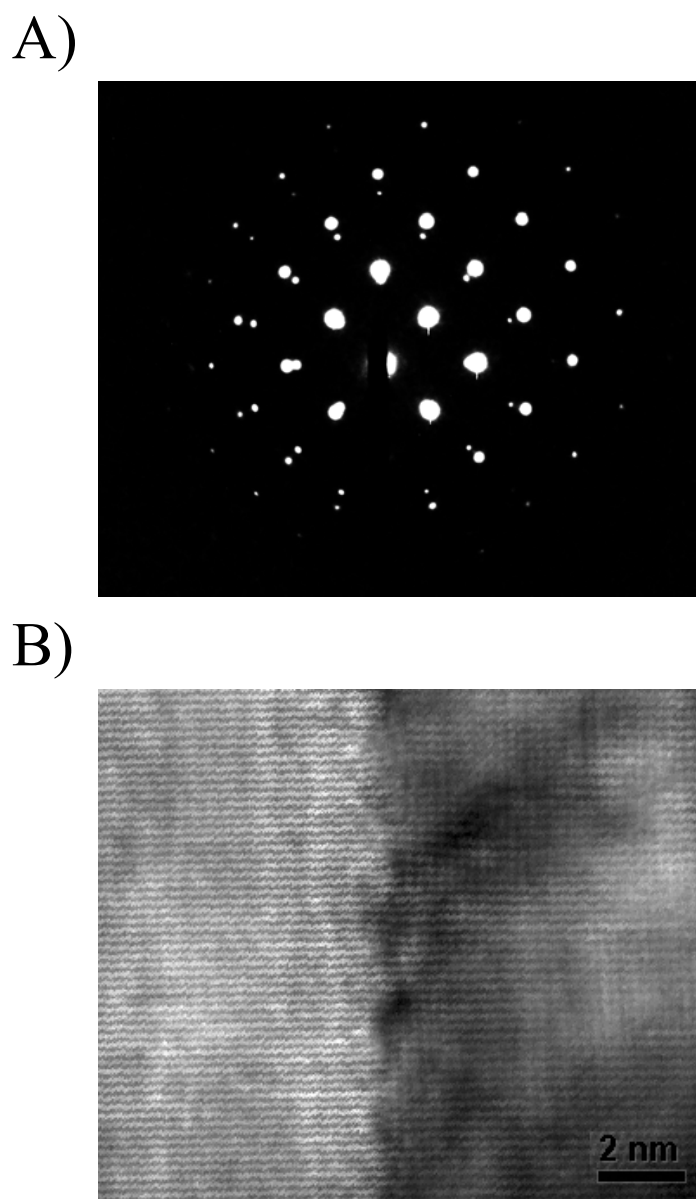
Figure 3.5. TEM images of 1.6% doped CGO thin film on MgO(100). A) SAED pattern, B) cross-section image (MgO substrate is on the left side of the image and the Ga-doped CdO film grown is on the right side)
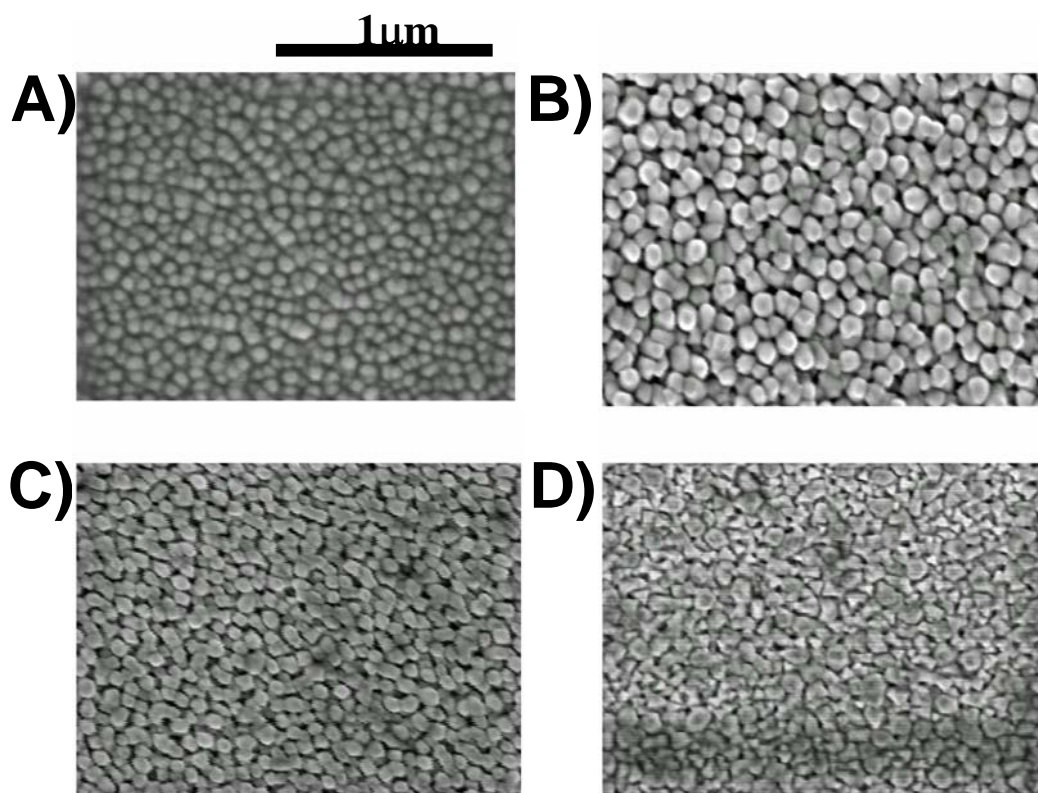
Figure 3.6. SEM images of CGO thin films grown on glass as a function of Ga doping level (given in atom %). (A) 0.7 %; (B) 1.6 %; (C) 3.3 %; (D) 4.9 %
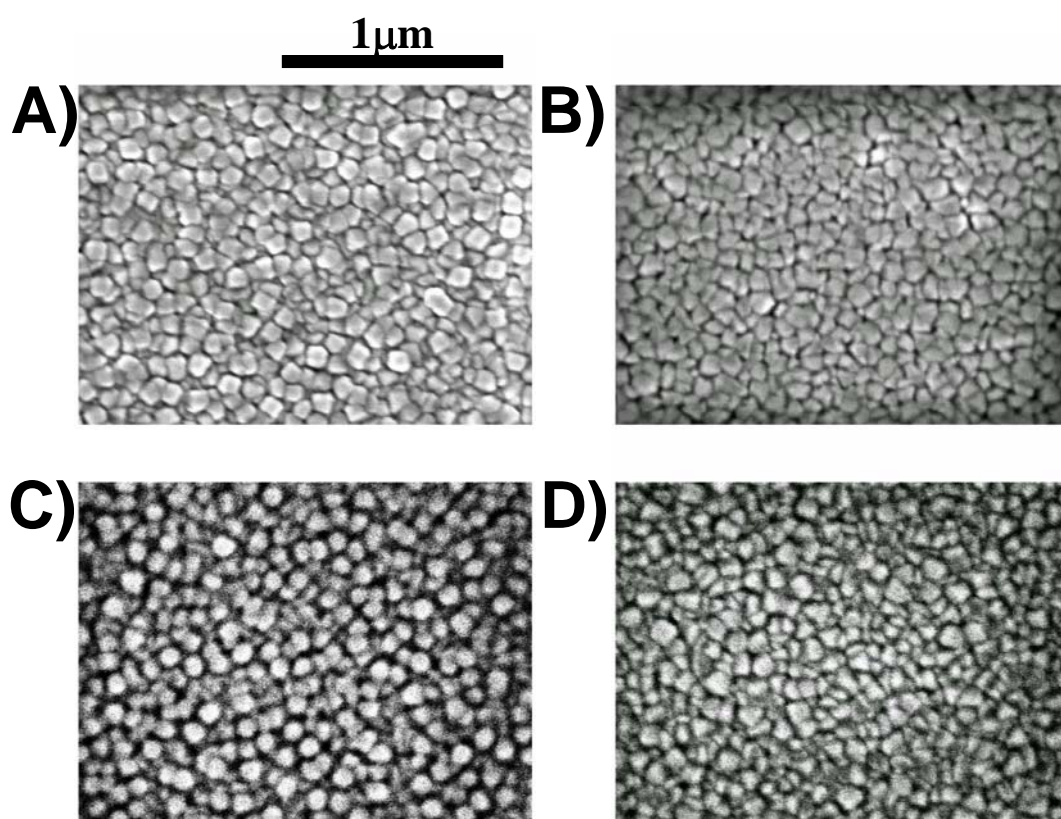
Figure 3.7. SEM images of CIO thin films grown on glass as a function of In doping level (given in atom %). (A) 1.2 %; (B) 1.6 %; (C) 3.2 %; (D) 4.3 %
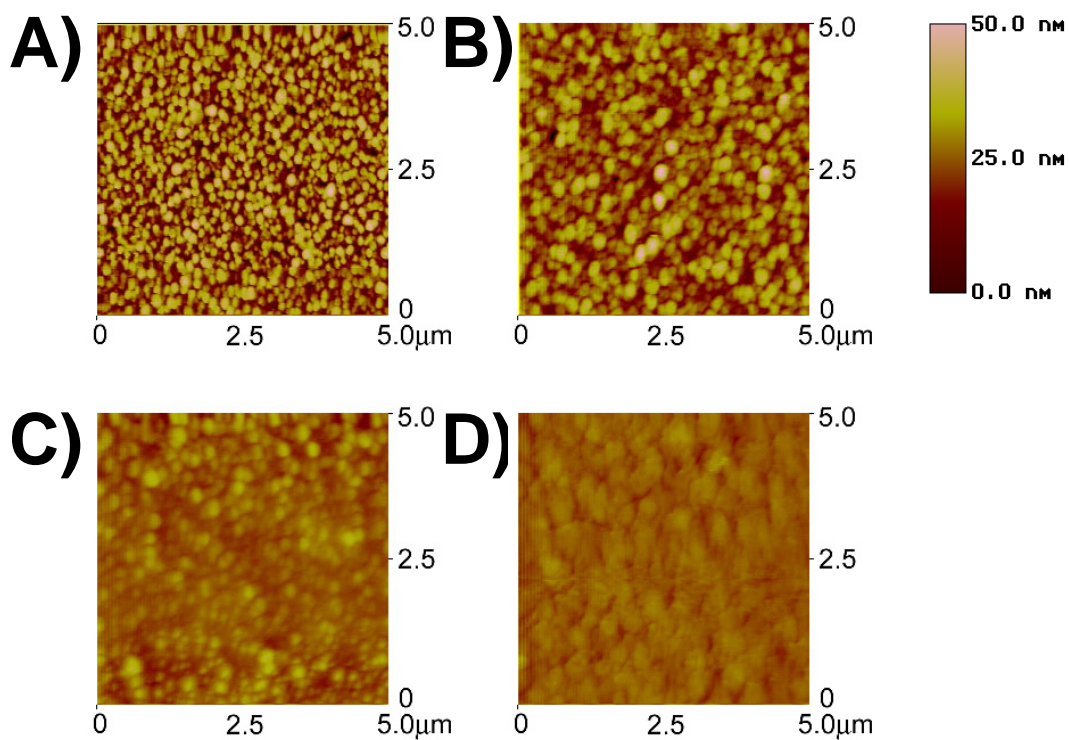
Figure 3.8.   AFM images of CGO and CIO thin films: (A) 3.3 % Ga-doped CdO

on glass, RMS roughness   = 8.9 nm; (B) 3.3 % Ga-doped CdO on

MgO(100); RMS roughness = 6.3 nm (C) 3.2 % In-doped CdO on

glass; RMS roughness = 2.5 nm (D) 3.2 % In-doped CdO

MgO(100); RMS roughness = 1.9 nm

A)
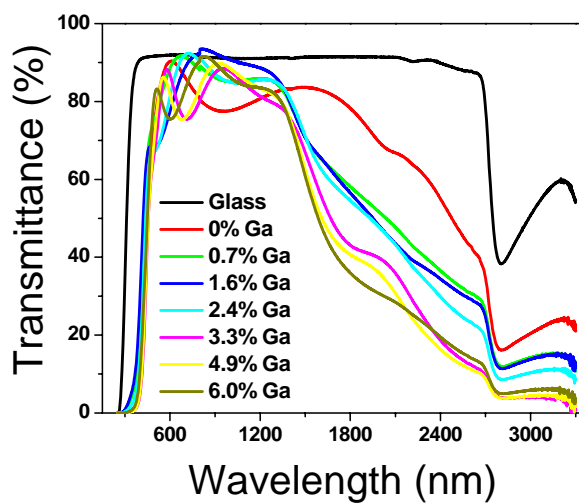
B)
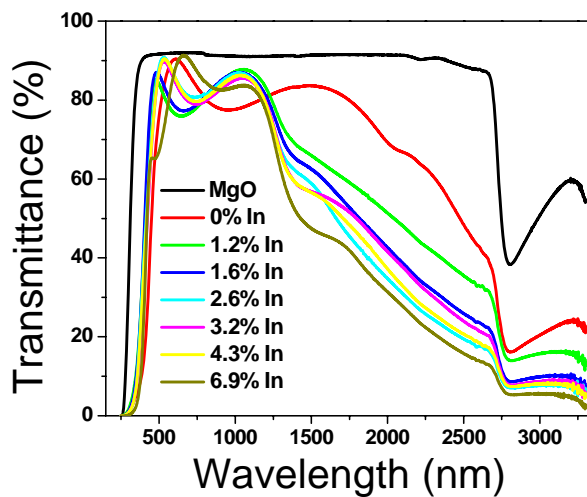
Figure 3.9. Transmission optical characterization of MOCVD-derived CGO (A) and CIO (B) thin films grown on glass as a function of Ga and In doping level

A)
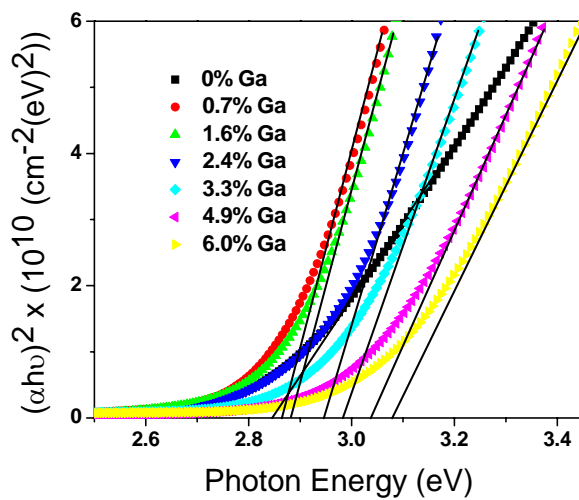
B)
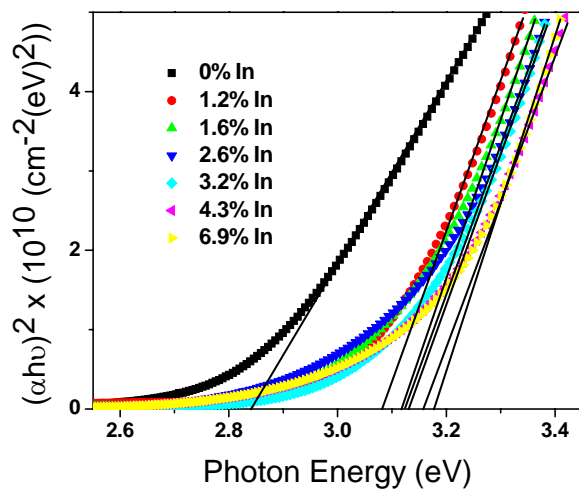
Figure 3.10. Transmission optical characterization of MOCVD-derived CGO (A) and CIO (B) thin films grown on glass as a function of Ga and In doping level; band gap estimations
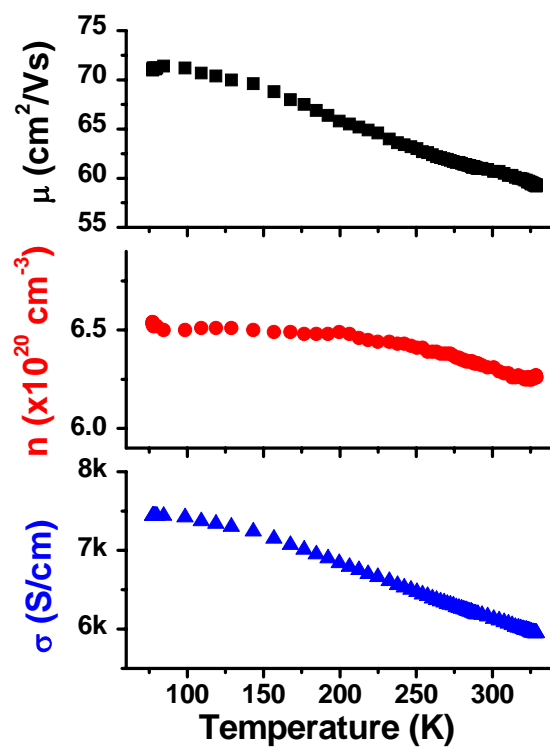
Figure 3.11. Variable temperature electrical conductivity and Hall effect measurements for a 2.7 atom % Ga-doped CdO thin film on MgO(100): carrier mobility (■), carrier concentration (●), and electrical conductivity (▲)

A)
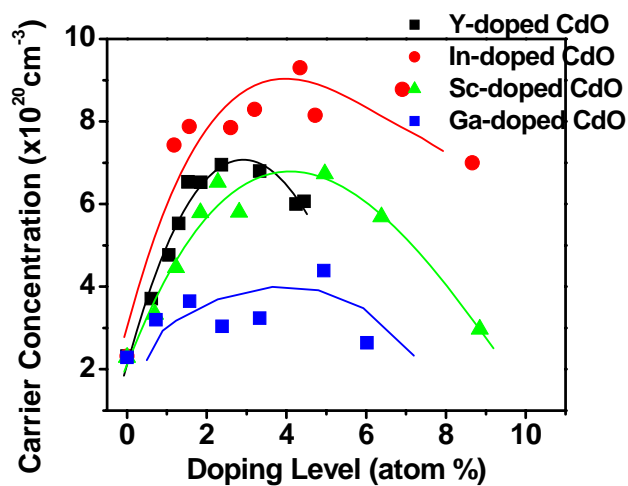
B)
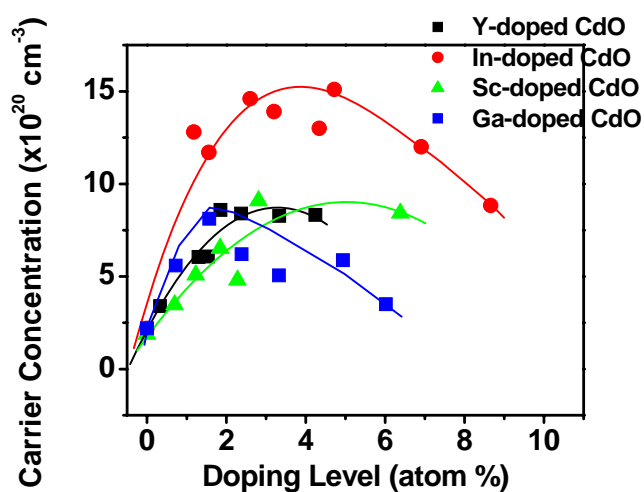
Figure 3.12. Room temperature four-probe charge transport measurements for Ga-, Y-, In-, and Sc-doped CdO thin films on glass (A) and on MgO(100) (B): carrier concentration. Lines are a guide to the eyes

A)
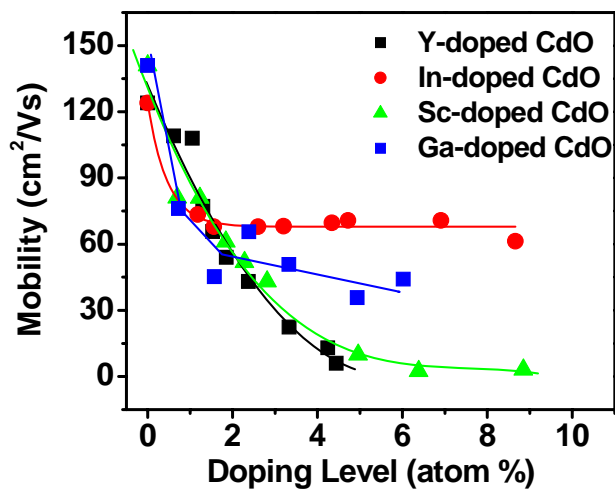
B)
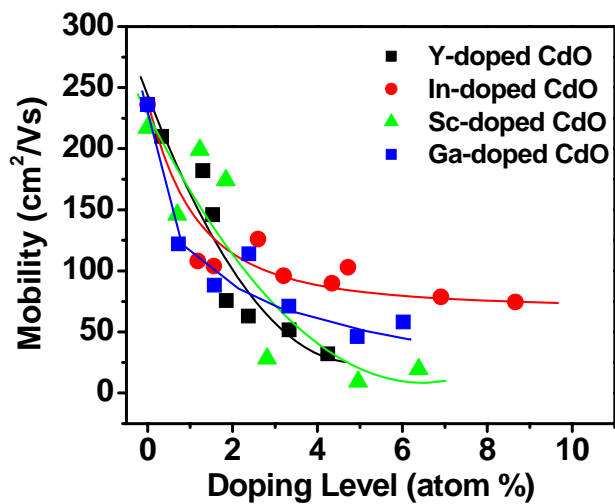
Figure 3.13. Room temperature four-probe charge transport measurements for Ga-, Y-, In-, and Sc-doped CdO thin films on glass (A) and on MgO(100) (B): mobility. Lines are a guide to the eyes

A)
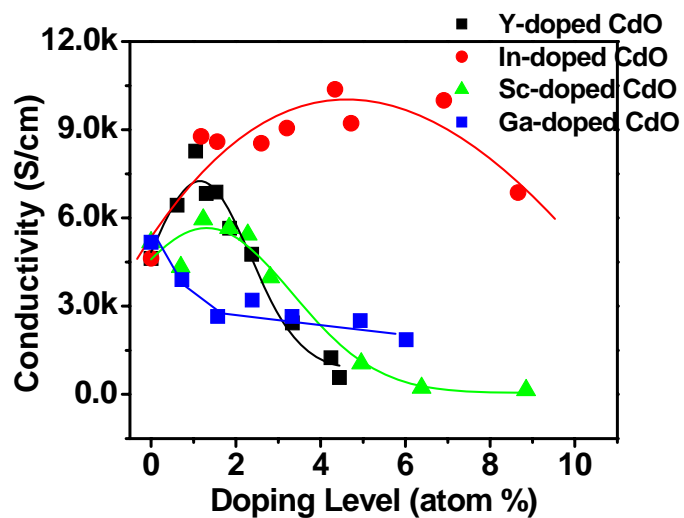
B)
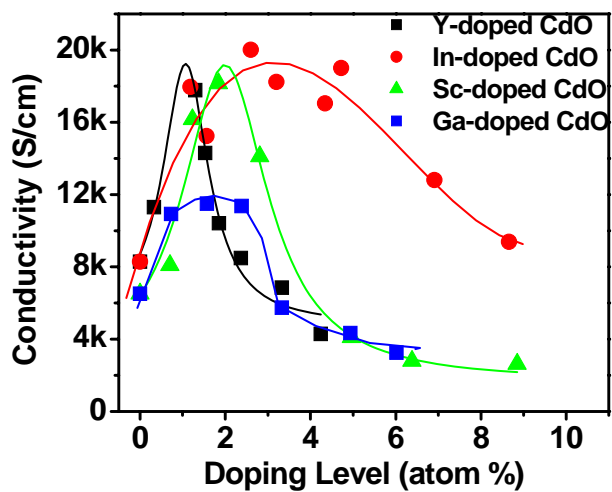
Figure 3.14. Room temperature four-probe charge transport measurements for Ga-, Y-, In-, and Sc-doped CdO thin films on glass (A) and on MgO(100) (B): electrical conductivity. Lines are a guide to the eyes

CHAPTER FOUR

Highly Transparent and Conductive CdO Thin Films as Anodes for Organic Light-Emitting Diodes. Film Microstructure and Morphology Effects on Performance

4.1. INTRODUCTION

Organic light-emitting diodes (OLEDs) have been receiving increasing research attention since the first report in 1987, due to their potential to replace liquid crystal displays (LCDs) in next-generation flat panel displays (FPDs).[1] Tin-doped indium oxide (ITO), with a typical electrical conductivity and visible range transparency of $3\text{-}5\times10^3$ S/cm and 85-90%, respectively, is currently the most widely used transparent anode material for OLEDs. However, it is by no means ideal due to: 1) the limited availability and high cost of indium; 2) the relatively low conductivity; 3) chemical instability in certain device structures;[2] and 4) the relatively low work function (4.3-4.7 eV).[3] To meet the rising demand for increased OLED device efficiency and larger display sizes, it will be necessary to develop novel transparent electrodes that are cheap, chemically more stable, possess superior electrical and optical properties, and have greater work functions. Recent advances in this area include using TiN,[4] high work function In_2O_3-based oxides (Zn-In-O, Zn-In-Sn-O, Ga-In-O, Ga-In-Sn-O),[5] ZnO-based oxides (Al-Zn-O, Ga-Zn-O, Zr-Zn-O),[6] SnO_2-based oxides (F-Sn-O, Sb-Sn-O),[7] conductive polymers (PANI, PEDOT:PSS),[8] and ultra-thin metals,[9] as OLED/PLED anodes.

CdO was one of the first transparent conducting oxide materials discovered and has been extensively employed for transparent electrodes in photovoltaic devices due to the nearly metallic conductivity.[10] However, there have been no reported attempts to fabricate OLEDs using CdO-based TCOs as the electrodes. Although the band gap of pure bulk CdO is only 2.3 eV,[11]

leading to relatively poor optical transparency in the short wavelength range, significant widening of the band gap can be achieved via a Burstein-Moss (B-M) shift using fluorine or aliovalent metal doping, due to the small effective CdO carrier mass.[12,13] For example, In-doping widens the band gap from 2.6 eV in pure CdO to 3.2 eV at 5 % In-doping,[12] which is comparable to reported band gap values for commercial ITO (3.0-3.7eV). Although CdO is somewhat toxic and thus not suitable for all applications in the display area, this can be overcome to some degree by encapsulation, which is normally used to extend OLED display lifetimes. In previous work from this laboratory, undoped and doped CdO thin films were successfully grown by an MOCVD technique using optimized metal-organic Cd precursors.[12,14] In-doped CdO thin films grown on glass by MOCVD exibit conductivities as high as 17,000 S/cm.[12] However, such films grown on amorphous glass substrates are relatively rough (RMS roughness ~ 10 nm), which could be a potential source of shorting when used as OLED anodes. It is our continued interest to investigate the feasibility of employing ITO-alternative materials such as these as transparent electrodes for OLEDs and to investigate the effects of surface morphology on OLED response. Our recent results reveal that high-quality epitaxial CdO thin films grown on MgO(100) are far more conductive and smoother than those grown on glass, with RMS roughnesses of 5~ 6 nm, enabling us to investigate anode morphology effects on OLED response using this material as a transparent model anode. In this contribution, we report the growth of high-quality CdO thin films on glass and single-crystal MgO(100) by MOCVD, and the resulting OLED response characteristics with these films as anodes for small-molecule OLEDs. Device response and

application potential are investigated and compared with those of control devices based on commercial ITO anodes. It is found that with appropriate attention to morphology, highly conductive CdO thin films are capable of efficiently injecting holes into OLED devices, rendering them promising anode materials for OLEDs.

4.2. THIN FILM GROWTH AND CHARACTERIZATION

CdO-based thin film growth was carried out in the previously described horizontal, cold-wall MOCVD reactor,[15] using metal-organic precursor $Cd(hfa)_2(N,N-DE-N',N'-DMEDA)$ (hfa = hexafluoroacetylacetonate; N,N-DE-N',N'-DMEDA = N,N-diethyl-N',N'-dimethyl-ethylenediamine).[12b] The $Cd(hfa)_2(N,N-DE-N',N'-DMEDA)$ precursor temperature/Ar carrier gas flow rates were optimized at 85 ^{o}C /45 sccm. The O_2 oxidizing gas was introduced at 400 sccm after saturating with distilled DI water. A system operating pressure of 4.3±0.1 Torr and a substrate temperature of 400 °C were maintained during thin film growth. Corning 1737F glass (Precision Glass and Optics, 2.54 × 2.54 cm^2) and double-side polished MgO(100) substrates (MTI Corporation, 2.54 × 2.54 cm^2) were used as substrates and were placed side-by-side on a SiC-coated susceptor for simultaneous growth. Both the glass and the MgO(100) substrate surfaces were cleaned with acetone prior to the film deposition. ITO-coated glass (sheet resistance =14.8 Ω/□, root-mean-square (RMS) roughness = 2.5 nm) was purchased from Colorado Concept Coating, LLC. Optical transparency

measurements were carried out with a Cary 500 Uv-Vis-NIR spectrophotometer. Film thicknesses were measured with a Tencor P-10 profilometer after etching a step in the film using 5% aqueous HCl solution. θ-2θ scans, rocking curves, and ϕ scans of the epitaxial thin films on MgO(100) substrates were obtained on a home-built Rigaku four-circle diffractometer using detector-selected Cu K_α radiation. Film surface morphology was examined using a Digital Instruments Nanoscope III atomic force microscope (AFM) operating in the contact mode. Film microstructure was imaged on a Hitachi S4500 FE scanning electron microscope (SEM). Transmission electron microscopic (TEM) images were obtained using a Hitachi 8100 microscope operating at 200 keV. Four-probe charge transport data were collected on Bio-Rad HL5500 Hall-effect measurement system at ambient temperature.

CdO thin films were grown on 1737F glass and single crystal MgO(100) at 400 ^{o}C at a growth rate of ~1.5 nm/min on glass and ~2.2 nm/min on MgO(100), respectively. The greater observed film growth rate on MgO(100) than on glass is likely due to epitaxy effects. All the films are phase-pure as judged from XRD, with highly crystalline fcc CdO microstructures. The as-deposited CdO thin films grown on MgO(100) also exhibit a highly biaxial textured structure (Figure 1). The rocking curve with a full-width-at-half-maximum (FWHM) of 0.7 ^{o} (Figure 1a) indicates good out-of-plane alignment. In-plane film orientation was investigated by ϕ-scans of the CdO (111) reflection at $\chi = 54.7$ ^{o} (Figure 1b), and the clear four-fold rotational symmetry of the CdO (111) reflections together with the small FWHMs of 0.7 ^{o} indicate excellent in-plane microstructual orientation of the films. The orientation relation between the CdO thin films and

the MgO(100) substrates is therefore CdO(100)‖MgO(100).

As-deposited CdO films are light-yellow but highly transparent. There is negligible difference in the transmittance spectra between films on glass and MgO(100) substrates. The optical transmittance spectrum of a thin film on MgO(100) is shown in Figure 2. The average transmittance exceeds 85% in the visible range, and the band gap is determined to be 2.8 eV from the spectra by extrapolating the linear portion of the plot of $(\alpha h\nu)^2$ vs. $h\nu$ to $\alpha = 0$ (Figure 2 inset). As-deposited CdO thin film samples exhibit n-type conductivity as determined by negative Hall coefficients. CdO thin films having a sheet resistance of 17.7 $\Omega/\square$ with a thickness of 180 nm, and 4.3 $\Omega/\square$ with a thickness of 267 nm, were obtained on glass and MgO(100), respectively -- comparable to or substantially lower than the sheet resistance of commercial ITO (14.8 $\Omega/\square$).

Smooth surfaces are essential for small-molecule OLED transparent bottom electrodes because the subsequently deposited upper organic semiconductor layers will assume the morphologies of the bottom electrode. The surface morphologies of the present as-deposited CdO thin films are uniform as judged by SEM and AFM images (Figures not shown). The RMS roughness of the CdO films determined by contact mode AFM is 8~10 nm on glass and 5~6 nm on MgO(100), over a 10 μm ×10 μm scan area. Cross-sectional TEM bright field images show that CdO on glass grows in a columnar microstructure, giving rise to more rough and discontinuous surfaces. No spikes are detected under AFM and TEM. The surface of epitaxial CdO films grown on MgO(100) is very smooth, with a very flat film surface (Figure 3).

4.3. DEVICE FABRICATION AND PROPERTIES

The as-deposited CdO thin films were transferred to a glove-box /twin-evaporator OLED fabrication facility, followed by thermal evaporation at 1×10^{-7} Torr of N,N'-di(1-napthyl)-N,N'-diphenylbenzidine (NPB) (25 nm), Alq/1% di-isoamylquinacridone (DIQA) (50 nm), 2,9-dimethyl-4,7-diphenyl-1,10-phenanthroline (BCP) (20 nm), Li (1 nm), and Mg/Ag (1:9, 100 nm). General details of device fabrication are described elsewhere.[16] Simultaneously, a control device with an identical multilayer structure was fabricated using commercial ITO on glass for comparison. The 0.2×0.5 cm^2 OLED emitting areas were defined by shadow masks. Steady state light output and *J-V* characteristics were measured with a Keithley 2400 source meter and an IL 1700 radiometer at 25°C under ambient atmosphere. External forward quantum efficiencies were estimated from current-density-voltage and luminance-current-density characteristics. We were not able to record accurate light output and *J-V* behavior for the device fabricated on CdO/glass electrode because such devices burn out within seconds. This likely reflects the rougher CdO/glass surface as confirmed by AFM and TEM, with the discontinuous columnar grains giving rise to much stronger local fields in the thin film device, leading to fast shorting. In contrast, the OLED devices fabricated on CdO/MgO(100) show good rectifying I-V behavior and are very stable at high driving voltages. Figure 4 shows steady state light output and I-V (*J-V*) data for devices based on CdO/MgO(100) and for a control device fabricated with plasma-cleaned commercial ITO/glass (14.8 $\Omega/\square$). Operating

characteristics are summarized in Table 1. The differences between the CdO device and the ITO control are attributed to differences in anodes because the two devices were fabricated in a parallel fashion. As can be seen in Figure 4, for both CdO- and ITO-based devices, light turn-on occurs simultaneously with current turn-on. It is clear that CdO anodes are capable of injecting holes into such devices, consistent with acceptable work function alignment with respect to the hole transport layer (NPB) highest occupied molecular orbital (HOMO) levels. Interestingly, the OLEDs with CdO anodes exhibit a turn-on voltage of 3.2 V, slightly lower than that of the commercial ITO-based control, 3.7 V. At driving voltages < 9 V, the light outputs of CdO devices and ITO controls are essentially identical. A maximum device luminance of 32,000 cd/m^2 is achieved for CdO devices, with an external forward quantum efficiency of 1.4 %, somewhat lower than that of the ITO control, 3.6%. Note that the respective operating voltage at 100 cd/m^2 for devices on CdO, 5.6 V, is comparable to that of the ITO control, 5.7 V. We suspect that the origin of the greater current flow and lower quantum efficiency in the CdO-based devices is interfacial and can be addressed via interfacial functionalization appropriate for CdO. This is currently under investigation.

4.4. CONCLUSIONS

In summary, this work demonstrates that highly conductive CdO thin films are capable of injecting holes into archetypical OLED devices as effective anodes. A maximum luminance of

32,000 cd/m^2 and an external forward quantum efficiency of 1.4 %, with a turn-on voltage of 3.2 V are achieved on CdO/MgO(100)-based devices. Importantly, this work also suggests the feasibility of employing other CdO-based TCOs as anodes for high-performance OLEDs. Interesting results are expected from the use of In-, Sn-, or other metal-doped CdO thin films as OLED anodes, which are more conductive and with broader transparency windows vs. undoped CdO and ITO.

OLED Anode	Sheet Resistance ($\Omega/\square$) (RMS Roughness (nm))	Turn-on Voltage (V) (Max. Light Output (cd/m^2))	Applied Bias at 100 cd/m^2 (V)	Max. External Forward Quantum Efficiency (%)
CdO/glass	17.7 (~10)	---[a]	---[a]	---[a]
CdO/MgO(100)	4.3 (5~6)	3.2 (32,000)	5.6	1.4
ITO-control	14.8 (2.5)	3.7 (69,000)	5.7	3.6

[a] not available due to the device shorting.

Table 4.1. Operating characteristics of OLED devices having the structure: TCO/NPB/AlQ:DIQA/BCP/Li/MgAg.

A)

B)
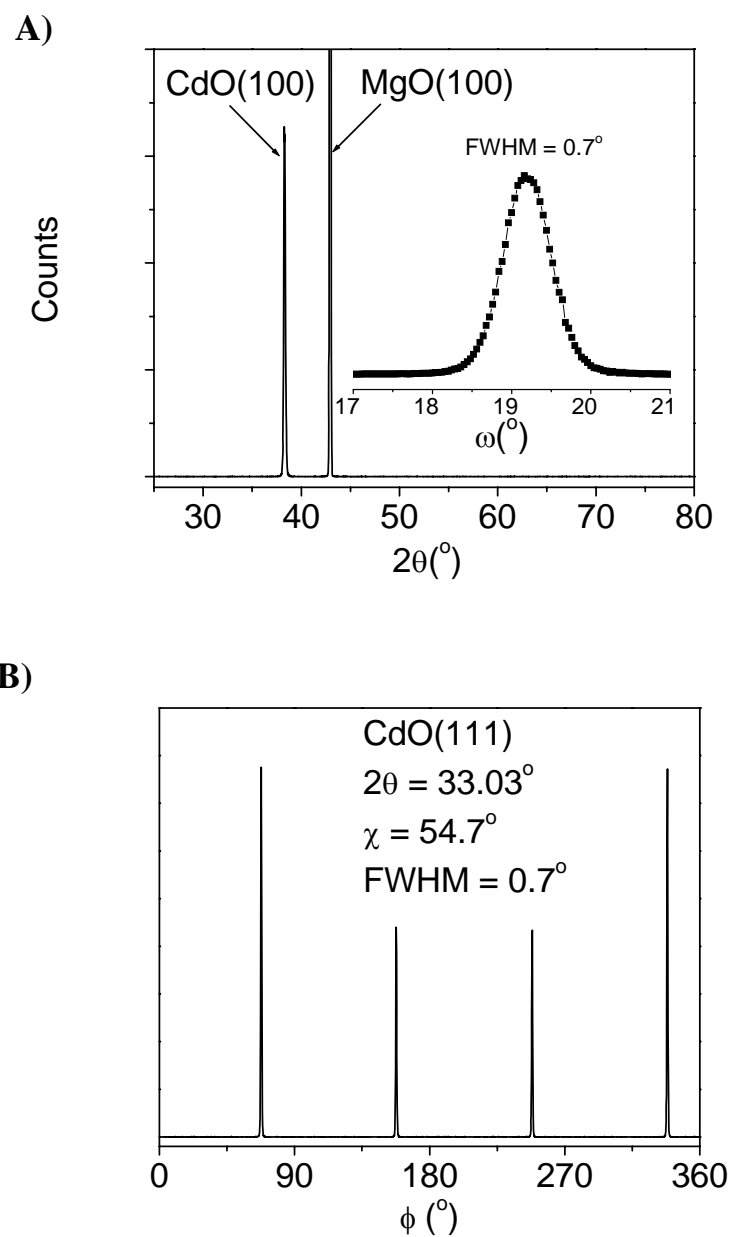
Figure 4.1.   A) θ-2θ x-ray diffractogram of as-deposited CdO thin film on MgO(100). Inset: rocking curve measured on the CdO (200) XRD peak; B) ϕ scans measured on the CdO(111) XRD peak with χ = 54.7°
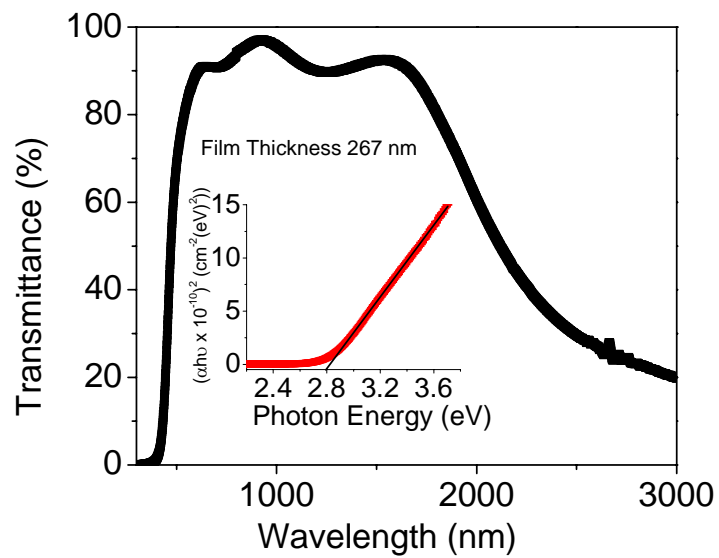
Figure 4.2.   Optical transparency of as-deposited CdO thin films on MgO(100).

Inset: derivation of the apparent optical band gap

A)
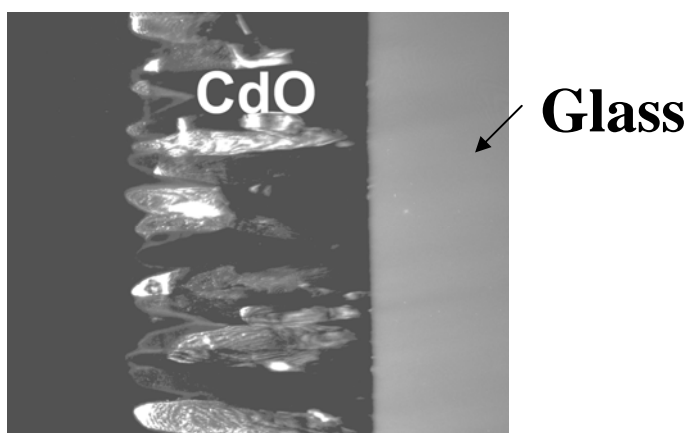
B)
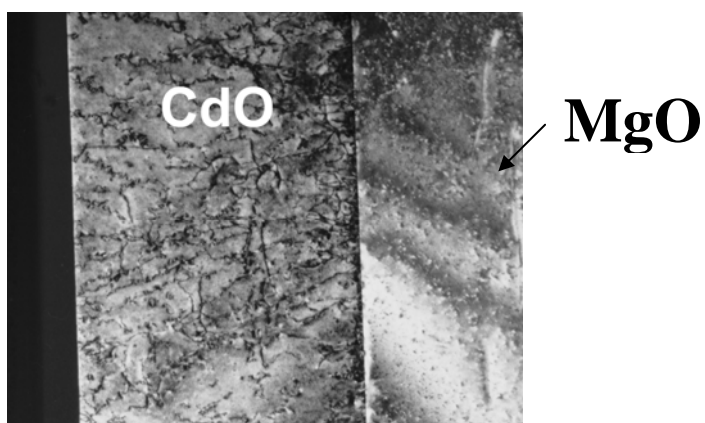
Figure 4.3.   Cross-section TEM images of as-deposited CdO thin film on a): glass;

b) MgO(100)
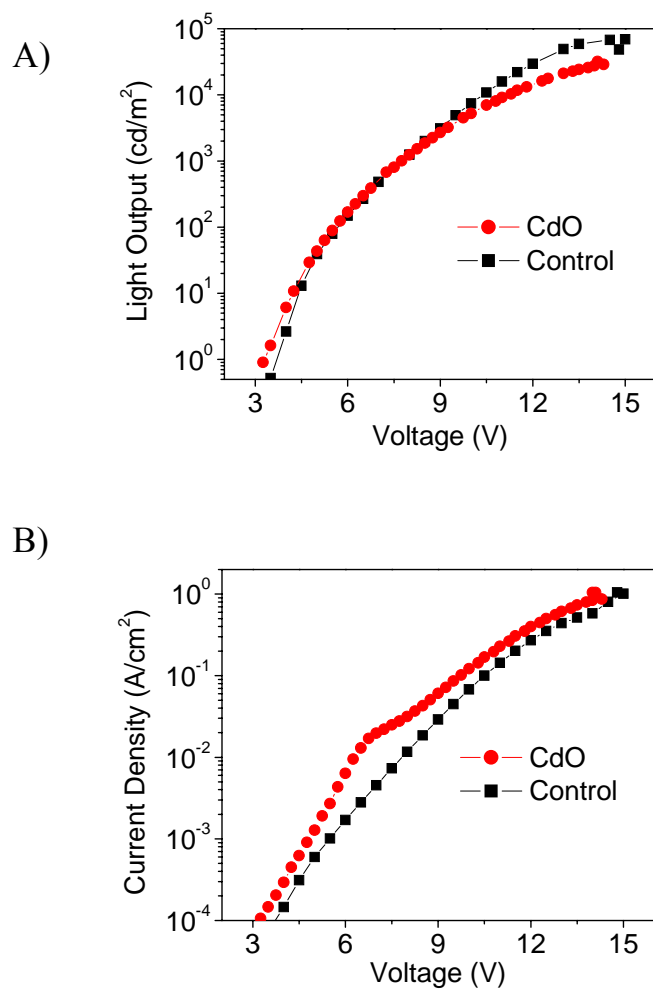
Figure 4.4. Steady state measurement of A) light output and B) current density as a function of bias for OLEDs of the structure CdO/NPB/AlQ:DIQA/BCP/Li/MgAg

REFERENCES

CHAPTER ONE

1   (a) Freeman, A. J.; Poeppelmeier, K. R.; Mason, T. O.; Chang, R. P. H.; Marks, T. J. *MRS Bull.* **2000**, *25*, 45. (b) Kawazoe, H.; Yanagi, H.; Ueda, K.; Hosono, H. *MRS Bull.* **2000**, *25*, 28. (c) Lewis, B. G.; Paine, D. C. *MRS Bull.* **2000**, *25*, 22. (d) Minami, T. *MRS Bull.* **2000**, *25*, 38. (e) Gordon, R. G. *MRS Bull.* **2000**, *25*, 52. (f) Granqvist, C. G.; Hultaker, A. *Thin Solid Films* **2002**, *411*, 1. (g) Hosono, H.; Ohta, H.; Orita, M.; Ueda, K.; Hirano, M. *Vacuum* **2002**, *66*, 419. (h) Coutts, T. J.; Young, D. L.; Li, X. *MRS Bull.* **2000**, *25*, 58.

2   (a) Ginley, D. S.; Bright, C. *MRS Bull.* **2000**, *25*, 15. (b) Mason, T. O.; Gonzalez, G. B.; Kammler, D. R.; Mansourian-Hadavi, N.; Ingram, B. J. *Thin Solid Films* **2002**, *411*, 106.

3   (a) Wu, X.; Dhere, R. G.; Albin, D. S.; Gessert, T. A.; DeHart, C.; Keane, J. C.; Duda, A.; Coutts, T. J.; Asher, S.; Levi, D. H.; Moutinho, H. R.; Yan, Y.; Moriarty, T.; Johnston, S.; Emery, K.; Sheldon, P. *Proceedings - NCPV Program Review Meeting, Lakewood, Co, USA* **2001**, 47. (b) Coutts, T. J.; Mason, T. O.; Perkins, J. D.; Ginley, D. S. *Electrochem. Soc. Proc.* **1999**, 274. (c) Kawamura, K.; Takahashi, M.; Yagihara, M.; Nakayama, T. In *Eur. Pat. Appl. EP 1271561, A2 20030102, CAN 138:81680, AN 2003:4983*, **2003**.

4   (a) Kammler, D. R.; Mason, T. O.; Young, D. L.; Coutts, T. J.; Ko, D.; Poeppelmeier, K. R.; Williamson, D. L. *J. Appl. Phys.* **2001**, *90*, 5979. (b) Zhao, Z. Y.; Morel, D. L.; Ferekides, C. S. *Thin Solid Films* **2002**, *413*, 203.

5   (a) Babcock, J. R.; Wang, A. C.; Metz, A. W.; Edleman, N. L.; Metz, M. V.; Lane, M. A.; Kannewurf, C. R.; Marks, T. J. *Chem. Vapor Depos.* **2001**, *7*, 239. (b) Asahi, R.; Wang, A.; Babcock, J. R.; Edleman, N. L.; Metz, A. W.; Lane, M. A.; Dravid, V. P.; Kannewurf, C. R.; Freeman, A. J.; Marks, T. J. *Thin Solid Films* **2002**, *411*, 101.

6   Wang, A.; Babcock, J. R.; Edleman, N. L.; Metz, A. W.; Lane, M. A.; Asahi, R.; Dravid, V. P.; Kannewurf, C. R.; Freeman, A. J.; Marks, T. J. *Proc. Natl. Acad. Sci. U. S. A.* **2001**, *98*, 7113.

7   Yan, M.; Lane, M.; Kannewurf, C. R.; Chang, R. P. H. *Appl. Phys. Lett.* **2001**, *78*, 2342.

8   (a) Coutts, T. J.; Young, D. L.; Li, X.; Mulligan, W. P.; Wu, X. *J. Vac. Sci. Technol. A-Vac. Surf. Films* **2000**, *18*, 2646. (b) Wu, X.; Coutts, T. J.; Mulligan, W. P. *J. Vac. Sci. Technol. A-Vac. Surf. Films* **1997**, *15*, 1057.

9   Koffyberg, F. P. *Phys. Rev. B* **1976**, *13*, 4470.

10   Burstein, E. *Phys. Rev.* **1954**, *93*, 632.

11   Shannon, R. D. *Acta Crystallogr.* **1976**, *A32*, 751.

12   Medvedeva, J.E.; Freeman, A. J. *to be published*.

13   Wimmer, E.; Krakauer, H.; Weinert, M.; Freeman, A. J. *Phys. Rev. B* **1981**, *24*, 864.

14 Hinds, B. J.; McNeely, R. J.; Studebaker, D. B.; Marks, T. J.; Hogan, T. P.; Schindler, J. L.; Kannewurf, C. R.; Zhang, X. F.; Miller, D. J. *J. Mater. Res.* **1997**, *12*, 1214.

15 Metz, A. W.; Ireland, J. R.; Zheng, J. G.; Lobo, R. P. S. M.; Yang, Y.; Ni, J.; Stern, C. L.; Dravid, V. P.; Bontemps, N.; Kannewurf, C. R.; Poeppelmeier, K. R.; Marks, T. J. *J. Am. Chem. Soc.* **2004**, *126*, 8477.

16 Fleeting, K. A.; Davies, H. O.; Jones, A. C.; O'Brien, P.; Leedham, T. J.; Crosbie, M. J.; Wright, P. J.; Williams, D. J. *Chem. Vapor Depos.* **1999**, *5*, 261.

17 Lyding, J. W.; Marcy, H. O.; Marks, T. J.; Kannewurf, C. R. *IEEE Trans. Instrum. Meas.* **1988**, *37*, 76.

18 Asahi, R.; Mannstadt, W.; Freeman, A. J. *Phys. Rev. B* **1999**, *59*, 7486; and references therein.

19 Lamoreaux, R. H.; Hildenbrand, D. L.; Brewer, L. *J. Phys. Chem. Ref. Data,* **1987**, *16*, 419.

20 JCPDS-International Centre for Diffraction Data *CdO: 05-0640*.

21 JCPDS-International Centre for Diffraction Data *Sc$_2$O$_3$: 05-0629*.

22 Ambrosini, A.; Duarte, A.; Poeppelmeier, K. R.; Lane, M.; Kannewurf, C. R.; Mason, T. O. *J. Solid State Chem.* **2000**, *153*, 41.

23 Vegard, L. *Z. Phys* **1921**, *5*, 17.

24 Morozova, L. V.; Komarov, A. V. *Russ. J. Appl. Chem.* **1995**, *68*, 1240.

25 (a) Dou, Y.; Egdell, R. G.; Walker, T.; Law, D. S. L.; Beamson, G. *Surf. Sci.* **1998**, *398*, 241.

(b) Dou, Y.; Fishlock, T.; Egdell, R. G.; Law, D. S. L.; Beamson, G. *Phys. Rev. B* **1997**, *55*, 13381.

26 Taga, N.; Odaka, H.; Shigesato, Y.; Yasui, I.; Kamei, M.; Haynes, T. E. *J. Appl. Phys.* **1996**, *80*, 978.

27 (a) Dingle, R. B. *Phil. Mag.* **1955**, *46*, 831. (b) Erginsoy, C. *Phys. Rev.* **1950**, *79*, 1013. (c) Frank, G.; Koestlin, H. *Appl. Phys. A: Solids and Surfaces* **1982**, *A27*, 197.

28 Chen, M.; Pei, Z. L.; Wang, X.; Yu, Y. H.; Liu, X. H.; Sun, C.; Wen, L. S. *J. Phys. D: Appl. Phys.* **2000**, *33*, 2538.

29 Bardeen, J.; Shockley, W. *Phys. Rev.* **1950**, *80*, 72.

30 (a) Zhang, D. H.; Ma, H. L. *Appl. Phys. A* **1996**, *A62*, 487. (b) Gilmore, A. S.; Al-Kaoud, A.; Kaydanov, V.; Ohno, T. R. *Mat. Res. Soc. Symp. Proc.* **2001**, *666*, F3.10/1. (c) Tahar, R. B. H.; Tahar, N. B. H. *J. Appl. Phys.* **2002**, *92*, 4498.

31 Cimino, A.; Marezio, M. *J. Phys. Chem. solids* **1960**, *17*, 57.

CHAPTER TWO

1   *Special Issue on Transparent Conducting Oxides*, (eds Ginley, D. S. & Bright, C.), MRS Bulletin **2000**, *25*, and references therein.

2   (a) Coutts, T. J.; Mason, T. O.; Perkins, J. D.; Ginley, D. S. in Transparent Conducting Oxides: Status and Opportunities in Basic Research, Photovaltaics for the 21st Century, (eds Kapur, V. K., et al.), *Electrochem. Soc. Proc*. **1999**, 274-288. (b) Wu, X.; Dhere, R. G.; Albin, D. S.; Gessert, T. A.; DeHart, C.; Keane, J. C.; Duda, A.; Coutts, T. J.; Asher, S.; Levi, D. H.; Moutinho, H. R.; Yan, Y.; Moriarty, T.; Johnston, S.; Emery, K.; Sheldon, P. *Proceedings - NCPV Program Review Meeting*, Lakewood, CO, United States, **2001**, Oct. 14-17, 47-48. (c) Kawamura, K.; Takahashi, M.; Yagihara, M.; Nakayama, T. *Eur. Pat. Appl*. **2003**, EP 1271561, A2 20030102, CAN 138:81680, AN 2003:4983.

3   (a) Wang, R.; King, L. L. H.; Sleight, A. W. *J. Mater. Res*. **1996**, *11*, 1659. (b) Wang, A.; Dai, J.; Cheng, J.; Chudzik, M. P.; Marks, T. J.; Chang, R. P. H.; Kannewurf, C. R. *Appl. Phys. Lett.* **1998**, *73*, 327. (c) Minami, T. in ref. 1 P.38 and references therein. (d) Edwards, D. D.; Mason, T. O.; Sinkler, W.; Marks, L. D.; Goutenoire, F.; Poeppelmeier, K. R. *J. Solid State Chem.* **1998**, *140*, 242-250. (e) Phillips, J. M.; Cava, R. J.; Thomas, G. A.; Carter, S. A.; Kwo, J.; Siegrist, T.; Krajewski, J. J.; Marshall. J. H.; Peck, W. F., Jr.; Rapkine, D. H. *Appl. Phys. Lett.* **1995**, *67*, 2246. (f) Ott, A. W.; Chang, R. P. H.; *Mater. Chem. Phys.* **1999**, *58*, 132. (g) Coutts, T. J.; Young, D. L.; Li, X. *J. Vac. Sci. Technol. A* **2000**, *18(6)*, 2646.

4   (a) Kammler, D. R.; Mason, T. O.; Young, D. L.; Coutts, T. J.; Ko, D.; Poeppelmeier, K. R.; Williamson, D. L. *J. Appl. Phys.* **2001**, *90*, 5979-5985. (b) Mason, T. O.; Gonzalez, G. B.; Kammler, D. R.; Mansourian-Hadavi, N.; Ingram, B. J. *Thin Solid Films*, **2002**, *411*, 106-114.

5   (a) Babcock, J. R.; Wang, A.; Metz, A. W.; Edleman, N. L.; Metz, M. V.; Lane, M. A.; Kannewurf, C. R.; Marks, T. J. *Chem. Vap. Deposition* **2001**, *7*, 239. (b) Wang, A.; Babcock, J. R.; Edleman, N. L.; Metz, A. W.; Lane, M. A.; Asahi, R.; Dravid, V. P.; Kannewurf, C. R.; Freeman, A. J.; Marks, T. J. *Proc. Nat. Acad. Sci.* **2001**, *98*, 7113-7116. (c) Asahi, R.; Wang, A.; Babcock, J. R.; Edleman, N. L.; Metz, A. W.; Lane, M. A.; Dravid, V. P.; Kannewurf, C. R.; Freeman, A. J.; Marks, T. J. *Thin Solid Films* **2002**, *411*, 101-105. (d) Metz, A.W.; Ireland, J.R.; Zheng, J.G.; Lobo, R.P.S.M.; Yang, Y.; Ni, J.; Stern, C.L.; Dravid, V.P.; Bontemps, N.; Kannewurf, C.R.; Poeppelmeier, K.R.; and Marks, T.J., *J. Am. Chem. Soc.* **2004**, *126*, 8477. (e) Jin, S.; Yang, Y.; Medvedeva, J.E.; Ireland, J.R.; Metz, A.W.; Ni, J.; Kannewurf, C.R.; Freeman, A.R.; and Marks, T.J. *J. Am. Chem. Soc.* **2004,** *126*, 13787.

6   Yan, M.; Lane, M.; Kannewurf, C. R.; Chang, R.P.H. *App. Phys. Lett.* **2001**, *78*, 2342-2344.

7   Zhao, Z.; Morel, D. L.; Ferekides, C. S. *Thin Solid Films* **2002**, *413*, 203-211.

8   Koffyberg, F. P. *Phys. Rev. B* **1976**, *13*, 4470.

9   (a) Burstein, E. *Phys. Rev.* **1954**, *93*, 632. (b) Moss, T.S. *Proc. Phys. Soc. A.* **1954**, *382*, 775.

10   (a) Ramakrishna Reddy, K. T.; Sravani, C.; Miles, R. W. *J Crys. Growth* **1998**, *184*, 1031-1034. (b) Phatak, G.; Lal, R. *Thin Solid Films* **1994**, *245*, 17.

11 Matsuura, N.; Johnson, D. J.; Amm, D. T. *Thin Solid Films* **1997**, *295*, 260.

12 a) Vigil, O.; Vaillant, L.; Cruz, F.; Santana, G.; Morales-Acevedo, A.; and Contreras-Puente, G. *Thin Solid Films* **2000**, *361*, 53. b) Murthy, L.C.S.; Rao, K.S.R.K. *Bull. Mater. Sci.* **1999**, *22*, 953.

13 (a) Subramanyam, T. K.; Uthanna, S.; Srinivasulu Naidu, B. *Physica Scripta* **1998**, *57*, 317. (b) Lewin, R.; Howson, R. P. Bishop, C. A.; Ridge, M.I.; *Vacuum* **1986**, *36*, 95-98. (c) Gurumurugan, K.; Mangalarj, D.; Narayandass, S.K.; Nakanishi, Y.; and Hatanaka, Y. *Appl. Surface Sci.* **1997**, *114*, 422. (d) Chu, T. L.; Chu, S. S. *J. Elec. Mater.* **1990**, *19*, 1003-1005

14 (a) Gulino, A.; Castelli, F.; Dapporto, P.; Rossi, P.; Fragalà, I. *Chem. Mater.* **2002**, *14*, 704-709. (b) Gulino, A.; Dapporto, P. Rossi, P.; Fragalà, I.; *Chem. Mater.* **2002**, *14*, 1441-1444. (c) Gulino, A.; Dapporto, P.; Rossi, P.; Fragalà, I.; *Chem. Mater.* **2002**, *14*, 4955.

15 Schulz, D. L.; Marks, T. J.; in *CVD of Non-Metals*, Rees, W. S. ed. (VCH, New York), pp 39-150.

16 Shannon, R.D. *Acta Crystallogr.* **1976**, *A32*, 751.

17 (a) Dou, Y. Egdell, R. G.; Walker, T.; Law, D. S. L.; Beamson, G. *Surface Science*, **1998**, *398*, 241-258. (b) Dou, Y.; Fishlock, T.; Egdell, R. G.; Law, D. S. L.; Beamson, G. *Phys. Rev. B*, **1997**, *55*, R13381-R13384.

18 Gulino A.; Fragalà, I. *J. Mater. Chem.* **1999**, *9*, 2837-2841.

19 Hinds, B.J.; McNeely, R.J.; Studebaker, D.B.; Marks, T.J.; Hogan, T.P.; Schindler, J.L.; Kannewurf, C.R.; Zhang, X.F.; Miller, D. *J. Mater. Res.* **1997**, *12*, 1214.

20   Rees, W. S., Jr.; Carris, M. W. *Inorg. Synth.* **1997**, *31*, 302-306.

21   Lyding, J. W.; Marcy, H. O.; Marks, T. J.; Kannewurf, C. R. *IEEE Trans. Instrum. Meas.* **1988**, *37*, 76.

22   Wimmer, E.; Krakauer, H.; Weinert, M.; Freeman, A. J. *Phys. Rev. B* **1981**, *24*, 864.

23   Asahi, R.; Mannstadt, W.; Freeman, A. J. *Phys. Rev. B* **1999**, *59*, 7486; and references therein.

24   In-doped CdO: Jin, S.; Yang, Y.; Medvedeva, J.E.; Ireland, J.R.; Metz, A.W.; Ni, J.; Hersam, M.C.; Freeman, A.R.; and Marks, T.J., *to be published.*

25   Medvedeva, J. E.; Freeman, A. J., Combining high conductivity with complete optical transparency: A band structure approach. *Europhysics Letters* **2005,** 69, (4), 583-587.

26   Taga, N.; Odaka, H.; Shigesato, Y.; Yasui, I.; Kamei, M.; Haynes, T. E. *J. Appl. Phys.* **1996**, *80*, 978-984.

27   Morozova, L. V.; Komarov, A. V. *Russ. J. Appl. Chem.* **1995**, *68*, 1240.

CHAPTER THREE

1. Coutts, T. J.; Mason, T. O.; Perkins, J. D.; Ginley, D. S., *Proc. - Electrochem. Soc.* **1999,** *99-11*, 274.

2. Coutts, T. J.; Young, D. L.; Li, X., *MRS Symp. Proc.* **2000,** *623*, 199.

3. Freeman, A. J.; Poeppelmeier, K. R.; Mason, T. O.; Chang, R. P. H.; Marks, T. J., *MRS Bull.* **2000,** *25*, 45.

4. Ginley, D. S.; Bright, C., *MRS Bull.* **2000,** *25*, 15.

5. Gordon, R. G., *MRS Bull.* **2000,** *25*, 52.

6. Granqvist, C. G.; Hultaker, A., *Thin Solid Films* **2002,** *411*, 1.

7. Hosono, H.; Ohta, H.; Orita, M.; Ueda, K.; Hirano, M., *Vacuum* **2002,** *66*, 419.

8. Kawamura, K.; Takahashi, M.; Yagihara, M.; Nakayama, T. European Patent Application, 2003, EP1271561, A2 20030102, CAN 138:81680, AN 2003:4983

9. Kawazoe, H.; Yanagi, H.; Ueda, K.; Hosono, H., *MRS Bull.* **2000,** *25*, 28.

10. Lewis, B. G.; Paine, D. C., *MRS Bull.* **2000,** *25*, 22.

11. Mason, T. O.; Gonzalez, G. B.; Kammler, D. R.; Mansourian-Hadavi, N.; Ingram, B. J., *Thin Solid Films* **2002,** *411*, 106.

12. Minami, T., *MRS Bull.* **2000,** *25*, 38.

13. Wu, X.; Dhere, R. G.; Albin, D. S.; Gessert, T. A.; DeHart, C.; Keane, J. C.; Duda, A.; Coutts, T. J.; Asher, S.; Levi, D. H.; Moutinho, H. R.; Yan, Y.; Moriarty, T.; Johnston, S.; Emery, K.; Sheldon, P., *Proc. NCPV Prog. Rev. Meet., Lakewood, Co, USA* **2001**, 47.

14. Coutts, T. J.; Young, D. L.; Li, X.; Mulligan, W. P.; Wu, X., *J. Vac. Sci. Technol., A* **2000,** *18*, 2646.

15. Coutts, T. J.; Young, D. L.; Li, X. N., *MRS Bull.* **2000,** *25*, 58.

16. Edwards, D. D.; Mason, T. O.; Sinkler, W.; Marks, L. D.; Goutenoire, F.; Poeppelmeier, K. R., *J. Solid State Chem.* **1998,** *140*, 242.

17. Ott, A. W.; Chang, R. P. H., *Mater. Chem. Phys.* **1999,** *58*, 132.

18. Phillips, J. M.; Cava, R. J.; Thomas, G. A.; Carter, S. A.; Kwo, J.; Siegrist, T.; Krajewski, J. J.; Marshall, J. H.; Peck, W. F.; Rapkine, D. H., *Appl. Phys. Lett.* **1995,** *67*, 2246.

19. Wang, A. C.; Dai, J. Y.; Cheng, J. Z.; Chudzik, M. P.; Marks, T. J.; Chang, R. P. H.; Kannewurf, C. R., *Appl. Phys. Lett.* **1998,** *73*, 327.

20. Wang, R. P.; King, L. L. H.; Sleight, A. W., *J. Mater. Res.* **1996,** *11*, 1659.

21. Asahi, R.; Wang, A.; Babcock, J. R.; Edleman, N. L.; Metz, A. W.; Lane, M. A.; Dravid, V. P.; Kannewurf, C. R.; Freeman, A. J.; Marks, T. J., *Thin Solid Films* **2002,** *411*, 101.

22. Babcock, J. R.; Wang, A. C.; Metz, A. W.; Edleman, N. L.; Metz, M. V.; Lane, M. A.; Kannewurf, C. R.; Marks, T. J., *Chem. Vap. Deposition* **2001,** *7*, 239.

23. Jin, S.; Yang, Y.; Medvedeva, J. E.; Ireland, J. R.; Metz, A. W.; Ni, J.; Kannewurf, C. R.; Freeman, A. J.; Marks, T. J., *J. Am. Chem. Soc.* **2004,** *126*, 13787.

24. Kammler, D. R.; Mason, T. O.; Young, D. L.; Coutts, T. J.; Ko, D.; Poeppelmeier, K. R.; Williamson, D. L., *J. Appl. Phys.* **2001,** *90*, 5979.

25. Metz, A. W.; Ireland, J. R.; Zheng, J. G.; Lobo, R.; Yang, Y.; Ni, J.; Stern, C. L.; Dravid, V. P.; Bontemps, N.; Kannewurf, C. R.; Poeppelmeier, K. R.; Marks, T. J., *J. Am. Chem. Soc.* **2004,** *126*, 8477.

26. Yan, M.; Lane, M.; Kannewurf, C. R.; Chang, R. P. H., *Appl. Phys. Lett.* **2001,** *78*, 2342.

27. Yang, Y.; Jin, S.; Medvedeva, J. E.; Ireland, J. R.; Metz, A. W.; Ni, J.; Hersam, M. C.; Freeman, A. J.; Marks, T. J., *J. Am. Chem. Soc.* **2005,** *127*, 8796.

28. Zhao, Z. Y.; Morel, D. L.; Ferekides, C. S., *Thin Solid Films* **2002,** *413*, 203.

29. Koffyberg, F. P., *Phys. Rev. B* **1976,** *13*, 4470.

30. Burstein, E., *Phys. Rev.* **1954,** *93*, 632.

31. Moss, T. S., *Proc. Phys. Soc. A* **1954,** *382*, 775.

32. Phatak, G.; Lal, R., *Thin Solid Films* **1994,** *245*, 17.

33. Reddy, K. T. R.; Sravani, C.; Miles, R. W., *J. Cryst. Growth* **1998,** *185*, 1031.

34. Matsuura, N.; Johnson, D. J.; Amm, D. T., *Thin Solid Films* **1997,** *295*, 260.

35. Murthy, L. C. S.; Rao, K., *Bull. Mater. Sci.* **1999,** *22*, 953.

36. Vigil, O.; Vaillant, L.; Cruz, F.; Santana, G.; Morales-Acevedo, A.; Contreras-Puente, G., *Thin Solid Films* **2000,** *361*, 53.

37. Chu, T. L.; Chu, S. S., *J. Electron. Mater.* **1990,** *19*, 1003.

38. Gurumurugan, K.; Mangalaraj, D.; Narayandass, S. K.; Nakanishi, Y.; Hatanaka, Y., *Appl. Surf. Sci.* **1997,** *113/114*, 422.

39. Lewin, R.; Howson, R. P.; Bishop, C. A.; Ridge, M. I., *Vacuum* **1986,** *36*, 95.

40. Subramanyam, T. K.; Uthanna, S.; Naidu, B. S., *Phys. Scr.* **1998,** *57*, 317.

41. Gulino, A.; Castelli, F.; Dapporto, P.; Rossi, P.; Fragala, I., *Chem. Mater.* **2002,** *14*, 704.

42. Gulino, A.; Dapporto, P.; Rossi, P.; Fragala, I., *Chem. Mater.* **2002,** *14*, 4955.

43. Gulino, A.; Dapporto, P.; Rossi, P.; Fragala, I., *Chem. Mater.* **2002,** *14*, 1441.

44. Wang, A.; Babcock, J. R.; Edleman, N. L.; Metz, A. W.; Lane, M. A.; Asahi, R.; Dravid, V. P.; Kannewurf, C. R.; Freeman, A. J.; Marks, T. J., *Proc. Natl. Acad. Sci. U. S. A.* **2001,** *98*, 7113.

45. Schulz, D. L.; Marks, T. J. In *CVD of Non-metals*; Rees, W. S., Ed.; VCH: New York; pp 39-150

46. Medvedeva, J. E.; Freeman, A. J., *Europhys. Lett.* **2005,** *69*, 583.

47. Hinds, B. J.; McNeely, R. J.; Studebaker, D. B.; Marks, T. J.; Hogan, T. P.; Schindler, J. L.; Kannewurf, C. R.; Zhang, X. F.; Miller, D. J., *J. Mater. Res.* **1997,** *12*, 1214.

48. Jablonski, Z.; Rychlowskahimmel, I.; Dyrek, M., *Spectrochim. Acta, Part A* **1979,** *35*, 1297.

49. Utsunomi.K, *Bull. Chem. Soc. Jpn.* **1971,** *44*, 2688.

50. Wang, A. C.; Edleman, N. L.; Babcock, J. R.; Marks, T. J.; Lane, M. A.; Brazis, P. R.; Kannewurf, C. R., *J. Mater. Res.* **2002,** *17*, 3155.

51. Lyding, J. W.; Marcy, H. O.; Marks, T. J.; Kannewurf, C. R., *IEEE Trans. Instrum. Meas.* **1988,** *37*, 76.

52. Cimino, A.; Marezio, M., *Phys. Chem. Solids* **1960,** *17*, 57.

53. Dingle, R. B., *Phil. Mag.* **1955,** *46*, 831.

54. Erginsoy, C., *Phys. Rev.* **1950,** *79*, 1013.

55. Frank, G.; Koestlin, H., *Appl. Phys. A* **1982,** *A27*, 197.

56. Bardeen, J.; Shockley, W., *Phys. Rev.* **1950,** *80*, 72.

57. Chen, M.; Pei, Z. L.; Wang, X.; Yu, Y. H.; Liu, X. H.; Sun, C.; Wen, L. S., *J. Phys. D: Appl. Phys.* **2000,** *33*, 2538.

58. Zhang, D. H.; Ma, H. L., *Appl. Phys. A* **1996,** *62*, 487.

59. Gilmore, A. S.; Al-Kaoud, A.; Kaydanov, V.; Ohno, T. R., *MRS Symp. Proc.* **2001,** *666*, F3.10/1.

60. Tahar, R. B. H.; Tahar, N. B. H., *J. Appl. Phys.* **2002,** *92*, 4498.

61. Taga, N.; Odaka, H.; Shigesato, Y.; Yasui, I.; Kamei, M.; Haynes, T. E., *J. Appl. Phys.* **1996,** *80*, 978.

CHAPTER FOUR

1   (a) Burrows, P. E.; Gu, G.; Bulovic, V.; Shen, Z.; Forrest, S. R.; Thompson, M. E. IEEE Transactions on Electron Devices 1997, 44, 1188. (b) OLED issue, J. Soc. Information Display, 2004, 20, No. 6.

2   Schlatmann, A. R.; Floet, D. W.; Hilberer, A.; Garten, F.; Smulders, P. J. M.; Klapwijk, T. M.; Hadziioannou, G. Appl. Phys. Lett. 1996, 69, 1764.

3   Schlaf, R.; Parkinson, B. A.; Lee, P. A.; Nebesny, K. W.; Armstrong, N. R. Appl. Phys. Lett. 1998, 73, 1026.

4   Adamovich, V.; Shoustikov, A.; Thompson, M. E. Adv. Mater. 1999, 11, 727.

5   Cui, J.; Wang, A.; Edleman, N. L.; Ni, J.; Lee, P.; Armstrong, N. R.; Marks, T. J. Adv. Mater. 2001, 13, 1476.

6   Kim, H.; Horwitz, J. S.; Kim, W. H.; Makinen, A. J.; Kafafi, Z. H.; Chrisey, D. B. Thin Solid Films 2002, 420, 539, and reference therein.

7   (a) Andersson, A.; Johansson, N.; Broms, P.; Yu, N.; Lupo, D.; Salaneck, W. R. Adv. Mater. 1998, 10, 859. (b) Vaufrey, D.; Ben Khalifa, M.; Besland, M. P.; Sandu, C.; Blanchin, M. G.; Teodorescu, V.; Roger, J. A.; Tardy, J. Synth. Met. 2002, 127, 207.

8   (a) Gustafsson, G.; Cao, Y.; Treacy, G. M.; Klavetter, F.; Colaneri, N.; Heeger, A. J. Nature 1992, 357, 477. (b) Kim, W. H.; Makinen, A. J.; Nikolov, N.; Shashidhar, R.; Kim, H.; Kafafi, Z. H. Appl. Phys. Lett. 2002, 80, 3844.

9   Hatton, R. A.; Willis, M. R.; Chesters, M. A.; Rutten, F. J. M.; Briggs, D. J. Mater. Chem. 2003, 13, 38.

10 Coutts, T. J.; Mason, T. O.; Perkins, J. D.; Ginley, D. S. Electrochem. Soc. Proc. 1999, 274.

11 Koffyberg, F. P. Phys. Rev. B 1976, 13, 4470.

12 (a) Wang, A.; Babcock, J. R.; Edleman, N. L.; Metz, A. W.; Lane, M. A.; Asahi, R.; Dravid, V. P.; Kannewurf, C. R.; Freeman, A. J.; Marks, T. J. Proc. Natl. Acad. Sci. U. S. A. 2001, 98, 7113. (b) Metz, A. W.; Ireland, J. R.; Zheng, J. G.; Lobo, R. P. S. M.; Yang, Y.; Ni, J.; Stern, C. L.; Dravid, V. P.; Bontemps, N.; Kannewurf, C.R.; Poeppelmeier, K. R.; and Marks, T. J., J. Am. Chem. Soc., 2004, 126, 8477. (c) Jin, S.; Yang, Y.; Medvedeva, J. E.; Ireland, J. R.; Metz, A. W.; Ni, J.; Kannewurf, C. R.; Freeman, A. J.; and Marks, T. J., J. Am. Chem. Soc., 2004, 126, 13787.

13 Yan, M.; Lane, M.; Kannewurf, C. R.; Chang, R. P. H. Appl. Phys. Lett. 2001, 78, 2342.

14 Babcock, J. R.; Wang, A. C.; Metz, A. W.; Edleman, N. L.; Metz, M. V.; Lane, M. A.; Kannewurf, C. R.; Marks, T. J. Chem. Vapor Deposition. 2001, 7, 239.

15 Hinds, B. J.; McNeely, R. J.; Studebaker, D. B.; Marks, T. J.; Hogan, T. P.; Schindler, J. L.; Kannewurf, C. R.; Zhang, X. F.; Miller, D. J. J. Mater. Res. 1997, 12, 1214.

16 Huang, Q. L.; Cui, J.; Veinot, J. G. C.; Yan, H.; Marks, T. J. Appl. Phys. Lett. 2003, 82, 331.